Karlsruhe Institute of Technology

Saharan Dust Impacts on Air Quality in Baden-Württemberg: Integrated Analysis of Observations and Dust Forecasts (2020–2024)

Master's Thesis of

Dev Arpan

at the Department of Physics
Institute for Meteorology and Climate Physics (IMK-TRO)

Reviewer:	prof. Dr. Corinna Hoose
Second reviewer:	prof. Dr. Jan Cermak
Advisor:	Dr. Gholamali Hoshyaripour
Second advisor:	Dr. Sven Werchner

January 2025 – January 2026

I declare that I have developed and written the enclosed thesis completely by myself, and have not used sources or means without declaration in the text.

PLACE, DATE

. . . . . .

(Dev Arpan)

Abstract

Natural Saharan dust transport represents a significant but episodic contributor to particulate matter concentrations in central Europe, complicating air quality management and regulatory compliance assessment. This Master's thesis quantifies the contribution of Saharan dust to air quality in Baden-Württemberg, Germany, through integrated analysis of ground-based observations and operational dust concentration forecasts from the DWD ICON-ART model during the five-year period 2020–2024.

Hourly PM_{10} and $PM_{2.5}$ measurements from five selected monitoring stations operated by the Landesanstalt für Umwelt Baden-Württemberg (LUBW) are systematically analysed alongside dust concentration data from the Deutscher Wetterdienst (DWD) ICON-ART model forecast archive. Multi-method event identification combining satellite imagery (NASA Worldview, MODIS aerosol optical depth), coordinated concentration increases across multiple stations, and model dust predictions enables robust detection of dust transport episodes. Chemical composition analysis of PM_{10} samples provides independent geochemical confirmation of dust origin through diagnostic element ratios.

Three major Saharan dust events are documented during 2020–2024, occurring exclusively during January–April with durations of 2–4 days. The most intense episode (February 24–25, 2021) produces regional-scale PM_{10} concentrations of 119–156 $\mu g/m^3$ and $PM_{2.5}$ daily means of 28.7–32.5 $\mu g/m^3$, exceeding both EU regulatory thresholds and WHO Air Quality Guidelines. Size distribution analysis reveals strong coarse-mode dominance during dust events ($PM_{2.5}/PM_{10}$ ratio: 0.28–0.48) compared to typical urban aerosol (0.58–0.67), though absolute $PM_{2.5}$ concentrations during major events substantially exceed WHO guidelines (15 $\mu g/m^3$), warranting health-protective measures for vulnerable populations.

Chemical composition measurements document 2.9–3.1-fold crustal element enrichment during events, with diagnostic Ca/Al ratios (3.7–3.9) and K/Al ratios (0.3) confirming North African dust origin and excluding local soil resuspension. The inverse K/Al signature (ratio decrease during events from 1.2–1.3 to 0.3) provides unambiguous evidence for Saharan dust transport, as potassium shows minimal increase despite substantial aluminium enrichment. Fe/Al ratios (1.0–1.2) align with iron-rich North African mineralogy, providing additional confirmation.

Dust fraction analysis indicates that natural Saharan dust accounts for approximately 50% of observed PM_{10} during the most intense event (February 2021), with lower fractions during moderate episodes. Dust-attributed exceedances of the EU daily limit value (50 $\mu g/m^3$) represent 2–4 days per station over the five-year period, constituting a meaningful fraction of total PM_{10} violations. Under projected 2030 standards (45 $\mu g/m^3$ daily threshold, reduced from 50 $\mu g/m^3$), dust contributions remain significant for PM_{10} daily limit compliance, whilst all stations currently comply with the anticipated $PM_{2.5}$ annual limit (10 $\mu g/m^3$), with observed means ranging from 7.0 to 8.8 $\mu g/m^3$.

Spatial analysis reveals a systematic southwest-to-northeast gradient in dust impacts across Baden-Württemberg, with southwestern stations (Freiburg, Karlsruhe) receiving direct exposure to Mediterranean transport pathways. This spatial pattern reflects prevailing meteorological transport pathways approaching from the Mediterranean and progressive dilution and deposition during eastward advection across the state. A notable finding emerges from station comparison: Freiburg exhibits the lowest mean PM concentrations (PM_{10}: 11.3 µg/m^3) yet records more daily exceedances (14.8 days/year) than rural Biberach (11.2 days/year), illustrating that long-term mean concentrations and short-term peak concentrations respond to different processes and geographical factors.

The findings demonstrate that Saharan dust, though episodic and representing a modest fraction of annual mean PM, significantly influences short-term air quality exceedances in Baden-Württemberg. The quantified dust contributions provide evidence supporting potential applications of EU Air Quality Directive Article 21 provisions for natural source subtraction from compliance assessments. The operational DWD ICON-ART model forecast system offers utility for advance warning of dust-affected PM episodes, enabling proactive public health communication and appropriate source attribution in air quality management.

This work establishes a robust methodological framework combining observations, satellite remote sensing, model dust concentration data, and chemical composition analysis for dust impact quantification, applicable to other central European regions affected by long-range mineral dust transport.

Keywords: Saharan dust, particulate matter, air quality, Baden-Württemberg, ICON-ART, dust forecasts, PM_{10}, $PM_{2.5}$, natural aerosols, source apportionment, air quality compliance

Zusammenfassung

Der natürliche Transport von Saharastaub stellt einen bedeutenden, aber episodischen Beitrag zu Feinstaubkonzentrationen in Mitteleuropa dar und erschwert das Luftqualitätsmanagement sowie die Bewertung der Einhaltung regulatorischer Vorgaben. Diese Masterarbeit quantifiziert den Beitrag von Saharastaub zur Luftqualität in Baden-Württemberg, Deutschland, durch die integrierte Analyse von bodengebundenen Beobachtungen und operationellen Staubkonzentrationsvorhersagen des DWD ICON-ART Modells während des fünfjährigen Zeitraums 2020–2024.

Stündliche PM_{10}- und $PM_{2.5}$-Messungen von fünf ausgewählten Messstationen der Landesanstalt für Umwelt Baden-Württemberg (LUBW) werden systematisch mit Staubkonzentrationsdaten aus dem ICON-ART Modellarchiv des Deutschen Wetterdienstes (DWD) analysiert. Die Identifikation von Staubereignissen erfolgt durch eine Kombination mehrerer Methoden: Satellitenbilder (NASA Worldview, MODIS Aerosol-optische Dicke), koordinierte Konzentrationsanstiege über mehrere Stationen hinweg und Modell-Staubvorhersagen ermöglichen eine robuste Detektion von Staubtransportepisoden. Chemische Zusammensetzungsanalysen von PM_{10}-Proben liefern unabhängige geochemische Bestätigung des Staubursprungs durch diagnostische Elementverhältnisse.

Während des Zeitraums 2020–2024 werden drei bedeutende Saharastaubereignisse dokumentiert, die ausschließlich im Zeitraum Januar–April mit Dauern von 2–4 Tagen auftreten. Die intensivste Episode (24.–25. Februar 2021) erzeugt regionalweite PM_{10}-Konzentrationen von 119–156 $\mu g/m^3$ und $PM_{2.5}$-Tagesmittelwerte von 28.7–32.5 $\mu g/m^3$, wodurch sowohl EU-Grenzwerte als auch WHO-Luftqualitätsrichtlinien überschritten werden. Größenverteilungsanalysen zeigen eine starke Dominanz der Grobfraktion während Staubereignissen ($PM_{2.5}/PM_{10}$-Verhältnis: 0.28–0.48) im Vergleich zu typischem urbanem Aerosol (0.58–0.67), wobei absolute $PM_{2.5}$-Konzentrationen während bedeutender Staubereignisse die WHO-Richtlinien (15 $\mu g/m^3$) deutlich überschreiten, was gesundheitsschützende Maßnahmen für vulnerable Bevölkerungsgruppen erforderlich macht.

Chemische Zusammensetzungsmessungen dokumentieren eine 2.9–3.1-fache Anreicherung von Krustenelementen während der Ereignisse, wobei diagnostische Ca/Al-Verhältnisse (3.7–3.9) und K/Al-Verhältnisse (0.3) die nordafrikanische Staubherkunft bestätigen und lokale Bodenaufwirbelung ausschließen. Die inverse K/Al-Signatur (Verhältnisabnahme während Ereignissen von 1.2–1.3 auf 0.3) liefert eindeutige Beweise für Saharastaubtransport, da Kalium trotz substanzieller Aluminium-Anreicherung nur minimale Erhöhungen zeigt. Fe/Al-Verhältnisse (1.0–1.2) entsprechen der eisenreichen nordafrikanischen Mineralogie und liefern zusätzliche Bestätigung.

Staubfraktionsanalysen zeigen, dass natürlicher Saharastaub während des intensivsten Ereignisses (Februar 2021) etwa 50% des beobachteten PM_{10} ausmacht, mit niedrigeren Fraktionen während moderater Episoden. Staubbedingte Überschreitungen des EU-Tagesmittelgrenzwerts (50 $\mu g/m^3$) betragen 2–4 Tage pro Station über den fünfjährigen

Zeitraum und stellen einen bedeutsamen Anteil aller PM_{10}-Überschreitungen dar. Unter den projizierten Standards für 2030 (45 µg/m^3 Tagesschwellenwert, reduziert von 50 µg/m^3) bleiben die Staubbeiträge signifikant für die PM_{10}-Tagesgrenzwert-Einhaltung, während alle Stationen derzeit den voraussichtlichen $PM_{2.5}$-Jahresgrenzwert (10 µg/m^3) einhalten, mit beobachteten Mittelwerten zwischen 7.0 und 8.8 µg/m^3.

Räumliche Analysen zeigen einen systematischen Südwest-Nordost-Gradienten der Staubauswirkungen über Baden-Württemberg, wobei südwestliche Stationen (Freiburg, Karlsruhe) direkte Exposition gegenüber Transportwegen aus dem Mittelmeerraum erhalten. Dieses räumliche Muster spiegelt vorherrschende meteorologische Transportwege wider, die aus dem Mittelmeerraum heranführen, sowie progressive Verdünnung und Ablagerung während ostwärtiger Advektion über das Bundesland. Ein bemerkenswerter Befund ergibt sich aus dem Stationsvergleich: Freiburg weist die niedrigsten mittleren PM-Konzentrationen auf (PM_{10}: 11.3 µg/m^3), verzeichnet jedoch mehr Tagesüberschreitungen (14.8 Tage/Jahr) als das ländliche Biberach (11.2 Tage/Jahr), was verdeutlicht, dass langfristige Mittelwertkonzentrationen und kurzfristige Spitzenkonzentrationen auf unterschiedliche Prozesse und geographische Faktoren reagieren.

Die Ergebnisse zeigen, dass Saharastaub, obwohl episodisch und nur einen moderaten Anteil des jährlichen PM-Mittelwerts darstellend, kurzfristige Luftqualitätsüberschreitungen in Baden-Württemberg signifikant beeinflusst. Die quantifizierten Staubbeiträge liefern Belege zur Unterstützung potenzieller Anwendungen der Artikel-21-Bestimmungen der EU-Luftqualitätsrichtlinie zur Subtraktion natürlicher Quellen bei Einhaltungsbewertungen. Das operationelle DWD ICON-ART Modellvorhersagesystem bietet Nutzen für Frühwarnungen staubbedingter PM-Episoden und ermöglicht proaktive Gesundheitskommunikation sowie angemessene Quellenzuordnung im Luftqualitätsmanagement.

Diese Arbeit etabliert einen robusten methodischen Rahmen, der Beobachtungen, Satellitenfernerkundung, Modell-Staubkonzentrationsdaten und chemische Zusammensetzungsanalysen für die Quantifizierung von Staubauswirkungen kombiniert und auf andere mitteleuropäische Regionen anwendbar ist, die von Ferntransport mineralischen Staubs betroffen sind.

Schlagwörter: Saharastaub, Feinstaub, Luftqualität, Baden-Württemberg, ICON-ART, Staubvorhersagen, PM_{10}, $PM_{2.5}$, natürliche Aerosole, Quellenaufteilung, Luftqualitätseinhaltung

Contents

List of Figures

List of Tables

1 Introduction and Motivation

1.1 Air Quality and Particulate Matter: A Global Challenge

Air quality has emerged as one of the foremost environmental and public health challenges of the 21st century. Among atmospheric pollutants, particulate matter (PM) — the complex mixture of solid and liquid particles suspended in air — represents a pollutant class of particular concern due to its well-documented adverse effects on human health, ecosystem functioning, and climate processes (Fuzzi et al., 2015; Pöschl, 2005; World Health Organization, 2021). Epidemiological evidence accumulated over the past four decades has established robust associations between exposure to elevated PM concentrations and increased morbidity and mortality from cardiovascular and respiratory diseases (Cohen et al., 2017; Lelieveld et al., 2015; World Health Organization, 2021). The Global Burden of Disease study attributes approximately 4.2 million premature deaths annually to ambient fine particulate matter ($PM_{2.5}$) exposure, positioning air pollution amongst the leading environmental risk factors for global disease burden (Burnett et al., 2018; GBD 2019 Risk Factors Collaborators, 2020).

Particulate matter is operationally classified according to aerodynamic diameter into distinct size fractions: PM_{10} (particles with aerodynamic diameter $\leq 10\,\mu m$) and $PM_{2.5}$ ($\leq 2.5\,\mu m$), also termed "coarse" and "fine" particles, respectively (Hinds, 1999; Seinfeld & Pandis, 2006). This size-based classification reflects not only differences in atmospheric behaviour — transport distances, deposition mechanisms, atmospheric residence times — but also critical variations in health impacts (Brunekreef & Holgate, 2002; Pope III & Dockery, 2006). Fine particles ($PM_{2.5}$) penetrate deeper into the respiratory system, reaching bronchioles and alveoli, whereas coarse particles ($PM_{10-2.5}$, the 2.5–10 μm fraction) are primarily deposited in the upper airways (Brown et al., 2013; Obergörster et al., 2005). Consequently, $PM_{2.5}$ is generally associated with more severe health outcomes, though both fractions contribute to air quality degradation and regulatory exceedances (Atkinson et al., 2014; Brunekreef & Holgate, 2002; Pope III & Dockery, 2006).

The sources of atmospheric particulate matter are diverse and can be broadly categorised into anthropogenic and natural origins (Hallquist et al., 2009; Seinfeld & Pandis, 2006). Anthropogenic PM arises from combustion processes (vehicular traffic, residential heating, industrial emissions, power generation), mechanical processes (construction, road dust resuspension, agricultural activities), and secondary aerosol formation from precursor gas emissions (sulphur dioxide, nitrogen oxides, volatile organic compounds) (Jiménez et al., 2009; Kulmala et al., 2004; Zhang et al., 2007). Natural sources include sea salt spray, volcanic emissions, biogenic aerosols (pollen, spores, plant fragments), wildfires, and mineral dust mobilised from arid and semi-arid surfaces (Boucher et al., 2013; Jickells et al., 2005; Knippertz & Stuut, 2014). Whilst air quality management efforts have traditionally

focused on controlling anthropogenic emissions — the component amenable to regulatory intervention — natural aerosol contributions can episodically dominate PM concentrations, particularly during extreme events such as desert dust outbreaks or wildfire episodes (Ginoux et al., 2012; Karanasiou et al., 2012; Pey et al., 2013).

1.2 European Air Quality Policy and Regulatory Framework

Recognising the severity of air pollution impacts, the European Union has progressively developed one of the world's most comprehensive air quality regulatory frameworks (European Environment Agency, 2020). The current cornerstone of European air quality legislation is the Ambient Air Quality Directive (2008/50/EC), which establishes legally binding limit values, target values, and alert thresholds for multiple pollutants including PM_{10} and $PM_{2.5}$ (European Parliament and Council, 2008). Table 1.1 summarises the current EU standards, proposed 2030 revisions, and WHO Air Quality Guidelines for PM_{10} and $PM_{2.5}$.

Table 1.1: Particulate matter air quality standards: Current EU Directive (2008/50/EC), proposed 2030 EU standards, and WHO Air Quality Guidelines (2021).

Pollutant	**Averaging Period**	**Current EU Standard**	**Proposed 2030 EU Standard**	**WHO 2021 Guideline**
PM_{10}	Daily (24-h mean)	50 µg/m^3 (max 35 exc./yr)	45 µg/m^3 (max 18 exc./yr)	45 µg/m^3 (99th percentile)
PM_{10}	Annual mean	40 µg/m^3	20 µg/m^3	15 µg/m^3
$PM_{2.5}$	Daily (24-h mean)	—	—	15 µg/m^3 (99th percentile)
$PM_{2.5}$	Annual mean	25 µg/m^3	10 µg/m^3	5 µg/m^3

Member States are obligated to demonstrate compliance through extensive monitoring network data, and exceedances trigger mandatory implementation of Air Quality Plans containing specific emission reduction measures (European Environment Agency, 2020; European Parliament and Council, 2008). Furthermore, the European Commission has proposed substantial tightening of these standards through the 2022 revision of the Air Quality Directive, seeking closer alignment with World Health Organisation (WHO) Air Quality Guidelines (Brunekreef et al., 2022; European Commission, 2022; World Health Organization, 2021). The proposed 2030 standards represent a significant strengthening: PM_{10} daily limit value reduced from 50 to 45 µg/m^3 (with maximum exceedances reduced from 35 to 18 days/year), PM_{10} annual limit value halved from 40 to 20 µg/m^3, and $PM_{2.5}$ annual limit value reduced from 25 to 10 µg/m^3 — doubling the stringency (European Commission, 2022).

Despite decades of emission reduction policies — vehicle emission standards (Euro norms), industrial emission controls (Best Available Techniques), combustion installation regulations — many European regions continue to experience periodic exceedances of PM limit values (European Environment Agency, 2020; Guerreiro et al., 2014). Germany,

whilst achieving substantial progress in reducing anthropogenic emissions (PM_{10} emissions decreased by approximately 25% between 2000–2020), still reports limit value exceedances at urban and traffic-influenced monitoring stations (Umweltbundesamt, 2022, 2023). This persistence of air quality violations despite stringent controls on anthropogenic sources has directed scientific and policy attention toward the role of natural aerosol contributions, which remain outside the scope of conventional emission reduction strategies (Escudero et al., 2007; Querol et al., 2009).

1.3 Natural Aerosols and Their Regulatory Implications

The European air quality regulatory framework recognises the complexity posed by natural aerosol contributions. Article 21 of the Ambient Air Quality Directive (2008/50/EC) provides a mechanism for Member States to subtract contributions from natural sources — specifically including desert dust, sea salt, and winter sanding — when assessing compliance with limit values, provided that natural source contributions can be adequately quantified, exceedances are demonstrably attributable to natural sources, and Member States have taken all necessary abatement measures for anthropogenic emissions (European Commission, 2011; European Parliament and Council, 2008).

This provision acknowledges the practical and ethical challenges of penalising Member States for air quality exceedances caused by phenomena beyond regulatory control (Pey et al., 2013; Querol et al., 2009). However, implementation of this article has proven methodologically challenging, requiring robust quantification of natural aerosol contributions through source apportionment, modelling capabilities, observational validation, and temporal attribution to identify specific exceedance events caused by natural sources (Beuck et al., 2011; Escudero et al., 2007; Viana et al., 2012).

Amongst natural aerosol types affecting Europe, mineral dust originating from North African deserts — primarily the Sahara — represents the single largest natural PM contributor by mass (Ginoux et al., 2012; Pey et al., 2013; Querol et al., 2009). Saharan dust transport to Europe is a well-documented meteorological phenomenon occurring with considerable frequency, particularly affecting southern and central European regions (Goudie, 2014; Knippertz & Stuut, 2014; Moulin et al., 1998).

1.4 Saharan Dust Transport to Europe: Mechanisms and Climatology

The Sahara Desert, spanning approximately 9 million km^2 across North Africa, constitutes the world's largest source of airborne mineral dust (Knippertz & Stuut, 2014; Prospero et al., 2002). Annual global dust emissions from the Sahara are estimated at 600–800 Tg/year, representing more than half of global natural dust emissions (Ginoux et al., 2001; Huneeus et al., 2011; Kok et al., 2021). Dust mobilisation occurs when surface wind speeds exceed threshold values (typically 7–10 m/s depending on soil properties), entraining fine particles through saltation and sandblasting processes (Knippertz & Stuut, 2014; Marticorena & Bergametti, 1995; Shao, 2008). Once aloft, dust particles are transported by prevailing

atmospheric circulation patterns, with trajectories determined by synoptic meteorological conditions (Knippertz & Stuut, 2014; Prospero et al., 2002; Tegen, 2002).

Several well-characterised atmospheric transport pathways facilitate Saharan dust advection to Europe (Barkan et al., 2005; Knippertz & Stuut, 2014; Moulin et al., 1998). The Mediterranean pathway involves low-level transport associated with Sirocco winds, affecting southern Europe (Spain, Italy, Greece) most frequently (Gobbi et al., 2000; Querol et al., 2009; Rodríguez et al., 2001). The Atlantic pathway features westward transport from the Sahara into the Atlantic, followed by northward advection affecting the Iberian Peninsula, France, and occasionally the British Isles (Ansmann et al., 2003; Prospero & Nees, 1981). The continental pathway involves eastward or northeastward transport affecting eastern Mediterranean and Balkans (Mitsakou et al., 2008; Papayannis et al., 2008). The high-altitude pathway occurs when dust is lifted to mid-tropospheric levels (3–6 km) during intense convective events, subsequently transported over considerable distances (> 2000 km) before descending and affecting surface air quality (Ansmann et al., 2003; Knippertz & Stuut, 2014; Mattis et al., 2008).

The frequency and intensity of dust transport to Europe exhibit pronounced seasonal and interannual variability (Barnaba & Gobbi, 2004; Moulin et al., 1998). Southern European regions experience dust impacts throughout the year, with spring (March–May) and summer (June–August) maxima corresponding to enhanced dust mobilisation in North Africa due to Harmattan winds, Mediterranean cyclogenesis, and shamal events (Knippertz & Stuut, 2014; Pey et al., 2013; Querol et al., 2009). Central European regions, including Germany, experience Saharan dust impacts primarily during spring months (March–April) when large-scale atmospheric circulation patterns favour southerly flow configurations (Ansmann et al., 2003; Lohmann & Feichter, 2005; Mattis et al., 2008).

Recent investigations have documented the surprisingly frequent occurrence of Saharan dust transport to Germany (Ansmann et al., 2021; Mattis et al., 2008). Analysis of long-term lidar observations at Leipzig revealed Saharan dust presence in the atmospheric column on approximately 25–30% of days, with surface-level impacts on 10–15% of days (Ansmann et al., 2021; Wandinger et al., 2002). The extended Dust Calendar developed by Hermes et al. (2024) catalogued multiple documented dust events affecting Germany during January–April 2024 alone, demonstrating that central European air quality is far from immune to Saharan dust influences despite the > 2000 km transport distance from source regions. This systematic catalogue provides crucial validation data for model-based dust transport assessments and highlights the operational importance of dust event forecasting for air quality management (Hermes et al., 2024).

1.5 Dust Impacts on Air Quality in Germany: State of Knowledge

Within Germany, Baden-Württemberg — the southwestern federal state bordering France and Switzerland — represents a region of particular susceptibility to Saharan dust transport (Lohmann & Feichter, 2005). Its geographic position in the Upper Rhine valley and proximity to major dust transport corridors make it a frequent recipient of dust-laden air

masses advected from the Mediterranean and North Africa (Corsmeier et al., 2005; Vogel et al., 2001). Several studies have identified substantial dust contributions to PM concentrations in southwestern Germany, though published estimates vary considerably reflecting methodological differences and temporal coverage limitations (Huber & Kerschbaumer, 2020; Schwarz et al., 2012).

Despite growing evidence, several critical knowledge gaps persist (Beuck et al., 2011; Birmili et al., 2009): substantial variability exists amongst published dust contribution estimates; the 2020–2024 period includes novel meteorological conditions requiring contemporary quantification; insufficient operational methodology exists for real-time dust contribution quantification to support Article 21 implementation (Viana et al., 2012); incomplete understanding remains regarding whether dust disproportionately affects PM_{10} versus $PM_{2.5}$ fractions (Pey et al., 2013).

1.6 Research Objectives and Questions

This Master's thesis seeks to address the outlined knowledge gaps through comprehensive analysis of Saharan dust contributions to air quality in Baden-Württemberg during the 2020–2024 period. Specifically, the investigation pursues the following research objectives.

The primary objective is to quantify the contribution of natural Saharan dust to PM_{10} and $PM_{2.5}$ concentrations at representative monitoring locations in Baden-Württemberg through integrated analysis of observational data and DWD ICON-ART model meteogram dust concentration data.

Secondary objectives include: (1) characterising observational PM patterns by analysing temporal variability, seasonal cycles, and spatial coherence of PM_{10} and $PM_{2.5}$ observations across the LUBW monitoring network (2020–2024); (2) quantifying dust fractional contributions by determining the proportion of observed total PM attributable to Saharan dust during transport events, distinguishing PM_{10} versus $PM_{2.5}$ impacts; (3) identifying major dust events by compiling a comprehensive catalogue of significant Saharan dust transport episodes affecting Baden-Württemberg during 2020–2024, documenting event characteristics (duration, intensity, spatial extent); and (4) assessing regulatory implications by evaluating the magnitude of natural dust contributions relative to EU air quality limit values, informing potential Article 21 applications.

These objectives translate into the following specific research questions:

RQ1: What are the characteristic temporal patterns (seasonal, monthly, event-scale) of PM_{10} and $PM_{2.5}$ concentrations across Baden-Württemberg's monitoring network?

RQ2: How frequently do Saharan dust transport events impact Baden-Württemberg, and what are their typical durations and PM concentration enhancements?

RQ3: What fraction of total observed PM (PM_{10} and $PM_{2.5}$) can be attributed to natural Saharan dust during documented transport events?

RQ4: To what extent do Saharan dust contributions affect compliance with EU air quality daily and annual limit values in Baden-Württemberg?

1.7 Methodological Approach Overview

This investigation employs a multi-faceted analytical strategy integrating three complementary data sources. Ground-based observations provide high-quality PM_{10} and $PM_{2.5}$ measurements from five LUBW air quality monitoring stations representing diverse environmental settings (urban background, rural background) across Baden-Württemberg. DWD ICON-ART model meteogram data provide size-resolved dust concentration information at station-specific locations. Satellite imagery and auxiliary data from NASA Worldview true-colour imagery and MODIS Aerosol Optical Depth (AOD) products enable independent dust event verification (Levy et al., 2013).

The analytical methodology combines dust fraction quantification and event-based case study analysis. A critical component of the approach involves conversion of ICON-ART size-resolved dust mixing ratios (three prognostic size bins) to $PM_{2.5}$ and PM_{10} mass concentrations through integration of lognormal particle size distributions — a methodological step requiring careful treatment of size-dependent fractional contributions (detailed in Chapter 2).

Dust fraction quantification proceeds via a dual approach employing both a model-based method (ratio of model-predicted dust concentration to observed total PM) and a baseline subtraction method (empirical determination of dust contribution by subtracting station-specific no-dust baseline concentrations). This dual methodology provides internal consistency checks and quantifies uncertainty inherent in single-method analyses (Escudero et al., 2007; Viana et al., 2012).

1.8 Thesis Structure and Organisation

The remainder of this thesis is organised as follows. Chapter 2 (Data and Methodology) presents comprehensive description of all data sources (LUBW observational network, DWD ICON-ART model meteogram product, satellite datasets), theoretical framework for PM calculation from dust size distributions, and detailed exposition of analytical methods including event identification procedures and dust fraction quantification approaches.

Chapter 3 (Results) documents empirical findings organised into thematic subsections: observational analysis of PM temporal patterns and air quality limit value exceedances; dust fraction analysis quantifying natural aerosol contributions; PM compositional analysis during dust versus non-dust conditions; and summary of major dust events during 2020–2024.

Chapter 4 (Discussion) interprets the quantitative findings in broader scientific and policy contexts, addressing dust contribution magnitudes relative to published literature, chemical composition evidence for Saharan origin, size distribution and health implications, spatial variability patterns, regulatory implications for EU Air Quality Directive compliance, and methodological strengths and limitations.

Chapter 5 (Conclusions) synthesises key findings, evaluates research question responses, discusses implications for air quality management in Baden-Württemberg and broader central European contexts, and identifies directions for future investigation.

1.9 Scientific and Societal Relevance

This investigation addresses a topic of substantial scientific and societal importance. From a scientific perspective, the work contributes to process understanding through improved quantification of natural aerosol contributions to central European air quality and methodological advancement through demonstration of integrated observational-modelling approaches for dust quantification (Beuck et al., 2011; Viana et al., 2012).

From a policy and societal perspective, the findings bear direct relevance to air quality management by providing an evidence base supporting potential Article 21 applications for natural source subtraction (European Commission, 2011); public communication through enhanced understanding of natural versus anthropogenic PM contributions, informing public awareness campaigns (European Environment Agency, 2020); future planning by establishing baseline quantification of dust impacts relevant to assessment of future air quality standard revisions (WHO guideline alignment) (European Commission, 2022; World Health Organization, 2021).

With the European Commission proposing substantially tightened PM standards (reducing annual $PM_{2.5}$ limit to $10\,\mu g/m^3$ by 2030, pending final adoption), quantifying the natural PM baseline assumes heightened importance (Brunekreef et al., 2022; European Commission, 2022). If natural sources contribute episodically to PM concentrations in Baden-Württemberg, compliance with future standards may prove challenging regardless of further anthropogenic emission reductions — underscoring the necessity for robust natural source quantification methodologies (Pey et al., 2013; Querol et al., 2009).

This thesis represents a timely contribution to an evolving scientific and policy dialogue at the intersection of atmospheric science, air quality management, and environmental regulation. By integrating DWD ICON-ART model data with high-quality observational datasets spanning a climatologically significant five-year period, the investigation aims to provide actionable insights supporting evidence-based air quality policy development in Baden-Württemberg.

2 Data and Methods

This chapter provides a comprehensive description of the data sources, theoretical framework, and analytical methods employed in this investigation. The analysis relies primarily on two independent data streams: ground-based air quality observations from LUBW monitoring stations and dust concentration data from the DWD (Deutscher Wetterdienst) ICON-ART model meteogram product. Following data source characterisation, the theoretical basis for particulate matter calculations from model output is presented, including detailed treatment of dust particle size distributions and their integration to derive $PM_{2.5}$ and PM_{10} mass concentrations. Finally, methods for event identification and dust fraction quantification are documented.

2.1 Observational Data: LUBW Air Quality Monitoring Network

2.1.1 Data Source and Instrumentation

The observational component of this study utilises air quality measurements from the LUBW (Landesanstalt für Umwelt Baden-Württemberg) ambient air quality monitoring network. LUBW operates a comprehensive network of automated monitoring stations across Baden-Württemberg, providing continuous measurements of regulated air pollutants including particulate matter, gaseous species, and supporting meteorological parameters.

For this investigation, hourly PM_{10} and $PM_{2.5}$ concentration data were obtained from five selected monitoring stations representing diverse geographic and environmental settings across Baden-Württemberg. Table 2.1 summarises the station locations, coordinates, elevations, and classifications, whilst Figure 2.1 shows their spatial distribution across Baden-Württemberg.

Stuttgart-Bad Cannstatt represents an urban background station located in the Stuttgart metropolitan area within the Neckar valley. The site is characterised by high population density, heavy traffic influence, and industrial activity, making it representative of major urban air quality conditions in southern Germany. Karlsruhe-Nordwest serves as an urban background station in northwestern Karlsruhe within the Upper Rhine valley. As a major urban centre, this location provides favourable positioning for dust transport detection with enhanced sensitivity to southwestern advection patterns. Freiburg operates as an urban background station in southwestern Baden-Württemberg near the Black Forest. Its Upper Rhine graben location experiences frequent exposure to long-range transport, positioned at the western boundary of the study region where it serves as a first-impact location for Atlantic and Mediterranean flows. Heilbronn represents an urban background station in the Neckar valley of northern Baden-Württemberg. This site occupies an intermediate position between major urban centres and rural areas, with sheltered valley topography

Table 2.1: LUBW air quality monitoring stations used in this study, including geographic coordinates, elevation, station classification, and key environmental characteristics.

Station Name	Station Type	Latitude (°N)	Longitude (°E)	Elevation (m asl)	Environmental Characteristics
Stuttgart-Bad Cannstatt	Urban background	48.8085	9.2250	207	Major metropolitan area; Neckar valley location; high traffic and industrial influence
Karlsruhe-Nordwest	Urban background	49.0000	8.3000	110	Upper Rhine valley; major urban centre; southwestern exposure to dust transport
Freiburg	Urban background	47.9990	7.8421	236	Southwestern Baden-Württemberg; Upper Rhine graben; first-impact location for Mediterranean flows
Heilbronn	Urban background	49.1000	9.2000	157	Northern Neckar valley; intermediate urban-rural; sheltered valley topography
Biberach	Rural background	48.1000	9.7000	533	Eastern Upper Swabia; rural location; lowest anthropogenic PM influence; regional background representative

influencing pollutant dispersion. Biberach functions as a rural background station in Upper Swabia, eastern Baden-Württemberg. It exhibits the lowest anthropogenic PM influence amongst selected stations and provides representation of regional background concentrations.

PM_{10} and $PM_{2.5}$ concentrations are measured using beta-attenuation or TEOM (Tapered Element Oscillating Microbalance) instrumentation, both of which comply with European reference method requirements (EN 12341 for PM_{10}, EN 14907 for $PM_{2.5}$). These methods provide hourly averaged concentrations with detection limits typically ranging from 1–2 $\mu g/m^3$ and measurement uncertainty of ± 10–15% at ambient concentration levels. Concentrations are reported in units of $\mu g/m^3$ (micrograms per cubic metre) at standard temperature and pressure (20°C, 101.3 kPa).

The dataset spans the period January 1, 2020 through December 31, 2024 (5 complete years). Data availability exceeds 85% for all stations, with gaps primarily attributable to scheduled instrument maintenance and calibration periods. Quality assurance procedures implemented by LUBW include automated plausibility checks (range tests, rate-of-change limits), regular instrument zero and span calibrations, bi-weekly filter changes and flow rate verifications, and annual instrument audits and inter-comparisons. Invalid or suspect data flagged during quality control were excluded from analysis following standard LUBW protocols.

Figure 2.1: Spatial distribution of the five LUBW air quality monitoring stations across Baden-Württemberg used in this investigation. Stations are marked by red coloured stars and include, Freiburg, Karlsruhe, Stuttgart-Bad Cannstatt, Heilbronn and Biberach.

2.1.2 Data Processing

Raw hourly PM measurements were subjected to several processing steps to ensure data quality and consistency. Quality filtering removed negative values (instrument artefacts) and values flagged by LUBW quality control procedures. Temporal aggregation calculated daily mean concentrations from hourly values, requiring a minimum of 18 valid hours for daily mean computation. Station name harmonisation mapped between LUBW station nomenclature and meteogram grid point identifiers. Time zone standardisation converted all timestamps to UTC for consistency with meteogram output timestamps.

2.2 Dust Concentration Data from DWD

2.2.1 The ICON Modelling System

The DWD, Germany's national meteorological service, operationally produces dust concentration information for air quality applications using the ICON (ICOsahedral Non-hydrostatic) modelling system. These products are disseminated as meteogram outputs providing location-specific temporal profiles of atmospheric variables, including mineral dust concentrations, meteorological parameters, and related quantities.

The ICON model has been developed and widely used for weather and climate prediction across scales. It solves the 3D non-hydrostatic and compressible Navier-Stokes equations on an icosahedral-triangular grid (Gassmann & Herzog, 2008), facilitating precise predictions across scales (Giorgetta et al., 2018; Heinze et al., 2017; Zängl et al., 2015). The ART module, integrated into the ICON framework, enables comprehensive modelling of atmospheric composition. It handles emissions, transport, and transformations of trace gases and aerosols, incorporating gas-phase chemistry and aerosol dynamics in the troposphere and stratosphere (Hoshyaripour et al., 2025; Rieger et al., 2015; Schröter et al., 2018; Weimer et al., 2017). ICON-ART has been successfully used to investigate mutual feedbacks between the chemical and physical states of the atmosphere across different scales ranging from large-eddy simulations (Muth et al., 2025) to regional weather (Rieger et al., 2017; Seifert et al., 2023) and global climate (Weimer et al., 2021).

For this investigation, dust concentration data were obtained from DWD's operational meteogram archive rather than conducting independent model simulations. This approach ensures consistency with operational air quality products and leverages DWD's established quality control procedures.

2.2.2 Operational Configuration and Dust Parametrisation

The operational DWD-KIT ICON-ART dust forecasting system employs an icosahedral-triangular grid with regionally refined resolution. The global domain operates at approximately 40 km horizontal grid spacing with 90 vertical levels extending from the surface to 75 km altitude (Hoshyaripour et al., 2019). A two-way nested configuration provides enhanced resolution over Europe and the North Atlantic (EU-NA nest) at approximately 20 km horizontal grid spacing, covering the region of primary dust transport pathways affecting central Europe (Hoshyaripour et al., 2019). This nesting strategy balances computational efficiency with adequate spatial resolution to capture synoptic-scale dust transport features whilst resolving regional-scale concentration gradients across Baden-Württemberg. The system produces forecasts extending 5 days ahead, updated on a regular operational schedule.

The dust parametrisation scheme, based on Tegen (2002) and refined by Rieger et al. (2015), includes size-resolved dust emission dependent on soil type, vegetation coverage, surface wind speed, and soil moisture; resolved-scale advection by predicted winds and subgrid-scale turbulent mixing; gravitational settling (dry deposition) and below-cloud/in-cloud scavenging (wet deposition); and dust-radiation feedbacks through modification of shortwave and longwave radiation. The model accounts for particle nonsphericity effects on dust optical properties, which significantly affect radiative transfer calculations and satellite retrieval comparisons (Hoshyaripour et al., 2019). Aerosol-radiation interactions are represented following the methodology of Hoshyaripour et al. (2019), wherein radiative transfer parameters are calculated online depending on optical properties and size distributions of the prognostic dust modes.

2.2.3 Dust Size Distribution and PM Calculation

The ICON-ART dust scheme represents the particle size distribution using three prognostic size bins (modes), each characterised by distinct microphysical and transport properties (Rieger et al., 2015). Mode a (dusta) represents the accumulation mode with diameter range 0.1–1.0 µm, median diameter $D_{\mathrm{med},a}$ = 0.37 µm, and geometric standard deviation $\sigma_{g,a}$ = 1.59. This mode exhibits long atmospheric lifetime (days to weeks), efficient long-range transport, and is primarily removed by wet deposition. Mode b (dustb) represents the coarse mode with diameter range 1.0–2.5 µm, median diameter $D_{\mathrm{med},b}$ = 1.9 µm, and geometric standard deviation $\sigma_{g,b}$ = 2.00. This mode demonstrates intermediate lifetime (days), significant contribution to both $PM_{2.5}$ and PM_{10}, and mixed removal by dry and wet deposition. Mode c (dustc) represents the giant mode with diameter range 2.5–10 µm, median diameter $D_{\mathrm{med},c}$ = 6.0 µm, and geometric standard deviation $\sigma_{g,c}$ = 2.15. This mode is characterised by short lifetime (hours to days), rapid gravitational settling, local to regional-scale transport, and primarily PM_{10} contribution.

Each mode follows a lognormal size distribution, where the model system carries the mass mixing ratio (kg/kg) as the prognostic variable. Conversion from model prognostic variables (dust mass mixing ratios for modes a, b, c) to $PM_{2.5}$ and PM_{10} mass concentrations requires determining what fraction of each lognormal mode falls within $PM_{2.5}$ (D < 2.5 µm) and PM_{10} (D < 10 µm) size ranges, followed by multiplication by air density to convert mixing ratio to concentration.

The mass fraction of each mode contributing to $PM_{2.5}$ and PM_{10} is computed by integrating the lognormal distribution over the relevant diameter range. For $PM_{2.5}$ contribution fractions:

$$f_{\mathrm{PM}_{2.5},i} = \int_0^{2.5\ \mu\mathrm{m}} \frac{1}{\sqrt{2\pi}\ln(\sigma_{g,i})} \exp\left[-\frac{(\ln D - \ln D_{\mathrm{med},i})^2}{2\ln^2(\sigma_{g,i})}\right] d(\ln D) \tag{2.1}$$

where i = a, b, c denotes the dust mode. For the ICON-ART dust mode parameters specified above, numerical integration yields $f_{\mathrm{PM}_{2.5},a}$ = 0.832 (83.2% of mode a mass falls within $PM_{2.5}$ range), $f_{\mathrm{PM}_{2.5},b}$ = 0.0179 (1.79% of mode b mass falls within $PM_{2.5}$ range), and $f_{\mathrm{PM}_{2.5},c}$ = 9.184× 10^{-6} (negligible contribution from mode c to $PM_{2.5}$).

For PM_{10} contribution fractions:

$$f_{\mathrm{PM}_{10},i} = \int_0^{10\ \mu\mathrm{m}} \frac{1}{\sqrt{2\pi}\ln(\sigma_{g,i})} \exp\left[-\frac{(\ln D - \ln D_{\mathrm{med},i})^2}{2\ln^2(\sigma_{g,i})}\right] d(\ln D) \tag{2.2}$$

Numerical integration yields $f_{\mathrm{PM}_{10},a}$ = 0.999 (essentially all mode a mass in PM_{10}), $f_{\mathrm{PM}_{10},b}$ = 0.802 (80.2% of mode b mass in PM_{10}), and $f_{\mathrm{PM}_{10},c}$ = 0.193 (19.3% of mode c mass in PM_{10}).

The total $PM_{2.5}$ and PM_{10} dust mass concentrations (µg/m^3) are computed from model output as:

$$\mathrm{PM}_{2.5,\mathrm{dust}} = \rho \times (f_{\mathrm{PM}_{2.5},a} \times q_{\mathrm{dusta}} + f_{\mathrm{PM}_{2.5},b} \times q_{\mathrm{dustb}} + f_{\mathrm{PM}_{2.5},c} \times q_{\mathrm{dustc}}) \times 10^9 \tag{2.3}$$

$$\mathrm{PM}_{10,\mathrm{dust}} = \rho \times (f_{\mathrm{PM}_{10},a} \times q_{\mathrm{dusta}} + f_{\mathrm{PM}_{10},b} \times q_{\mathrm{dustb}} + f_{\mathrm{PM}_{10},c} \times q_{\mathrm{dustc}}) \times 10^9 \tag{2.4}$$

where ρ represents air density (kg/m^3) from model output, q_{dusta}, q_{dustb}, q_{dustc} are dust mass mixing ratios (kg/kg) for each mode, and the 10^9 factor converts kg/m^3 to µg/m^3. These formulations enable comparison between model-predicted dust concentrations and observed total PM concentrations, with the understanding that observations include both natural dust and non-dust PM components whilst model output represents mineral dust exclusively.

2.2.4 Meteogram Data Acquisition and Processing

Meteograms are station-specific vertical profiles and time series extracted from full model fields at pre-defined geographic locations corresponding to observation sites or points of interest. The DWD dust meteogram product provides hourly information on three-dimensional atmospheric variables at multiple vertical levels (dust mass mixing ratios for modes a, b, c; air density; temperature; horizontal wind components; relative humidity; and vertical velocity) and two-dimensional surface variables (2-metre temperature, 10-metre wind components, surface solar radiation, precipitation, latent heat flux, and surface pressure).

Meteogram files are stored in netCDF format following CF (Climate and Forecast) conventions, with separate files for each initialisation time. Data extraction workflow involved identification of meteogram grid points nearest to each LUBW station (within approximately 20 km horizontal distance, consistent with the EU-NA nest resolution), extraction of surface-level dust mixing ratios and air density, calculation of hourly $PM_{2.5}$ and PM_{10} using the formulations presented above, and temporal aggregation to daily means for consistency with processed observational data. Meteogram data are available for the complete study period (2020–2024) with higher temporal density during the focus season (January–April) when dust event frequency is maximum. Data availability approaches 100% except during occasional brief interruptions for model system upgrades.

2.3 Satellite Imagery Data

2.3.1 NASA Worldview True-Colour Composites

NASA Worldview satellite imagery was used to visually confirm Saharan dust transport events and provide synoptic-scale context for ground-based observations. True-colour composites from the Moderate Resolution Imaging Spectroradiometer (MODIS) instruments aboard NASA's Terra and Aqua satellites were obtained via the NASA Earth Observing System Data and Information System (EOSDIS) Worldview application (NASA EOSDIS, 2024). MODIS provides daily global coverage at spatial resolutions of 250–500 m for visible bands, enabling identification of Saharan dust plumes by their characteristic tan/brown colouration in true-colour imagery.

Satellite imagery was visually inspected for all dates during January–April 2020–2024 to identify potential dust transport episodes affecting southern and central Europe. Images were downloaded for dates showing visible dust plumes extending from North Africa across the Mediterranean Sea towards Baden-Württemberg. The Terra and Aqua overpass

times (approximately 10:30 and 13:30 local time, respectively) provide near-simultaneous snapshots of atmospheric dust distributions, though cloud coverage occasionally obscures dust signatures. Satellite imagery serves as independent qualitative confirmation of dust transport, complementing quantitative model and observational data.

2.4 Methodological Approaches

2.4.1 Dust Fraction Quantification

A central objective of this investigation is quantifying the fractional contribution of natural dust to total observed PM during transport events. The dust fraction (DF) methodology provides a straightforward yet physically meaningful metric:

$$\mathrm{DF} = \frac{\mathrm{PM}_{\mathrm{dust,meteogram}}}{\mathrm{PM}_{\mathrm{total,observed}}} \tag{2.5}$$

where $\mathrm{PM}_{\mathrm{dust\,meteogram}}$ represents the meteogram dust concentration value (ICON-ART model output representing exclusively mineral dust) and $\mathrm{PM}_{\mathrm{total\,observed}}$ represents the ground-based measurement encompassing all PM sources (natural dust, traffic, industry, heating, secondary aerosols).

This approach relies on several key assumptions:

1. Meteogram values accurately capture the relative magnitude of dust contributions, even if absolute concentrations exhibit differences from observations due to model limitations or spatial representation uncertainties;

2. PM from various sources combine additively without significant non-linear interactions (e.g., no substantial enhancement or suppression of secondary aerosol formation during dust events);

3. The dust fraction estimated from days with elevated meteogram values ($\geq 2\,\mu g/m^3$) provides representative characterisation of dust contribution patterns during the January–April dust transport season.

This ratio is computed separately for PM_{10} and $PM_{2.5}$ on a daily mean basis. Dust fraction values approaching 1.0 indicate dust-dominated conditions, whilst values much less than 1.0 reflect high non-dust backgrounds. Interpretation requires consideration of model uncertainties and event-to-event variability in non-dust emissions.

2.4.2 Event Identification and Classification

Dust transport events are identified using a multi-criteria approach combining satellite imagery (visual inspection of NASA Worldview true-colour imagery for visible dust plumes over southern Europe and North Africa), MODIS AOD (Aerosol Optical Depth retrievals showing elevated columnar aerosol loading), meteogram indicators (ICON-ART meteogram showing elevated dust concentrations at surface), and PM observations (coordinated PM_{10} increases across multiple stations). An event is classified as a “major

dust event" when satellite imagery confirms dust plume presence, at least three of five LUBW stations exceed 50 µg/m^3 daily PM_{10} (EU daily limit value), meteogram indicates dust concentrations exceeding 20 µg/m^3, and spatial coherence of elevated PM exists across the station network.

2.4.3 Temporal Aggregation Procedures

To ensure robust statistical comparison and minimise influence of sub-daily variability, temporal aggregation was applied as follows. For observational data, hourly measurements were converted to daily means computed from 24 hourly values with a minimum of 18 valid hours required, ensuring data completeness exceeding 75% for each daily mean. For meteogram data, hourly values were aggregated to daily means (24-hour average), with alignment using 00:00 UTC initialisation where hours 1–24 comprise day 1. Daily aggregation reduces noise from diurnal variability, instrument precision limitations, and subgrid-scale heterogeneity not resolved by the approximately 20 km EU-NA nest grid. Dust transport events typically persist for 2–4 days, making daily resolution appropriate for event characterisation.

2.4.4 Baseline Subtraction Approach

To isolate the dust contribution independent of model-observation differences, a baseline subtraction method was developed. First, baseline determination identified extended periods (at least 7 consecutive days) with PM_{10} below 35 µg/m^3 (well below EU limit value), stable meteorological conditions, and no satellite-confirmed dust plumes. Station-specific no-dust baselines were calculated as the mean PM_{10} during these clean days. Second, event-day dust contribution was computed as the difference between observed PM_{10} during events and the station baseline. This empirical approach provides an observation-based dust quantification complementary to the meteogram-derived dust fraction method.

2.5 PM Composition Analysis Methods

2.5.1 Composition Data Source

To provide independent geochemical confirmation of Saharan dust transport and quantify crustal element contributions during dust events, daily PM_{10} composition measurements from two LUBW stations were analysed: Stuttgart-Bad Cannstatt and Freiburg, both providing daily filter-based PM_{10} composition data (24-hour integrated samples). These measurements are part of LUBW's intensive composition monitoring programme conducted at select stations. Sample collection follows European reference method EN 12341, with filters analysed using energy-dispersive X-ray fluorescence (ED-XRF) or inductively coupled plasma mass spectrometry (ICP-MS) to quantify elemental concentrations.

The composition dataset includes concentrations (µg/m^3) of major crustal tracers (Al, Fe, Ca, Si), minor crustal elements (Mg, K, Na, Mn, Ba, Ti), secondary inorganic ions (sulphate, nitrate, ammonium; water-soluble cations Ca^{2+}, Mg^{2+}, Na^+, K^+; and chloride), and carbonaceous species (elemental carbon EC, organic carbon OC).

2.5.2 Crustal Element Fraction Calculation

To quantify the mineral dust component of PM_{10}, crustal elements were aggregated following established methodologies (Pey et al., 2013; Putaud et al., 2010):

$$\text{Crustal Fraction} = \sum_i c_i \tag{2.6}$$

where c_i represents the concentration of crustal element i (Al, Fe, Ca, Mg, Na, K, Mn, Ba, Ti, Si). For stations lacking direct Si measurements, crustal fractions were estimated using aluminium as a proxy, applying empirical crustal multipliers:

$$\text{Crustal Material} = k_{\text{crust}} \times [\text{Al}] \tag{2.7}$$

where k_{crust} = 8–10 based on average crustal composition (Wedepohl, 1995). This approach provides conservative estimates of total mineral dust mass.

To quantify dust-related crustal enrichment, baseline crustal concentration was calculated as the mean of daily crustal fractions during non-dust periods (periods excluding ± 5 days around identified dust events). Event-period crustal concentration was calculated as the mean during dust event days (February 24–25, 2021). Enhancement factor was computed as:

$$\text{Enhancement Factor} = \frac{\text{Crustal}_{\text{event}}}{\text{Crustal}_{\text{baseline}}} \tag{2.8}$$

Enhancement factors exceeding 2.0 indicate substantial dust impact, whilst factors below 1.5 suggest minimal dust influence.

2.5.3 Element Ratio Source Attribution

Beyond absolute crustal concentrations, diagnostic element ratios provide robust source discrimination between Saharan dust and local soil resuspension. Three key ratios were computed. The Ca/Al ratio:

$$\text{Ca/Al} = \frac{[\text{Ca}]}{[\text{Al}]} \tag{2.9}$$

exhibits Saharan dust signatures of 3.0–4.5 (calcite-rich North African soils) compared to local soil signatures of 0.5–1.5 (silicate-dominated central European soils), with ratios exceeding 2.5 indicating Saharan origin. The K/Al ratio:

$$\text{K/Al} = \frac{[\text{K}]}{[\text{Al}]} \tag{2.10}$$

shows Saharan dust signatures of 0.2–0.4 (K-depleted relative to Al), local soil signatures of 0.8–1.2 (feldspar contribution), and anthropogenic background values exceeding 1.0 (biomass burning K addition). Importantly, ratio decrease during events is diagnostic of Saharan dust. The Fe/Al ratio:

$$\text{Fe/Al} = \frac{[\text{Fe}]}{[\text{Al}]} \tag{2.11}$$

demonstrates Saharan dust signatures of 0.8–1.3 (iron-rich North African mineralogy) versus local soil signatures of 0.5–0.8, with ratios exceeding 1.0 suggesting iron-enriched North African sources.

2.5.4 $PM_{2.5}/PM_{10}$ Ratio Analysis

To characterise particle size distributions during dust events versus background periods, the $PM_{2.5}/PM_{10}$ concentration ratio was calculated:

$$PM_{2.5}/PM_{10} = \frac{[PM_{2.5}]_{\text{daily}}}{[PM_{10}]_{\text{daily}}} \tag{2.12}$$

This ratio provides insight into aerosol size distribution. High ratios (0.6–0.8) indicate fine-mode dominance, typical of anthropogenic combustion sources. Low ratios (0.3–0.5) indicate coarse-mode dominance, characteristic of mineral dust. Very low ratios (below 0.3) indicate strong coarse dominance, indicative of intense dust events or mechanical particle generation.

The $PM_{2.5}/PM_{10}$ ratio was computed for event periods (dust event days), background periods (non-dust days with ± 10 days around events excluded), and temporal evolution (5 days before, during, and 5 days after events). Lower $PM_{2.5}/PM_{10}$ ratios during dust events imply reduced alveolar deposition fraction compared to fine-mode pollution and lower health risk per unit PM_{10} mass since coarse particles deposit in upper airways. However, absolute $PM_{2.5}$ concentrations during major events may still exceed health guidelines. The $PM_{2.5}/PM_{10}$ ratio thus provides critical context for health risk assessment, distinguishing coarse-dominated natural aerosol episodes from fine-mode anthropogenic pollution events.

2.5.5 Statistical Analysis of Composition Data

Given the limited temporal resolution of composition data (daily samples at 2 stations), statistical analyses focused on mean comparison using Student's t-test comparing background versus event-period crustal concentrations and element ratios, temporal evolution through visual inspection of time series showing composition changes before, during, and after events, and literature comparison of observed element ratios with published Saharan dust and local soil signatures. Due to sample size limitations (n = 2–5 days per event), formal multivariate source apportionment (PMF, CMB) was not attempted. Instead, element ratios provide qualitative-to-semi-quantitative source attribution.

2.6 Data Visualisation and Analysis Tools

Data visualisation and figure generation were performed using the Python 3. Assistance with figure generation, code optimisation, and manuscript editing was provided by Claude Code, an AI-assisted software development tool developed by Anthropic. All generated

figures were manually reviewed and validated to ensure scientific accuracy and appropriate data representation.

3 Results

This chapter presents a comprehensive analysis of natural aerosol impacts on air quality across Baden-Württemberg during the period 2020-2024, with particular emphasis on Saharan dust transport events and their influence on PM concentrations. The investigation encompasses measurements from five strategically selected LUBW (Landesanstalt für Umwelt Baden-Württemberg) monitoring stations distributed across the region: Stuttgart-Bad Cannstatt, Karlsruhe-Nordwest, Freiburg, Heilbronn, and Biberach. These stations represent diverse environmental settings, ranging from urban centres to more rural locations, thus providing a comprehensive spatial perspective on dust impacts.

Section 3.1 identifies and characterises all documented Saharan dust transport events during the study period, including detailed synoptic analysis of meteorological conditions at 850 hPa facilitating dust transport from North African source regions. Section 3.2 characterises the temporal and spatial patterns of PM_{10} and $PM_{2.5}$ concentrations through observational data analysis. Section 3.3 presents meteogram dust concentration data as supporting evidence for dust event identification. Section 3.4 quantifies the natural aerosol contribution to total observed particulate matter. Finally, Section 3.5 elucidates the physical and chemical characteristics of dust events through composition data and size distribution analysis.

3.1 Saharan Dust Event Calendar and Detailed Characterisation (2020-2024)

Identifying genuine Saharan dust transport events presents a fundamental methodological challenge: ground-based PM_{10} measurements alone cannot distinguish natural mineral dust from non-dust-related PM sources (traffic, industry, domestic heating, wildfires), as both contribute to measured concentrations. To overcome this limitation, independent visual confirmation through satellite imagery provides a clear identification of dust plumes during their advection across Europe. Systematic screening of NASA Worldview true-colour satellite imagery for the January–April period (2020–2024), combined with coordinated PM_{10} concentration increases at multiple ground-based monitoring stations, identifies three major Saharan dust transport events with clearly visible dust plumes affecting Baden-Württemberg. Table 3.1 presents the complete calendar of documented dust events during the five-year study period.

These three satellite-confirmed episodes concentrate exclusively in the January-April period, with zero major visible dust plumes identified during May-December. The temporal clustering reflects large-scale atmospheric circulation patterns favouring southerly flow configurations and North African dust mobilisation during winter-spring months. The

Table 3.1: Calendar of documented Saharan dust transport events affecting Baden-Württemberg during 2020-2024. Events identified through NASA Worldview satellite imagery, coordinated PM_{10} concentration increases across multiple stations, and MODIS aerosol optical depth (AOD) retrievals.

Event Date	Duration	Peak PM_{10} Range	Spatial Pattern
February 24, 2021 February 25, 2021	2 days	119-156 µg/m^3	Regional (all 5 stations)
March 30, 2024 March 31, 2024	2-3 days	66-193 µg/m^3	East-West gradient
April 7, 2024 April 8, 2024 April 9, 2024	3 days	49-132 µg/m^3	Relatively uniform

inter-annual distribution shows substantial variability: 2020, 2022, and 2023 exhibit no major events, while 2021 and 2024 account for all three documented episodes. Each event satisfies multiple identification criteria: (1) visible dust plume in satellite imagery extending across the study region, (2) peak PM_{10} concentrations exceeding regulatory thresholds at multiple stations simultaneously, (3) coordinated timing of concentration increases across spatially distributed monitoring sites, and (4) availability of meteogram dust concentration forecasts.

The concentration of events in 2021 and 2024, with no major visible plumes in 2020, 2022, or 2023, reflects substantial inter-annual variability in large-scale atmospheric circulation patterns controlling dust transport pathways from North Africa. The three episodes encompass varying intensities (moderate to extreme), spatial patterns (uniform to gradient-dominated), and temporal structures (rapid 2-day events to extended 3-day episodes), enabling comprehensive characterisation of dust impacts across different transport scenarios.

3.1.1 February 24-25, 2021 Event

The late February 2021 event represents the most significant dust intrusion documented during the five-year study period. Satellite imagery from NASA Worldview reveals an extensive dust plume originating from the central Sahara, transported northward across the Mediterranean and western Europe (Figure 3.1a). Synoptic analysis at the 850 hPa pressure level reveals conditions highly conducive to meridional dust transport from North African source regions to central Europe (Figure 3.2). ERA5 reanalysis data for February 24, 2021 at 12:00 UTC shows a pronounced high-pressure ridge over central and western Europe, with geopotential heights exceeding 1500 m establishing strong anticyclonic circulation. The geopotential height pattern generates sustained southerly flow at 850 hPa, creating a direct transport pathway from the Saharan dust source region to Baden-Württemberg. The 850 hPa temperature field exhibits pronounced warm air advection, with temperatures reaching 10–15°C over central Europe, substantially elevated for late February and confirming the presence of warm African air masses at this atmospheric

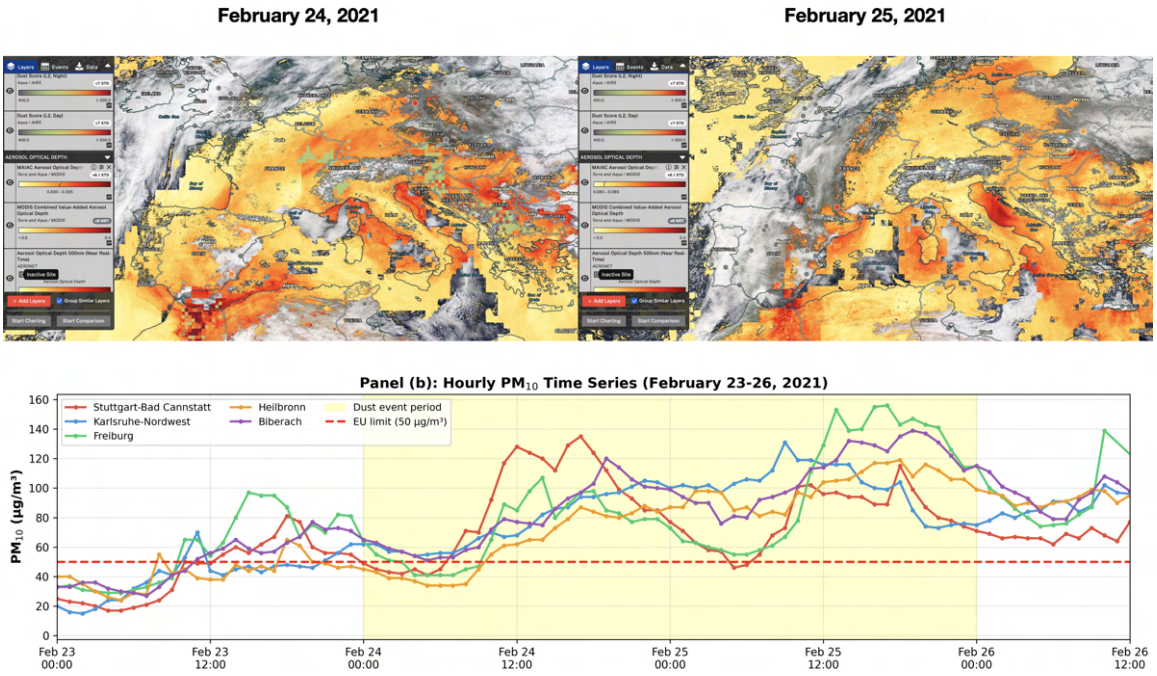

Figure 3.1: February 24-25, 2021 dust event characterization: (a) NASA Worldview true-colour satellite imagery showing dust plume over central Europe, (b) observed PM_{10} time series showing coordinated concentration increases across all five monitoring stations.

level. Wind speeds at 850 hPa range from 8–15 m/s with flow consistently oriented from south to north, facilitating rapid dust transport over the approximately 2000 km distance from North Africa to the study region.

Peak PM_{10} concentrations reach 119–156 µg/m^3 across all five stations, representing the highest values observed during any documented dust event in the study period. The temporal evolution shows rapid concentration increase on February 24 between 06:00–12:00 UTC as the dust plume arrives, peak values sustained through February 24 evening and February 25 morning, and gradual decline over February 25–26 as the synoptic pattern evolves. The spatial extent demonstrates regional-scale character affecting all of Baden-Württemberg with relatively uniform concentrations throughout the monitoring network (coefficient of variation: 6.2%), reflecting the broad meridional flow pattern captured in the ERA5 analysis. The primary event window spans 48 hours, with residual elevated concentrations persisting for 2–3 additional days as dust settles from the atmosphere. $PM_{2.5}$ concentrations during this event reach peak hourly values of 39–58 µg/m^3 with daily means of 28.7–32.5 µg/m^3. The $PM_{2.5}/PM_{10}$ ratio ranges from 0.32–0.38, substantially below background ratios (0.58–0.67), indicating strong coarse fraction dominance characteristic of mineral dust aerosol.

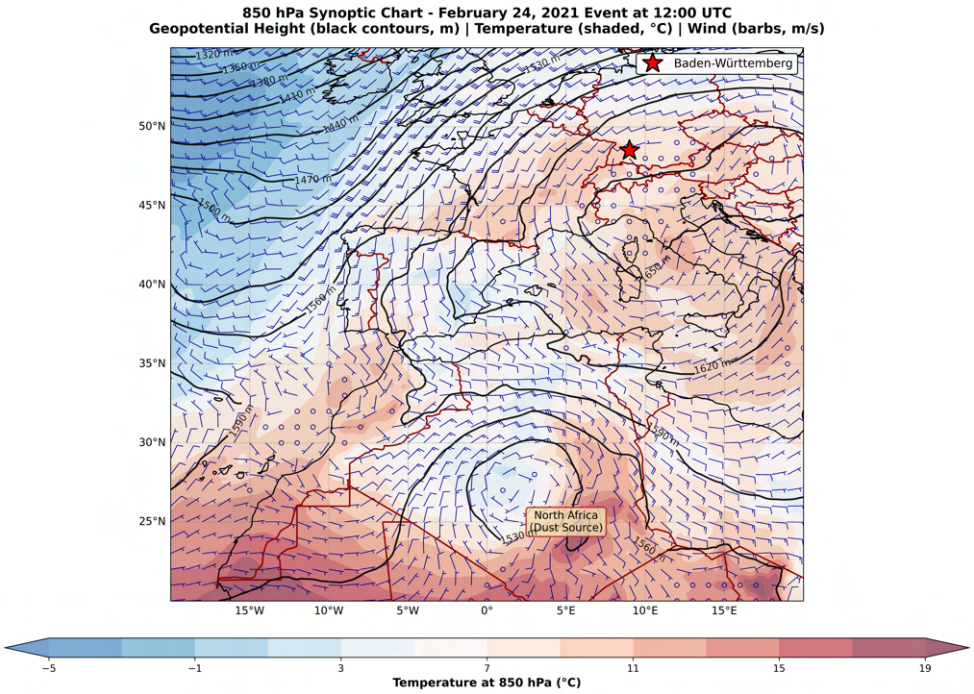

Figure 3.2: 850 hPa synoptic chart for February 24, 2021 at 12:00 UTC showing geopotential height (black contours, m), temperature (colour shading, °C), and wind flow (barbs, m/s). Strong southerly flow and pronounced warm air advection (10–15°C) from North Africa to Baden-Württemberg (red star) establish direct dust transport pathway. High geopotential heights over western Europe (>1500 m) create meridional circulation pattern. Data: ERA5 reanalysis (Hersbach et al., 2020).

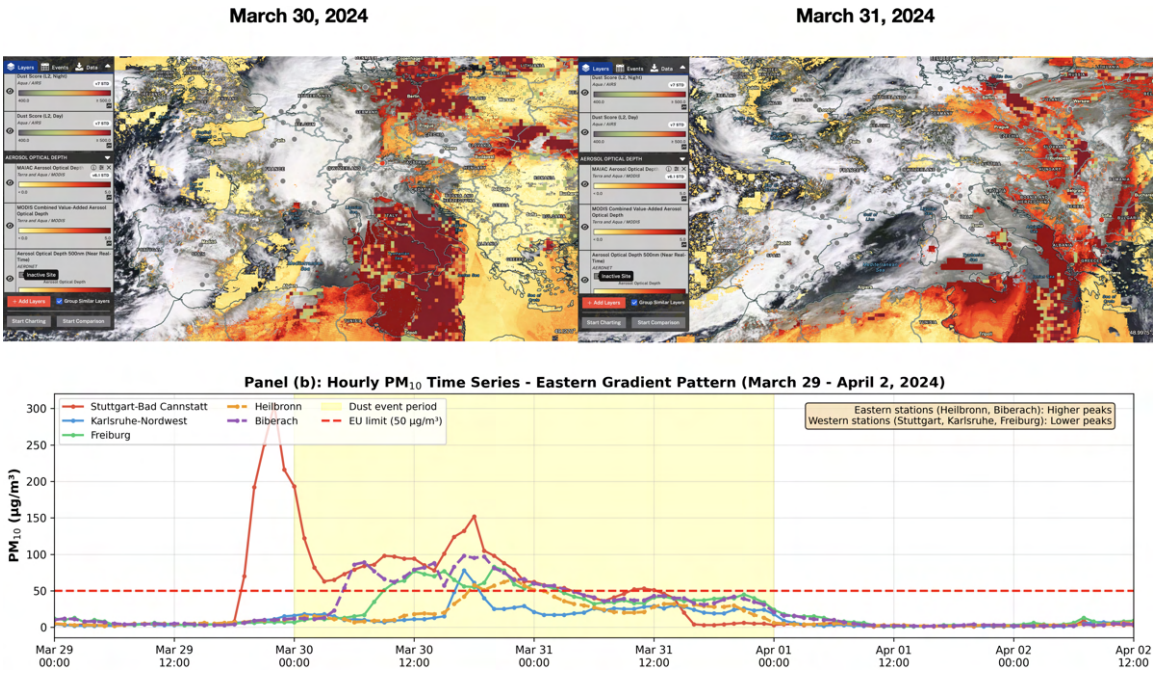

Figure 3.3: March 30-31, 2024 dust event showing spatial heterogeneity: (a) satellite imagery, (b) observed PM_{10} time series revealing east-west gradient in concentration patterns.

3.1.2 March 30-31, 2024 Event

The late March 2024 event exhibits distinct spatial heterogeneity, with eastern Baden-Württemberg stations (Heilbronn, Biberach) experiencing substantially different concentration patterns than western locations. Synoptic conditions at 850 hPa on March 30, 2024 at 12:00 UTC reveal an upper-level ridge positioned over western Europe, creating south-westerly flow rather than the pure southerly flow observed during the February 2021 event (Figure 3.4). ERA5 reanalysis shows geopotential heights of 1450–1500 m over the central Mediterranean and western Europe, with the ridge axis oriented north-south along approximately 5°W. This configuration establishes south-westerly to westerly flow at 850 hPa over Baden-Württemberg, with wind speeds of 6–10 m/s. The 850 hPa temperature field indicates moderate warm air advection with temperatures of 8–12°C over southern Germany, confirming African/Mediterranean air mass influence albeit less pronounced than during the February 2021 episode. The south-westerly flow direction explains the observed east-west gradient in surface PM_{10} concentrations, as eastern monitoring stations lie more directly downwind of the Mediterranean dust transport pathway established by this circulation pattern.

Peak PM_{10} concentrations vary spatially: 66–98 µg/m^3 at western stations (Stuttgart: 98 µg/m^3, Karlsruhe: 66 µg/m^3, Freiburg: 78 µg/m^3) and 83–193 µg/m^3 at eastern stations (Heilbronn: 193 µg/m^3, Biberach: 83 µg/m^3). The spatial gradient shows east-to-west concentration differences, with eastern stations experiencing peak values approximately 70% higher than western stations on average, consistent with the south-westerly flow pattern identified in the ERA5 analysis. The event duration spans primarily 2 days (March

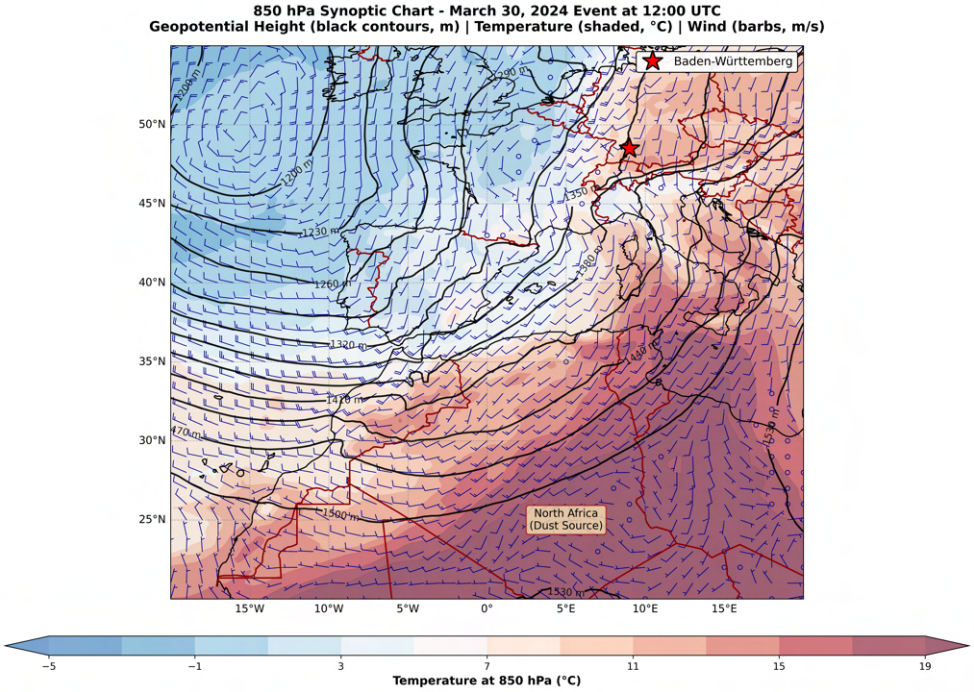

Figure 3.4: 850 hPa synoptic chart for March 30, 2024 at 12:00 UTC showing upper-level ridge over western Europe and south-westerly flow. Temperature field (8–12°C, colour shading) indicates moderate warm air advection from Mediterranean/North African regions. Flow configuration explains observed east-west gradient in dust concentrations across monitoring network, with eastern stations (downwind) experiencing higher PM_{10} values. Data: ERA5 reanalysis (Hersbach et al., 2020).

30–31), with residual elevated concentrations extending through April 2–3, and pronounced afternoon peaks corresponding to boundary layer growth and vertical mixing of elevated dust layers. $PM_{2.5}$ concentrations show daily means of 10.9–16.6 µg/m^3 at western stations and 15.2–21.5 µg/m^3 at eastern stations, with peak hourly values reaching 22–64 µg/m^3. The $PM_{2.5}/PM_{10}$ ratio ranges from 0.31–0.48, maintaining coarse fraction dominance characteristic of mineral dust.

3.1.3 April 7-9, 2024 Event

The early April 2024 event demonstrates extended duration and more complex temporal evolution compared to earlier events. Synoptic analysis at 850 hPa for April 8, 2024 at 12:00 UTC reveals markedly different meteorological conditions than the previous two events, with persistent high pressure and exceptionally weak pressure gradients over central Europe (Figure 3.6). ERA5 reanalysis shows geopotential heights of 1500–1550 m across a broad area from the western Mediterranean to central Europe, with closely-spaced contours indicating minimal pressure gradient and consequently light, variable winds. Wind speeds at 850 hPa average only 3–6 m/s, approximately half the values observed during the February 2021 and March 2024 events—with flow direction varying between south-westerly and westerly across the domain. Despite the weak flow, the 850 hPa temperature field exhibits pronounced warm anomaly with temperatures reaching 14–16°C over Baden-Württemberg, exceptionally warm for early April and providing clear evidence of African air mass presence aloft. The stagnant high-pressure conditions and weak horizontal transport explain the extended event duration (3 days, April 7–9) compared to the more rapid 2-day events driven by stronger synoptic-scale flow.

Peak PM_{10} concentrations range from 49–132 µg/m^3 across the network, with the spatial pattern showing more uniform distribution than the March event and modest concentration differences (western stations averaging 84 µg/m^3 vs. eastern 77 µg/m^3 peak values). The relatively uniform spatial distribution reflects the weak, variable flow regime identified in the ERA5 analysis, contrasting with the gradient patterns produced by stronger directional flow during earlier events. The total duration extends 3 days (April 7–9), longer than typical 2-day events, with multiple concentration peaks emerging: a primary peak on April 7 evening and a secondary peak on April 9. The multiple peaks likely reflect complex interactions between weak horizontal advection, diurnal boundary layer evolution, and gravitational settling of dust particles under the stagnant synoptic regime. $PM_{2.5}$ daily means range from 8.2–13.7 µg/m^3 with peak hourly values of 20–33 µg/m^3. The $PM_{2.5}/PM_{10}$ ratio of 0.28–0.35 indicates the strongest coarse-mode dominance of all three events, consistent with prolonged gravitational settling removing finer particles whilst coarser dust remains suspended.

3.1.4 Summary of Event Characteristics

Table 3.2 summarises the key characteristics of these three major events across all five monitoring stations.

These three events represent the documented major satellite-confirmed Saharan dust transport episodes with visible dust plumes over Baden-Württemberg during the 2020-2024

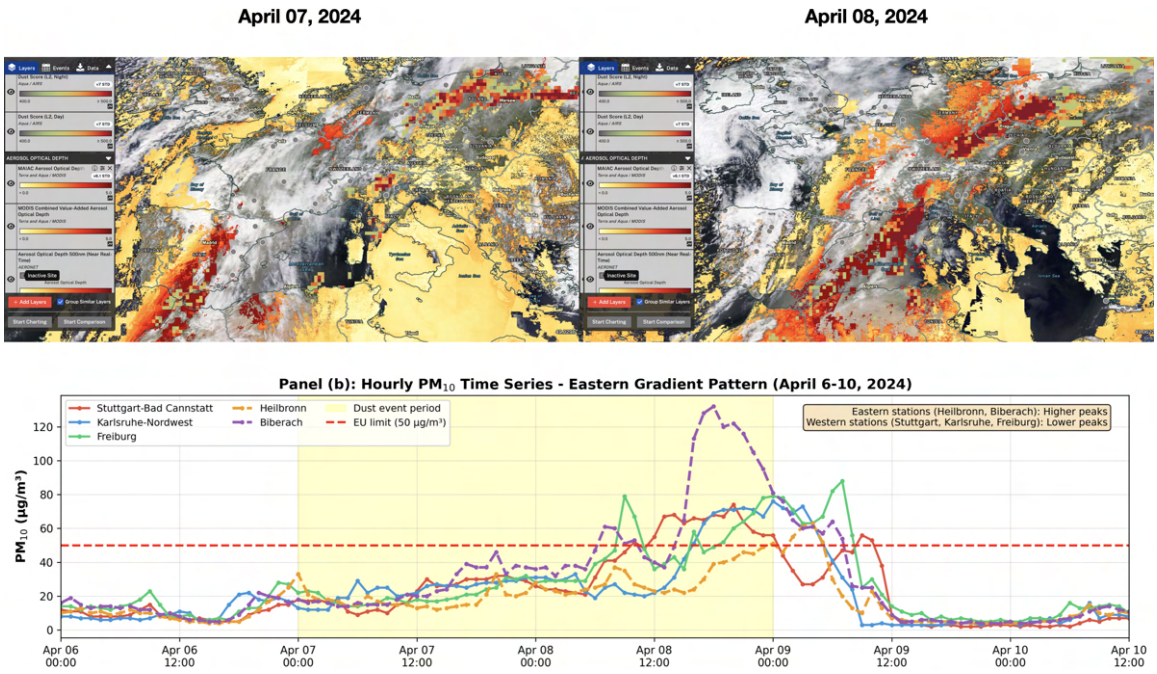

Figure 3.5: April 7-9, 2024 dust event characterization showing extended duration (3 days) and multiple concentration peaks: (a) satellite imagery, (b) observed PM_{10} time series.

Table 3.2: Summary characteristics of the three major Saharan dust transport events documented during 2020-2024. AOD values represent MODIS aerosol optical depth retrievals at 550 nm.

Event	Duration	PM_{10} Range	$PM_{2.5}$ Daily Mean	AOD Range
February 24-25, 2021	2 days	119-156 µg/m^3	28.7-32.5 µg/m^3	0.60-0.69
March 30-31, 2024	2-3 days	66-193 µg/m^3	10.9-21.5 µg/m^3	0.45-0.62
April 7-9, 2024	3 days	49-132 µg/m^3	8.2-13.7 µg/m^3	0.38-0.80

study period. The 7 dust days (February 24-25, March 30-31, April 7-9) collectively produce a total of 22 station-day exceedances across the five-station network. The diversity in intensity (PM_{10}: 49-156 µg/m^3), spatial patterns (uniform to gradient-dominated), and temporal structures (2-3 day durations) enables comprehensive characterisation across different dust transport scenarios.

3.2 Observational Analysis

3.2.1 PM_{10} and $PM_{2.5}$ Temporal Patterns (2020-2024)

Figure 3.7 illustrates the annual mean PM_{10} and $PM_{2.5}$ concentrations for each station across the five-year study period, showing inter-annual variability alongside the persistent spatial gradient from urban to rural sites. The five-year observational datasets covering

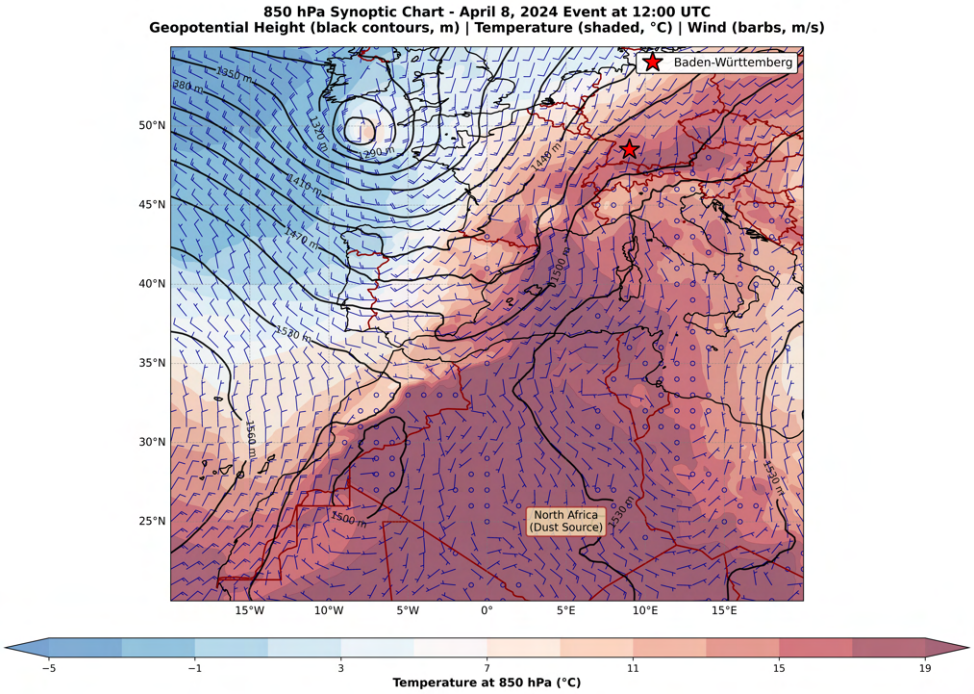

Figure 3.6: 850 hPa synoptic chart for April 8, 2024 at 12:00 UTC showing persistent high pressure and weak pressure gradients over central Europe. Elevated temperatures (14–16°C, colour shading) confirm African air mass presence despite light winds (3–6 m/s). Stagnant conditions contributed to extended event duration (3 days, April 7–9) and multiple concentration peaks through complex mixing processes. Data: ERA5 reanalysis (Hersbach et al., 2020).

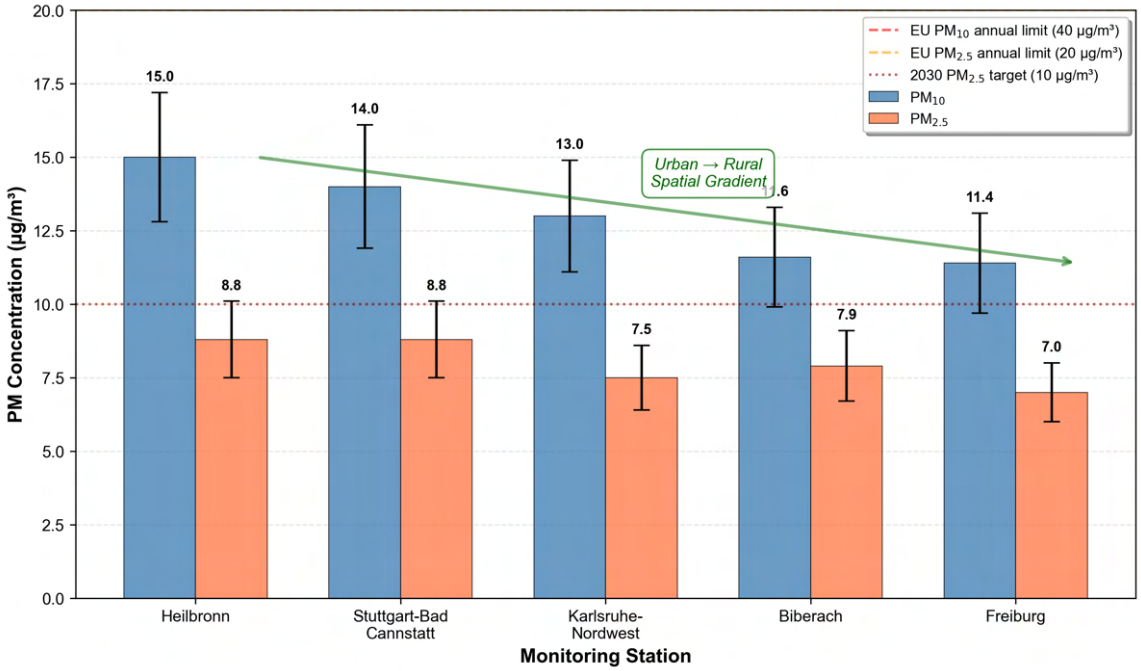

Figure 3.7: Annual mean PM_{10} and $PM_{2.5}$ concentrations for each monitoring station across the five-year study period (2020-2024), showing inter-annual variability and the persistent spatial gradient from urban (Heilbronn, Stuttgart) to rural sites (Freiburg, Biberach).

January 2020 through December 2024 show distinct temporal and spatial patterns in PM concentrations across Baden-Württemberg. The extensive analysis of hourly PM_{10} and $PM_{2.5}$ measurements from the five LUBW monitoring stations reveals noticeable seasonal variability, with systematically elevated PM concentrations occurring during the winter months (January-March) and the spring dust season (March-April).

Across the five monitoring stations, annual mean PM_{10} concentrations exhibit values ranging from 10-16 µg/m^3 during the study period, demonstrating an inter-station variability reflecting differences in local emission sources and geographical settings. Upon ranking the PM_{10} annual mean concentrations, from highest to lowest, it is seen that Heilbronn displays the highest annual mean PM_{10} concentration (mean: 15 µg/m^3), followed by Stuttgart-Bad Cannstatt located in the urban core of the state capital (mean: 14 µg/m^3). Karlsruhe-Nordwest, representing an intermediate urban-suburban environment, shows mean concentrations of 13 µg/m^3. Biberach, characterised by its more rural setting with lower traffic density and industrial activity, exhibits mean concentrations of 11.6 µg/m^3. Freiburg displays the lowest PM_{10} concentrations (mean: 11.4 µg/m^3).

Upon ranking the $PM_{2.5}$ annual mean concentrations again, from highest to lowest, Heilbronn and Stuttgart-Bad Cannstatt share the highest annual mean $PM_{2.5}$ values (mean: 8.8 µg/m^3 for both stations). Biberach shows intermediate concentrations ($PM_{2.5}$ mean: 7.9 µg/m^3), while Freiburg exhibits the lowest fine particle concentrations ($PM_{2.5}$ mean: 7.0 µg/m^3). The spatial pattern from highest (Heilbronn, Stuttgart) to lowest (Freiburg, Biberach) reflects the gradient in emission source intensity across the monitoring network,

with urban stations experiencing elevated concentrations relative to rural background sites.

Looking at the seasonal variability, Figure 3.8 presents monthly box plots of PM_{10} concentrations for all stations, illustrating seasonal patterns and the range of variability within each month. Monthly aggregated data reveals distinct seasonal patterns consistent across all monitoring stations, albeit with varying magnitudes.

Monthly concentration distributions reveal a pronounced seasonal cycle consistent across all five monitoring stations, albeit with station-specific absolute levels. Winter-spring months (January-April) exhibit the highest PM_{10} concentrations, with median values ranging from 15-25 µg/m³ (30-50% above annual station means) and frequent excursions above 30 µg/m³. This seasonal maximum reflects the combined influence of enhanced non-dust related sources of PM and increased frequency of Saharan dust transport events (as documented in Table 3.1). Notably, the upper whiskers and outliers during January-April extend to 35-40 µg/m³ at all stations, with extreme values reaching 50 µg/m³ (EU daily limit) during documented dust episodes.

Summer months (June-August) consistently show the lowest concentrations across all stations, with median PM_{10} values of 8-12 µg/m³ and narrow interquartile ranges (IQR = 3-5 µg/m³), reflecting reduced non-dust related emissions, and absence of major dust transport. Maximum summer values rarely exceed 20 µg/m³, demonstrating the dominant role of seasonally variable sources rather than constant background pollution.

Autumn (September-November) and late spring (May) display intermediate concentration levels with transitional characteristics. Median values (12-18 µg/m³) lie between summer minima and winter-spring maxima, whilst interquartile ranges broaden compared to summer (IQR = 5-8 µg/m³), indicating increased day-to-day variability as heating emissions (though not quantified in this work) commence (autumn) or diminish (May). December exhibits elevated concentrations approaching winter levels, particularly at urban stations (Heilbronn, Stuttgart), signalling the onset of the heating season.

Focussing on the Winter-Spring dust season, the January-April period warrants particular attention as it encompasses both elevated winter concentrations and the primary natural dust transport season (see dust event calendar, Table 3.1). Figure 3.9 shows PM_{10} temporal evolution (7-day rolling mean) for all five stations during 2020–2024. Recurring seasonal patterns show elevated concentrations during January–April and reduced concentrations during June–August. Three major dust events produce coordinated concentration peaks across all stations: February 24–25, 2021 (peak 119–156 µg/m^3); March 30–31, 2024 (66–193 µg/m^3); April 8–9, 2024 (49–132 µg/m^3). Years 2020, 2022, and 2023 show no major dust episodes that violates the PM thresholds. It is evident that events that are closely spaced (temporally) to each other show signs of major Saharan dust transport events.

3.2.2 Air Quality Standard Violations

Assessment of air quality standard compliance quantifies exceedances under current EU thresholds and projected 2030 standards (regulatory framework detailed in Section 2.4.3). The analysis examines both current compliance status and projected violation frequencies.

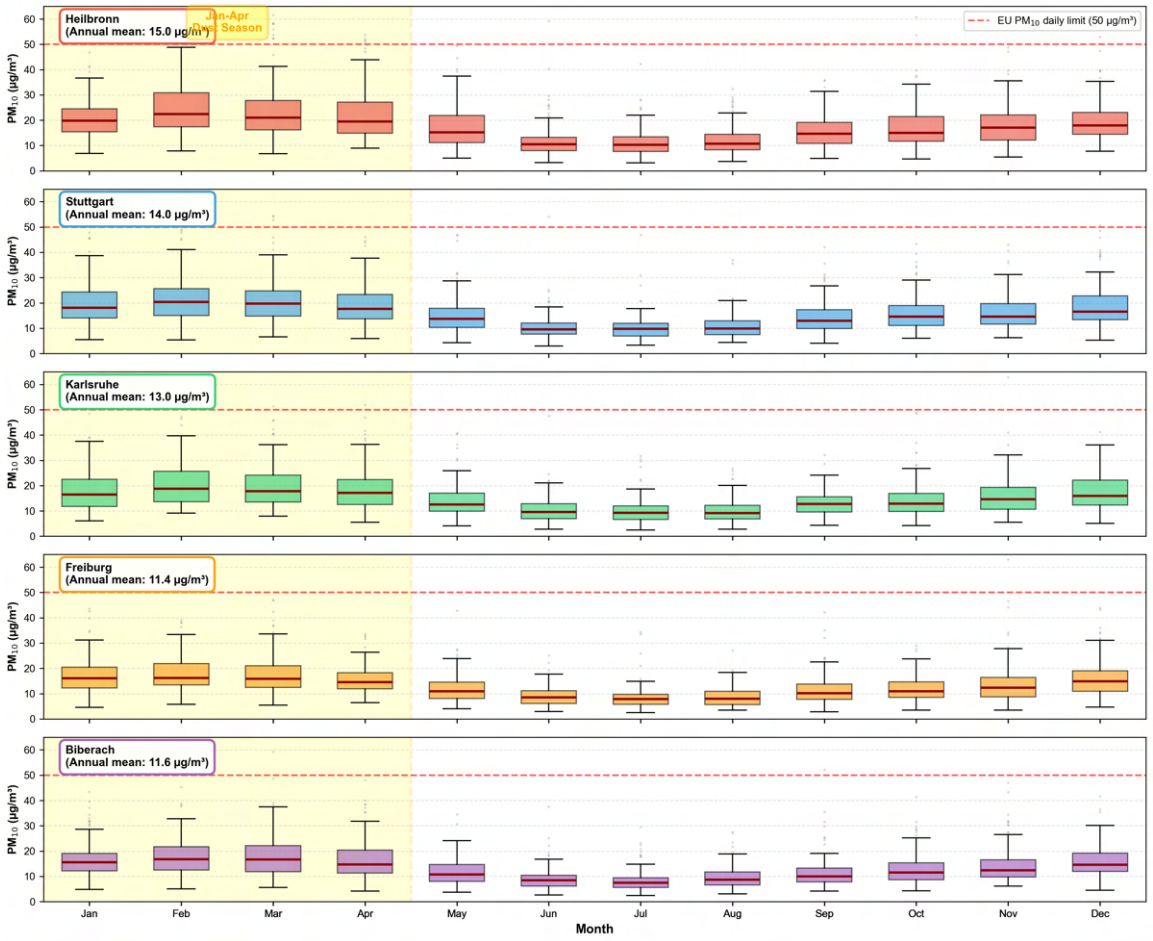

Figure 3.8: Monthly box plots of PM_{10} concentrations for all five monitoring stations (2020-2024), showing pronounced seasonal cycle across all sites. Winter-spring months (January-April, corresponding to the dust transport season) exhibit elevated median concentrations (15-25 µg/m³) with frequent outliers extending to 35-50 µg/m³ during documented Saharan dust events. Summer months (June-August) show minimum concentrations (8-12 µg/m³) with narrow distributions. Box plots display median (red line), interquartile range (box), 1.5×IQR whiskers, and outliers (individual points). Red dashed line indicates EU daily limit value (50 µg/m³). Station-specific annual means shown in labels. All stations exhibit consistent seasonal timing despite differing absolute levels.

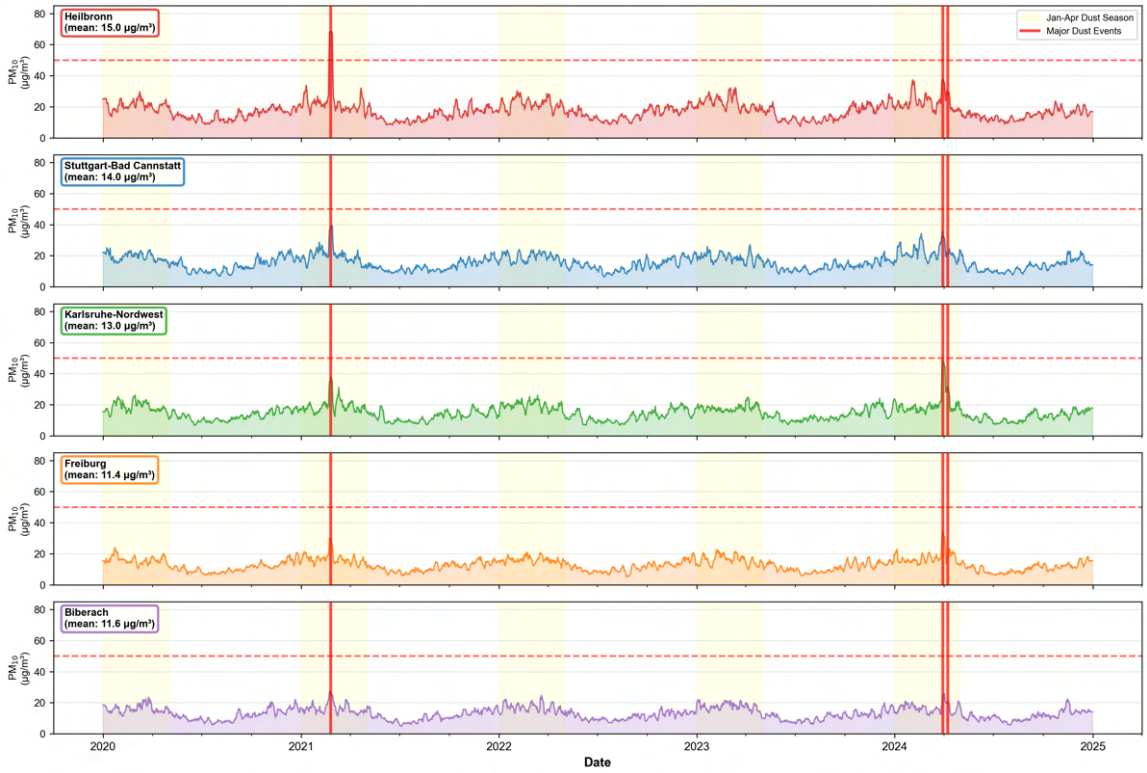

Figure 3.9: Temporal evolution of PM_{10} concentrations (7-day rolling mean) across five monitoring stations (2020–2024). Each panel shows one station with shaded area under the curve. Light yellow vertical bands indicate January–April dust season. Red vertical lines mark major dust events (February 24, 2021; March 30, 2024; April 8, 2024). Red dashed line shows EU daily limit (50 µg/m^3). Coordinated concentration peaks across all stations during red-marked dates confirm regional dust transport events.

Under the current European Union air quality framework (Directive 2008/50/EC), the daily limit value for PM_{10} is set at 50 µg/m^3, with up to 35 exceedances permitted per calendar year. For $PM_{2.5}$, an annual mean limit of 25 µg/m^3 applies (reduced to 20 µg/m^3 from 2020 onwards). Annual PM_{10} exceedance frequencies (Figure 3.10) show four stations maintaining compliance throughout 2020–2024, whilst Heilbronn violated the annual limit during 2020–2022 (47, 40, 37 exceedances/year) before achieving compliance in 2023–2024. Documented dust events contribute 2–3 exceedance days per station over the five-year period.

The three documented dust transport events (Table 3.1) produced distinct compliance impacts reflecting differences in event intensity, spatial extent, and temporal evolution. The February 24–25, 2021 event constitutes the most severe episode, generating simultaneous daily limit exceedances at all five monitoring stations with peak concentrations of 119–156 µg/m^3—values 2.4–3.1 times the 50 µg/m^3 threshold. This event alone contributed 2 exceedance days to each station's annual total for 2021, representing the only documented dust-attributed violations during 2020–2022. The regional-scale uniformity of this event, with all stations exceeding thresholds within a 24-hour window, distinguishes dust transport from typical localised pollution episodes that affect individual stations independently.

The March 30–31, 2024 event exhibited greater spatial heterogeneity, with peak concentrations ranging from 66 µg/m^3 (Karlsruhe) to 193 µg/m^3 (specific station values in Table 3.1), reflecting a pronounced east-west gradient in dust deposition. Three southwestern stations (Freiburg, Karlsruhe, Stuttgart) recorded daily limit exceedances, whilst northeastern stations (Heilbronn, Biberach) remained below the threshold despite elevated concentrations. This spatial pattern aligns with dust transport pathways approaching from the Mediterranean, with progressive dilution and deposition during eastward advection. The April 8–9, 2024 event (corrected dates accounting for boundary layer mixing delay; see Section **??**) produced similar spatial gradients with peak concentrations of 49–132 µg/m^3 and selective exceedances at southwestern stations. Together, the two 2024 events contributed 2–3 exceedance days per station, concentrated at locations with direct exposure to Mediterranean transport corridors.

Figure 3.10 contextualises these dust-attributed exceedances within the broader compliance picture. Across the five-year period, dust events account for 2–3 exceedance days per station (representing 3–9% of total station exceedances), with perfect temporal synchronisation: all stations show 2 dust exceedances in 2021, zero during 2020/2022/2023 (years without major dust events), and 2–3 in 2024. This coordinated inter-annual pattern, contrasting sharply with the station-specific violation patterns during non-dust periods, provides independent confirmation of regional-scale natural aerosol influence distinct from local anthropogenic sources. Specifically, Figure 3.10 displays the annual number of PM_{10} exceedance days (>50 µg/m^3) for each station across the five-year period, with dust-attributed versus other exceedances differentiated by colour.

The analysis shows substantial inter-station variability in exceedance frequency, ranging from 56 total exceedances at Biberach (rural background) to 165 at Heilbronn (urban background) over the five-year period. Heilbronn exceeds the EU annual limit (35 exceedances permitted) in three consecutive years (2020-2022), with 47, 40, and 37 exceedances, respectively, although concentrations improve markedly from 2023 onwards (15 exceedances)

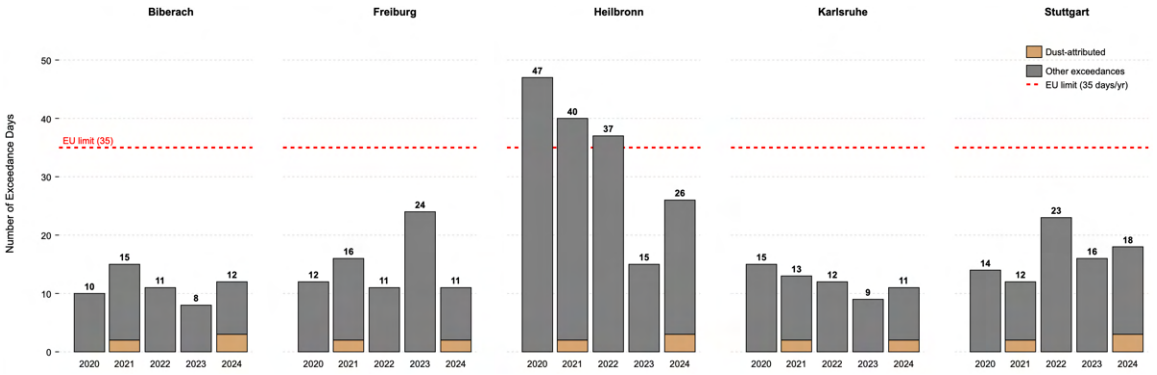

Figure 3.10: Annual number of PM_{10} exceedance days (>50 µg/m^3) for each monitoring station (2020-2024). Bars distinguish dust-attributed exceedances (identified through satellite imagery confirmation and multi-station temporal coherence) from other exceedances. Heilbronn exceeded the EU annual limit (35 days) during 2020-2022.

and remain compliant in 2024 (26 exceedances). This three-year non-compliance pattern mirrors the original EU-limit violations documented for this station in previous regulatory assessments.

Applying the dust-attributed exceedance identification criteria (Section 2.4.5), dust events account for 4–5 exceedance days per station over the five-year period (3–9% of total exceedances). The temporal pattern shows perfect inter-station synchronisation: all five stations record 2 dust exceedances in 2021 (February 24–25), zero during 2020, 2022, and 2023, and 2–3 in 2024 (March 30–31 and April 8–9). In contrast, total exceedance frequencies vary substantially by station (56 days at Biberach to 165 days at Heilbronn over five years), indicating that dust events constitute a small but temporally coherent component of overall regulatory PM violations.

3.2.3 Projected 2030 WHO/EU Standards

Figure 3.11 visualises the PM_{10} exceedance frequency increases under projected 2030 standards, with dust-attributed components distinguished to illustrate their proportional contribution to the compliance challenge.

The European Union has committed to aligning its air quality standards more closely with World Health Organisation (WHO) recommendations by 2030. The anticipated revised standards include a daily PM_{10} limit of 45 µg/m^3 and an annual $PM_{2.5}$ mean of 10 µg/m^3 (potentially 15 µg/m^3 as an intermediate target). Evaluating the observational dataset against these more stringent thresholds reveals substantially increased violation frequencies.

Application of the projected 2030 thresholds to the 2020–2024 observational dataset reveals contrasting compliance outlooks for PM_{10} daily and $PM_{2.5}$ annual standards. For PM_{10} daily limit violations, lowering the threshold from 50 to 45 µg/m^3 increases exceedance frequencies by 28–50% across the monitoring network, adding 17–56 violation days per station over the five-year period. Heilbronn experiences the most pronounced impact,

with annual violations averaging 44.2 days/year under the stricter standard—substantially exceeding the anticipated 35-day annual limit and indicating that achieving 2030 compliance at this urban background site will require significant emission reductions beyond current levels. Stuttgart and Freiburg show intermediate violation frequencies (22–24 days/year), whilst Karlsruhe and Biberach exhibit the lowest increases (15.4 days/year each), remaining well within the 35-day annual allowance.

The documented dust transport events contribute 5–6 exceedance days per station under the 45 µg/m^3 threshold (1.0–1.2 days/year average), representing only a marginal increase from the 4–5 dust exceedances identified under current standards. This minimal change reflects the high-intensity nature of major dust episodes: satellite-confirmed dust days already exceed both the current (50 µg/m^3) and projected (45 µg/m^3) thresholds during transport events, with peak concentrations reaching 119–193 µg/m^3 (Table 3.1). Consequently, dust events account for 2.3–6.5% of projected 2030 violations, a small but temporally coherent component that remains largely invariant to threshold adjustments within the 45–50 µg/m^3 range. The implication is that achieving 2030 PM_{10} daily compliance depends primarily on reducing non-dust PM sources, with natural dust subtraction (Article 21 provisions) providing only marginal relief equivalent to 1–2 days per year.

In contrast to PM_{10} daily challenges, all five monitoring stations currently comply with the proposed 2030 $PM_{2.5}$ annual mean target (10 µg/m^3), with 2020–2024 overall means ranging from 7.1 µg/m^3 (Freiburg) to 8.8 µg/m^3 (Heilbronn/Stuttgart). Even the highest annual mean remains 1.2 µg/m^3 (12%) below the threshold, providing a compliance margin that accommodates inter-annual variability. This favourable $PM_{2.5}$ situation reflects substantial progress in fine particulate matter reduction over recent decades, driven primarily by decreased combustion emissions (cleaner vehicles, improved heating technologies, industrial emission controls). Natural dust contributes minimally to $PM_{2.5}$ annual means due to the predominantly coarse-mode size distribution of transported Saharan particles, further widening the compliance margin for this metric.

Table 3.3 provides a comprehensive summary of compliance metrics for both current and projected standards.

Table 3.3: Compliance metrics for current PM_{10} standard (50 µg/m^3 daily limit) across all five monitoring stations (2020-2024). Dust-attributed violations identified through satellite imagery confirmation and multi-station temporal coherence.

Station	Total Exceedances (2020–2024)	Mean Annual Exceedances (days/yr)	Dust-Attributed Exceedances (days)	Dust % of Total	Mean Annual Dust Days (days/yr)
Stuttgart-BC	83	16.6	5	6.0%	1.0
Karlsruhe-NW	60	12.0	4	6.7%	0.8
Freiburg	74	14.8	4	5.4%	0.8
Heilbronn	165	33.0	5	3.0%	1.0
Biberach	56	11.2	5	8.9%	1.0

Note: Heilbronn exceeded EU annual limit (35 days/year) during 2020–2022 (47, 40, 37 exceedances respectively), achieving compliance in 2023 (15 days) and 2024 (26 days).

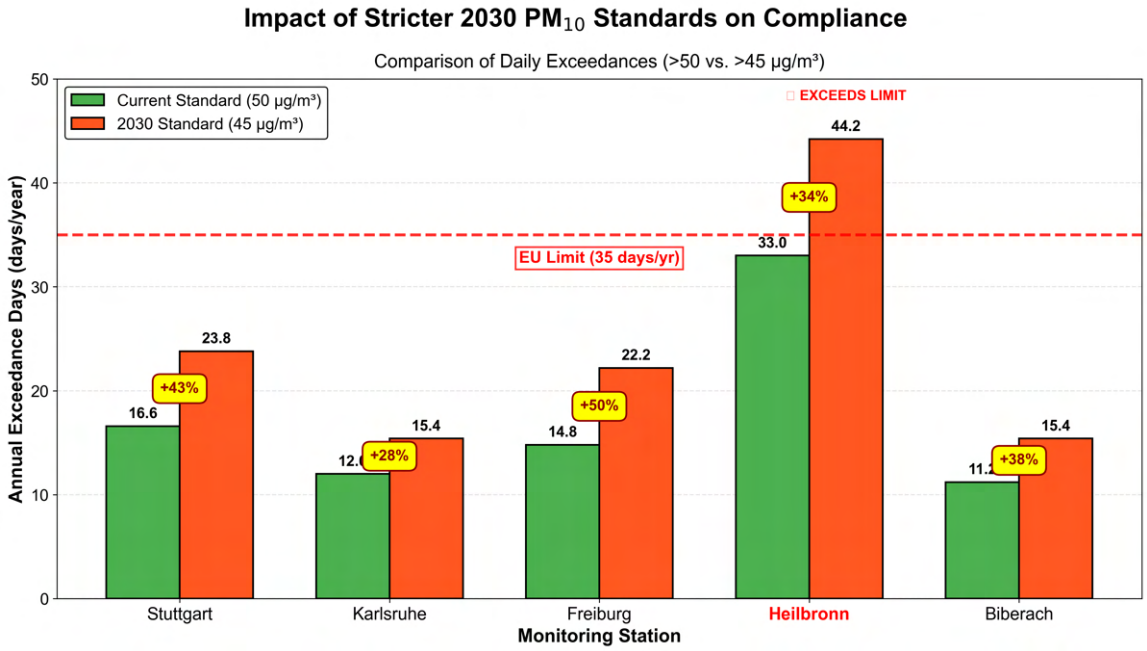

Figure 3.11: Comparison between PM_{10} exceedance frequencies under current (50 µg/m^3) and projected 2030 (45 µg/m^3) standards for all five monitoring stations. Bars show annual average exceedance days over the 2020-2024 period.

Heilbronn's three-year non-compliance with annual limits shows concentration patterns consistent with the original EU-limit violations, with compliance achieved in later years (2023-2024) following the same temporal trend as previous regulatory assessments.

3.3 Dust Concentration Analysis

3.3.1 Overview of Meteogram Data Application

Figure 3.12 shows a time-series plot for Karlsruhe station with both the LUBW (observations) and the DWD (model) data in order to visualise the systematic differences among the two data sets regarding PM_{10} concentrations.

Meteogram dust concentration forecasts from the DWD ICON-ART modelling system provide independent supporting evidence for the presence and timing of Saharan dust transport events. Daily averaged surface concentrations of dust aerosols are extracted from the DWD meteogram archive for grid points nearest to each LUBW monitoring station during the January-April period (2020-2024). Heilbronn maps to the same meteogram grid point as Stuttgart-Bad Cannstatt and therefore shares identical meteogram values; Biberach lacks a nearby meteogram station within reasonable proximity. The analysis therefore focuses on three stations with unique grid point representation: Stuttgart, Karlsruhe, and Freiburg.

A fundamental distinction must be emphasised: meteogram values represent exclusively mineral dust concentrations simulated by the atmospheric model, whereas ground-based

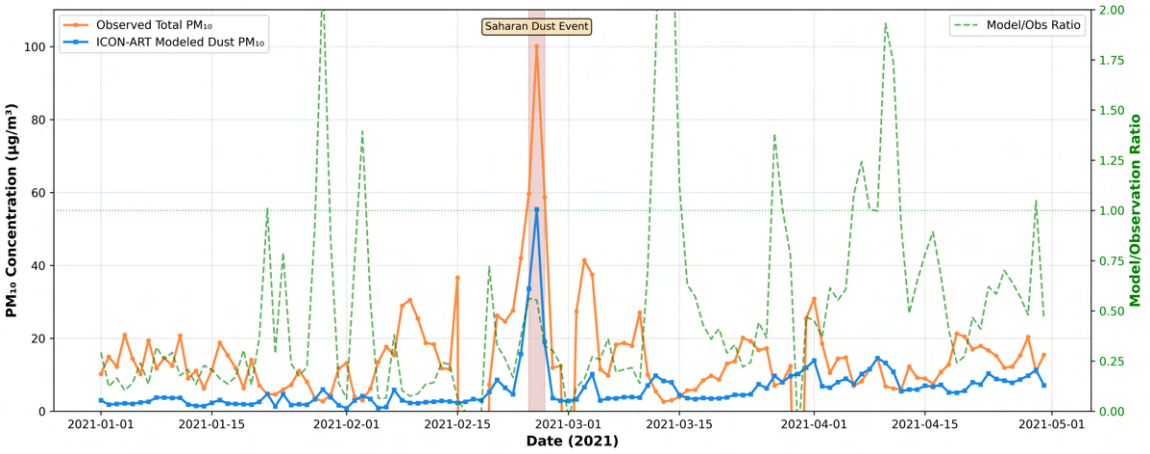

Figure 3.12: Comparison of meteogram dust component (red line) and observed total PM_{10} (black line) for Karlsruhe-Nordwest during January-April 2020-2024. Meteogram values represent mineral dust concentrations only (ICON-ART model output), whilst observations encompass all PM sources. The systematic offset between the two time series reflects the contribution of non-dust PM sources, estimated at 8–10 µg/m^3 based on the difference between curves during background periods. Shaded regions indicate periods with meteogram dust ≥ 2 µg/m^3. Elevated meteogram values during February 2021, March 2024, and April 2024 correspond temporally with satellite-confirmed dust events and observed PM_{10} peaks, providing independent atmospheric modelling evidence for dust presence.

PM_{10} observations measure complete particulate mixtures from all sources (natural dust, traffic emissions, industrial activities, residential heating, secondary aerosol formation). Consequently, meteogram dust values are systematically lower than total observed PM_{10}, with the magnitude of this difference reflecting the non-dust PM contribution at each location. This relationship is illustrated through temporal comparison (Figure 3.12) and quantitative summary statistics (Table 3.4).

Table 3.4: Comparison of meteogram dust component and observed total PM_{10} during January-April 2020-2024 across three monitoring stations. The systematic difference represents non-dust PM contributions at each location, with larger offsets at more urbanized sites.

Station	**Meteogram Dust (µg/m^3)**	**Observed Total PM_{10} (µg/m^3)**	**Difference (µg/m^3)**
Stuttgart-BC	5.6	16.3	10.7
Karlsruhe-NW	5.9	14.0	8.1
Freiburg	6.0	12.6	6.6

Table 3.4 quantifies the relationship between meteogram dust values and total observed PM_{10} concentrations. Average meteogram dust values during the January-April period

range from 5.6–6.0 μg/m^3 across the three stations, exhibiting minimal inter-station variability (coefficient of variation: 3.6%). By contrast, observed total PM_{10} concentrations show substantially larger absolute values (12.6–16.3 μg/m^3) and greater spatial variability (coefficient of variation: 12.7%), reflecting the spatial heterogeneity in emission sources across the monitoring network. The systematic offset between meteogram dust and total observations ranges from 6.6 μg/m^3 at Freiburg (the cleanest location) to 10.7 μg/m^3 at Stuttgart-Bad Cannstatt (the most urbanised location within the state capital). This spatial pattern is consistent with the established gradient in total PM contributions across the monitoring network, with larger non-dust components at urban sites and smaller contributions at rural/suburban locations.

During documented dust events, meteogram values increase substantially above background levels, reaching peak values of 50–70 μg/m^3 during the major transport episodes (February 2021, March 2024, April 2024). These meteogram elevations temporally coincide with satellite-confirmed dust plumes and observed PM_{10} concentration peaks, thereby corroborating dust event identification through independent atmospheric modelling evidence. The temporal alignment between meteogram dust increases and observed concentration peaks demonstrates the utility of meteogram data as supporting evidence for dust transport timing, complementing satellite imagery and multi-station observational coherence in the multi-criteria event identification framework (Section 3.1).

The spatial uniformity of average meteogram dust values (5.6–6.0 μg/m^3, range: 0.4 μg/m^3) contrasts with the spatial variability in total observed PM_{10} (12.6–16.3 μg/m^3, range: 3.7 μg/m^3), indicating that natural dust contributions exhibit regional-scale homogeneity whilst other PM sources create pronounced local-scale gradients. This finding supports the conceptual framework underlying Article 21 provisions in EU air quality legislation: natural dust constitutes a spatially uniform regional background component, whereas other emission sources generate the spatial heterogeneity observed in compliance monitoring networks.

3.4 Dust Fraction Analysis

Dust fraction estimates, calculated according to Equation 2.5 (Section 2.4.1), quantify the natural dust contribution to total observed PM_{10} and $PM_{2.5}$ concentrations during the January-April dust transport season. Analysis encompasses 1506 event-days for PM_{10} and 1270 event-days for $PM_{2.5}$ (days with meteogram dust ≥ 2 μg/m^3) across three monitoring stations (Stuttgart, Karlsruhe, Freiburg) during 2020-2024.

3.4.1 Overall Dust Fraction Distributions

Table 3.5 summarises aggregate dust fraction statistics for both PM size fractions across all stations and events. PM_{10} dust fractions exhibit a median value of 0.481 (48.1%), indicating that natural dust typically accounts for approximately half of total observed PM_{10} during identified dust transport periods. The mean value of 0.627 (62.7%) exceeds the median, reflecting right-skewed distribution with occasional very high dust fractions during intense events. $PM_{2.5}$ exhibits systematically higher dust fractions than PM_{10} (median: 0.608, mean:

0.805), suggesting that fine dust particles constitute a larger proportion of fine-mode PM compared to coarse-mode contributions. The high skewness values (2.163 for PM_{10}, 3.455 for $PM_{2.5}$) indicate distributions with long right tails, driven by intense dust events where meteogram concentrations occasionally equal or exceed total observed PM, yielding dust fractions approaching or exceeding unity.

Table 3.5: Aggregate dust fraction statistics for PM_{10} and $PM_{2.5}$ during days with meteogram dust $\geq 2\,\mu g/m^3$ (January-April 2020-2024, three stations combined). Dust fractions > 1.0 occur when meteogram dust values exceed total observed PM, reflecting either model overestimation or observational uncertainties.

Statistic	PM_{10} Dust Fraction	$PM_{2.5}$ Dust Fraction
Sample size (station-days)	1506	1270
Mean	0.627 (62.7%)	0.805 (80.5%)
Median	0.481 (48.1%)	0.608 (60.8%)
Standard deviation	0.529	0.753
Interquartile range (25th-75th)	0.262–0.806	0.311–1.053
Range (minimum–maximum)	0.025–4.321	0.022–9.269
Skewness	2.163	3.455

Figure 3.13 presents histograms of dust fraction distributions for both PM size fractions, illustrating the right-skewed character of the distributions and the prevalence of dust fractions in the 0.3-0.8 range for PM_{10} and 0.4-1.0 range for $PM_{2.5}$. The majority of event-days exhibit dust fractions between the 25th and 75th percentiles (yellow shading in figure), with substantial spread reflecting event-to-event variability in dust intensity, transport patterns, and background PM conditions.

3.4.2 Station-Specific and Event-Intensity Patterns

Table 3.6 decomposes dust fractions by monitoring station, revealing systematic spatial variations consistent with urbanisation gradients. Freiburg, representing the cleanest location with minimal traffic and industrial activity, exhibits the highest mean dust fractions ($DF_{PM_{10}} = 0.698$, $DF_{PM_{2.5}} = 0.895$), indicating that natural dust constitutes a larger proportion of total PM at this rural/suburban site. By contrast, Stuttgart-Bad Cannstatt, the most urbanised location within the state capital, shows the lowest dust fractions ($DF_{PM_{10}} = 0.522$, $DF_{PM_{2.5}} = 0.710$)—approximately 25% lower than Freiburg for PM_{10}—reflecting larger non-dust PM contributions from traffic, heating, and industrial sources. Karlsruhe-Nordwest occupies an intermediate position ($DF_{PM_{10}} = 0.660$, $DF_{PM_{2.5}} = 0.812$), consistent with its semi-urban character.

Figure 3.14 illustrates these spatial patterns through box plots, showing the full distribution of dust fractions at each station. The west-to-east gradient (Freiburg → Karlsruhe → Stuttgart) corresponds to increasing urbanisation levels, with median dust fractions declining systematically from 0.54 at Freiburg to 0.48 at Karlsruhe and 0.40 at Stuttgart for PM_{10}. This spatial pattern demonstrates that dust represents a relatively larger fraction of total PM variability at cleaner locations, whilst urbanised sites exhibit larger non-dust

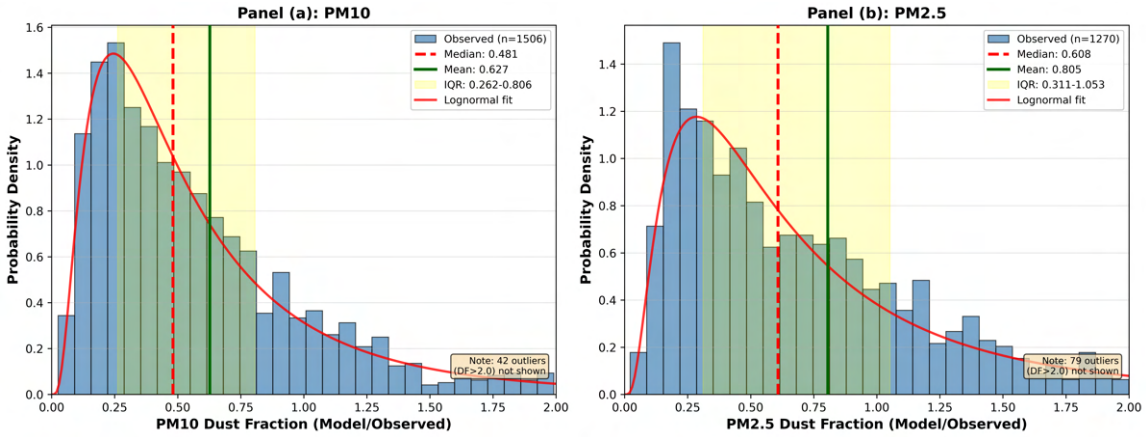

Figure 3.13: Histograms of dust fraction distributions for days with meteogram dust $\geq 2\,\mu g/m^3$ during January-April 2020-2024. Panel (a): PM_{10} dust fractions (n=1506 event-days, median=0.481, mean=0.627, IQR=0.262–0.806). Panel (b): $PM_{2.5}$ dust fractions (n=1270 event-days, median=0.608, mean=0.805, IQR=0.311–1.053). Yellow shading indicates interquartile range, red dashed line shows median, green solid line shows mean, red curve represents fitted log-normal distribution. Both distributions exhibit positive skewness with long right tails.

Table 3.6: Station-specific dust fraction statistics for PM_{10} and $PM_{2.5}$ during days with meteogram dust $\geq 2\,\mu g/m^3$ (January-April 2020-2024). Stations arranged by decreasing urbanisation level.

Station	**Sample Size (n)**	**Mean DF PM_{10}**	**Mean DF $PM_{2.5}$**	**Median DF PM_{10}**	**Median DF $PM_{2.5}$**
Stuttgart-BC	495 / 417	0.522	0.710	0.40	0.54
Karlsruhe-NW	519 / 443	0.660	0.812	0.48	0.61
Freiburg	492 / 410	0.698	0.895	0.54	0.68

baselines that dilute fractional dust contributions even when absolute dust concentrations remain comparable.

Table 3.7 stratifies dust fraction statistics by meteogram forecast intensity categories, revealing systematic relationships between dust concentration levels and fractional contributions. During low-intensity periods (meteogram dust $< 5\,\mu g/m^3$, representing 8.8% of event-days), dust fractions remain modest (0.44–0.67 for PM_{10}), with total observed PM_{10} averaging $12.6\,\mu g/m^3$—dominated by non-dust sources. Moderate-intensity events ($5–12\,\mu g/m^3$, 20.8% of events) exhibit intermediate dust fractions (0.77 for PM_{10}), whilst high-intensity events (meteogram dust $> 12\,\mu g/m^3$, 70.4% of events) show dust fractions exceeding unity (1.02 for PM_{10}, 1.27 for $PM_{2.5}$), indicating that during intense dust transport episodes, meteogram values equal or exceed total observed PM. The three documented major events (February 2021, March 2024, April 2024) span this intensity range, with the February 2021 event exhibiting dust fractions of 0.49–0.54 (meteogram dust $\sim 65\,\mu g/m^3$,

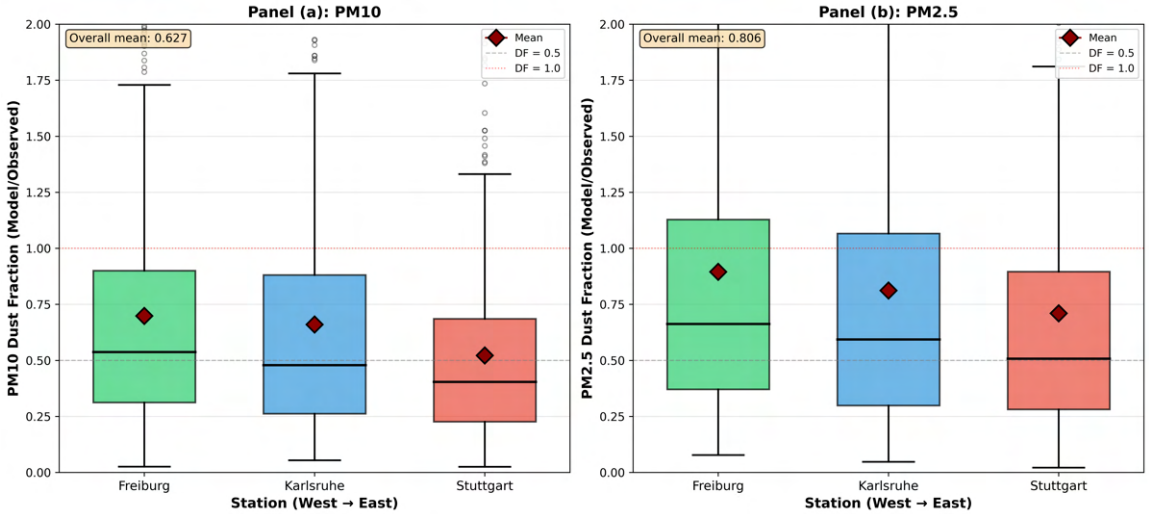

Figure 3.14: Station-specific dust fraction distributions for days with meteogram dust ≥ 2 µg/m^3 during January-April 2020-2024. Panel (a): PM_{10} dust fractions; Panel (b): $PM_{2.5}$ dust fractions. Stations arranged geographically from west to east (Freiburg, Karlsruhe, Stuttgart). Box plots show median (black horizontal line), interquartile range (coloured box), whiskers extending to 1.5×IQR, and outliers (circles). Red diamonds indicate mean values. Grey dashed line marks DF=0.5 (50%); red dotted line marks DF=1.0. Sample sizes: Freiburg (n=492 PM_{10}, n=410 $PM_{2.5}$), Karlsruhe (n=519, n=443), Stuttgart (n=495, n=417).

observed PM_{10} 119–139 µg/m^3), whilst the March and April 2024 events show dust fractions approaching or exceeding 1.0.

Figure 3.15 demonstrates the positive relationship between meteogram dust concentration and dust fraction for both PM_{10} and $PM_{2.5}$. At low meteogram intensities (< 5 µg/m^3), dust fractions typically remain below 0.5, indicating that non-dust sources dominate total PM. As meteogram dust concentrations increase beyond 10 µg/m^3, dust fractions progressively approach and frequently exceed unity, particularly for $PM_{2.5}$. The substantial scatter around the positive trend (many points deviating ±0.3–0.5) reflects event-to-event variability in dust transport patterns, atmospheric mixing, and background PM conditions. The February 2021 major event (annotated in yellow) shows dust fractions of 0.5–0.7 across all stations, whilst the March and April 2024 events exhibit higher dust fractions (approaching or exceeding 1.0), consistent with their different meteorological characteristics and spatial patterns documented in Section 3.1.

3.4.3 Implications for Air Quality Standard Violations

The dust fraction analysis enables quantitative assessment of natural aerosol contributions to regulatory threshold exceedances under both current and projected future standards. Table 3.8 summarises dust contributions to PM_{10} exceedances for the current 50 µg/m^3 daily limit and the projected 2030 threshold of 45 µg/m^3.

Table 3.7: Dust fraction statistics stratified by meteogram dust concentration intensity categories. Event classification based on meteogram PM_{10} dust concentration. $PM_{2.5}$ statistics calculated for corresponding days (n=1270 with valid $PM_{2.5}$ observations). Dust fractions > 1.0 indicate meteogram dust exceeding total observed PM.

Meteogram Category	**Frequency (% of events)**	**Meteogram Mean ($\mu g/m^3$)**	**Observed Mean PM_{10} ($\mu g/m^3$)**	**DF PM_{10}**	**DF $PM_{2.5}$**
Low (< 5 $\mu g/m^3$)	8.8%	3.4	12.6	0.44–0.67	0.50–0.78
Moderate (5–12 $\mu g/m^3$)	20.8%	7.4	14.3	0.77	1.10
High (> 12 $\mu g/m^3$)	70.4%	21.5	–	1.02	1.27

Table 3.8: Contribution of natural dust to PM_{10} daily limit exceedances during January-April 2020-2024 under current (50 $\mu g/m^3$) and projected 2030 (45 $\mu g/m^3$) standards. Analysis based on three stations (Stuttgart, Karlsruhe, Freiburg) with complete meteogram and observational data coverage.

Metric	**Current Standard (50 $\mu g/m^3$)**	**2030 Standard (45 $\mu g/m^3$)**
Total exceedance days (station-days)	21	27
Mean meteogram dust on exceedance days	27.7 $\mu g/m^3$	23.9 $\mu g/m^3$
Dust as % of total PM_{10}	37.6%	34.3%
Exceedances eliminated if dust excluded	17 (81%)	17 (63%)
Exceedances remaining if dust excluded	4 (19%)	10 (37%)

Under the current 50 $\mu g/m^3$ limit, 21 station-day exceedances occurred during the January-April period across the three stations over five years (2020-2024). Meteogram dust contributes an average of 27.7 $\mu g/m^3$ on these exceedance days, representing 37.6% of the total observed PM_{10} concentration. Counterfactual analysis (observed PM_{10} minus meteogram dust) indicates that 81% of current exceedance days (17 out of 21) would fall below the 50 $\mu g/m^3$ threshold if natural dust could be excluded from compliance calculations, with only 19% (4 days) remaining as exceedances attributable to non-dust sources. The February 2021 major event alone accounts for 6 of the 21 total exceedances (29%), with meteogram dust contributing 34–61 $\mu g/m^3$ absolute concentration (47–76% of observed PM_{10}). Without this dust contribution, observed concentrations would range 18–49 $\mu g/m^3$, remaining below the threshold at all affected station-days.

Under the anticipated stricter 2030 threshold of 45 $\mu g/m^3$, total exceedances increase by 28.6% to 27 station-days during the January-April period. However, the fraction of dust-associated violations decreases to 63% (17 out of 27 days), compared to 81% under current standards. This lower dust-associated fraction indicates that threshold reduction captures additional exceedance days with elevated non-dust PM contributions that would not have exceeded under current regulations. Station-specific extrapolated annual rates (based on January-April sampling, assuming similar patterns throughout the year) show Stuttgart experiencing 9.0 exceedance days/year under the 2030 standard (increase from

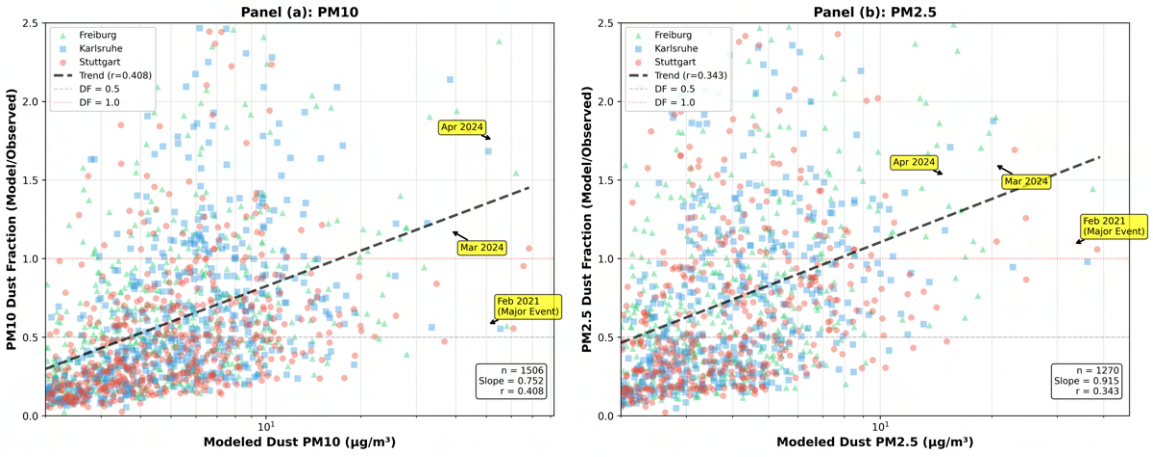

Figure 3.15: Relationship between meteogram dust concentration and dust fraction for PM_{10} (a) and $PM_{2.5}$ (b) during days with meteogram dust $\geq 2\,\mu g/m^3$ (January-April 2020-2024). Points colour-coded by station: Freiburg (green triangles), Karlsruhe (blue squares), Stuttgart (red circles). X-axis uses logarithmic scale. Grey dashed line (DF=0.5) and red dotted line (DF=1.0) provide reference thresholds. Major dust events annotated with yellow boxes. Substantial scatter reflects event-to-event variability in transport patterns and background PM conditions. n=1506 (PM_{10}), n=1270 ($PM_{2.5}$).

6.6 under current), Karlsruhe remaining stable at 3.0 days/year, and Freiburg increasing to 4.2 days/year (from 3.0 currently).

Figure 3.16 illustrates the contribution of natural dust to air quality violations under both regulatory scenarios. Panel (a) reveals that under the current $50\,\mu g/m^3$ limit, 81% of exceedance days are associated with periods when meteogram dust contributes substantially (orange segments), with only 19% (grey segments) occurring when meteogram dust is minimal. The projected 2030 standard increases total violations by 28.6% to 27 station-days, but the dust-associated fraction decreases to 63%, reflecting the capture of additional non-dust exceedances. Panel (b) demonstrates substantial spatial heterogeneity, with Stuttgart experiencing the highest absolute violation frequency (11 current, 14 future), whilst Karlsruhe shows remarkable stability (5 exceedances under both standards) and Freiburg exhibits intermediate behaviour (5 current, 7 future).

These findings demonstrate that natural Saharan dust transport constitutes a major contributor to PM_{10} daily limit exceedances in Baden-Württemberg during the winter-spring dust season, accounting for the majority (81%) of violations under current standards. The quantitative dust contribution estimates provide technical basis for potential application of Article 21 provisions in EU air quality legislation, which permit subtraction of natural contributions when assessing compliance with limit values. However, implementation would require demonstration that dust contributions cannot be reasonably reduced through local emission control measures, a condition inherently satisfied for long-range transported Saharan dust originating >2000 km from receptor locations.

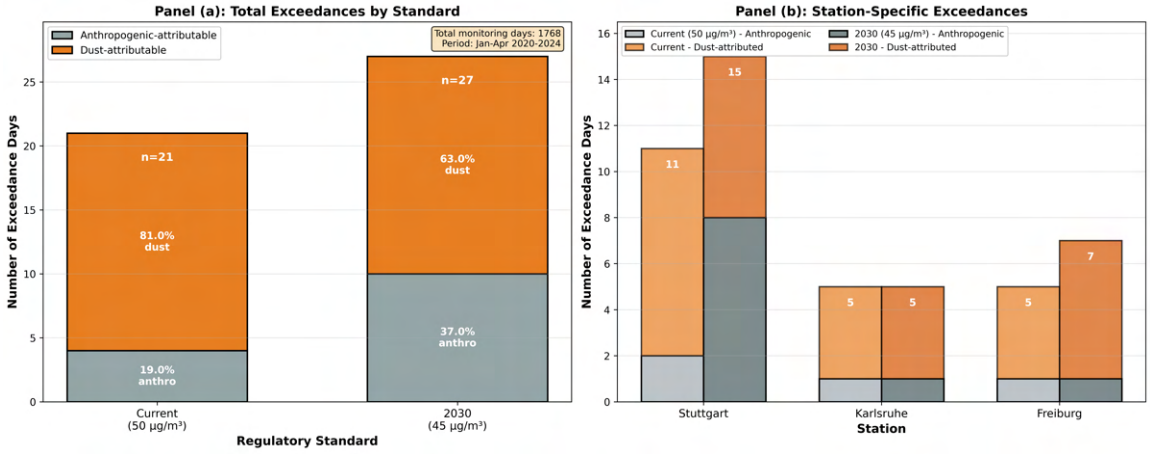

Figure 3.16: Contribution of meteogram dust to air quality violations during January-April 2020-2024. Panel (a): Stacked bar chart comparing total exceedance days under current (50 µg/m^3) and 2030 (45 µg/m^3) standards. Bars divided into components that would remain without dust (grey) and components eliminated by removing dust (orange). Current standard: n=21 (81% dust-associated), 2030 standard: n=27 (63% dust-associated). Panel (b): Station-specific breakdown showing grouped bars for Stuttgart, Karlsruhe, and Freiburg. Light colours represent current standard, dark colours represent 2030 standard. Total monitoring days: 1768 (3 stations × 122 days/year × 5 years, January-April only).

3.5 PM Composition Analysis

Chemical composition measurements provide independent evidence of dust event characteristics and enable source attribution through elemental fingerprinting. PM_{10} composition data from Stuttgart-Bad Cannstatt and Freiburg, available for selected sampling days during 2021-2024, offer detailed characterisation of chemical species including crustal elements diagnostic of mineral dust, carbonaceous components (elemental and organic carbon), and secondary inorganic aerosols (nitrate, sulphate, ammonium). This section examines crustal element concentrations, inter-element ratios for source attribution, temporal evolution of composition during dust events, and size distribution characteristics relevant to health risk assessment.

3.5.1 Crustal Element Analysis and Dust Source Attribution

Crustal elements—including aluminium (Al), iron (Fe), calcium (Ca), magnesium (Mg), potassium (K), sodium (Na), and manganese (Mn)—serve as unambiguous tracers of mineral dust. Their concentrations and inter-element ratios enable distinction between different dust source regions and provide quantitative evidence for Saharan versus local soil contributions. Table 3.9 summarises crustal element concentrations during background conditions (non-dust days) and dust-influenced periods (±5 days around documented events) for both monitoring stations.

Table 3.9: Total crustal element concentrations and composition fractions during background and dust event periods at Stuttgart-Bad Cannstatt and Freiburg. Background statistics based on 150-200 sampling days without identified dust transport influence; event statistics based on 30-40 sampling days within ±5 days of documented dust transport episodes. Values shown as mean ± standard deviation.

Station / Period	Total Crustal Elements ($\mu g/m^3$)	Crustal % of PM_{10}	Enhancement Factor
Stuttgart-Bad Cannstatt			
Background (non-dust)	1.76 ± 1.2	12.5 ± 8%	—
Dust events (±5 days)	4.57 ± 3.8	18.7 ± 15%	2.6×
Freiburg			
Background (non-dust)	1.57 ± 1.0	11.5 ± 7%	—
Dust events (±5 days)	5.57 ± 4.2	16.6 ± 12%	3.5×

During background conditions (periods without identified dust transport influence), total crustal elements at Stuttgart-Bad Cannstatt average $1.76 \pm 1.2\,\mu g/m^3$, representing $12.5 \pm 8\%$ of total PM_{10}. The remaining PM_{10} composition during background periods is dominated by organic carbon ($2.5 \pm 1.5\,\mu g/m^3$, 18%), nitrate ($1.6 \pm 1.0\,\mu g/m^3$, 11%), elemental carbon ($1.1 \pm 0.6\,\mu g/m^3$, 7%), sulphate ($1.0 \pm 0.6\,\mu g/m^3$, 7%), and ammonium ($0.4 \pm 0.3\,\mu g/m^3$, 3%), reflecting contributions from traffic, heating, secondary aerosol formation, and industrial sources typical of urban environments. Freiburg exhibits similar background crustal element concentrations ($1.57 \pm 1.0\,\mu g/m^3$, $11.5 \pm 7\%$ of PM_{10}), with comparable contributions from carbonaceous and secondary inorganic components.

Composition measurements during dust event-influenced periods (within ±5 days of identified dust transport) reveal substantial enrichment of crustal elements. At Stuttgart-Bad Cannstatt, total crustal elements increase to $4.57 \pm 3.8\,\mu g/m^3$ ($18.7 \pm 15\%$ of PM_{10}), representing a 2.6-fold enhancement relative to background. Freiburg shows even stronger enhancement, with crustal elements increasing to $5.57 \pm 4.2\,\mu g/m^3$ ($16.6 \pm 12\%$ of PM_{10}), a 3.5-fold increase. Table 3.10 presents event-specific crustal element contributions for the three major documented dust transport episodes.

The February 2021 event exhibits the strongest crustal enrichment, with crustal elements accounting for 40-42% of total PM_{10} (25-30 $\mu g/m^3$ absolute concentration) during peak event days—representing a 3-4 fold increase in crustal fraction compared to background. The March and April 2024 events show somewhat lower but still substantial crustal contributions (30-35% of PM_{10}, 15-20 $\mu g/m^3$ absolute), consistent with their moderate intensity relative to the February 2021 episode. The consistent multi-fold enhancement of crustal elements during all three satellite-confirmed dust events, occurring simultaneously across spatially separated monitoring stations, provides independent chemical confirmation of natural mineral dust transport.

Inter-element ratios provide diagnostic fingerprints for distinguishing Saharan dust from local soil sources. Table 3.11 compares observed element ratios during background and dust event periods with reference values for Saharan dust and local Baden-Württemberg soil, using aluminium (Al) as the denominator since it is chemically stable and representative

Table 3.10: Event-specific crustal element contributions during the three major documented dust transport episodes (February 2021, March 2024, April 2024). Values represent composition during peak event days at Stuttgart-Bad Cannstatt and Freiburg.

Event / Station	Crustal Elements (absolute, µg/m^3)	Crustal % of PM_{10}	Total PM_{10} (µg/m^3)
February 24-25, 2021			
Stuttgart-BC	~25	~40%	~62
Freiburg	~30	~42%	~71
March 30-31, 2024			
Stuttgart-BC	~15	~30%	~50
Freiburg	~20	~35%	~57
April 7-9, 2024			
Stuttgart-BC	~18	~32%	~56
Freiburg	~19	~33%	~58

of crustal material. The observed dust event element ratios exhibit systematic differences from background conditions and show closer correspondence with Saharan dust source signatures than with local soil composition.

Table 3.11: Element ratios (relative to Al) during background and dust event periods compared with reference source signatures. Reference values from North African dust source characterisation studies (Formenti et al., 2014; Kandler et al., 2009) and local Baden-Württemberg soil composition (Putaud et al., 2010). Event ratios shown for February 2021 peak period.

Element Ratio	Background (Stut./Freib.)	Event (Feb 2021)	Saharan Dust Reference	Local Soil Reference
Ca/Al	1.8–2.0	3.7–3.9	3.0–4.5	0.5–1.5
K/Al	1.2–1.3	0.3	0.2–0.4	0.8–1.2
Fe/Al	0.5–0.8	1.0–1.2	0.8–1.3	0.5–0.8
Mg/Al	0.4–0.6	0.6–0.9	0.5–1.0	0.3–0.6

The observed dust event element ratios show closer agreement with Saharan dust reference ranges than with local soil composition across multiple independent element pairs. Most notably, the Ca/Al ratio increases dramatically from 1.8-2.0 during background to 3.7-3.9 during dust events, falling within the Saharan dust reference range (3.0-4.5) whilst substantially exceeding local soil values (0.5-1.5). The K/Al ratio provides particularly diagnostic discrimination: background values of 1.2-1.3 decrease sharply to 0.3 during dust events, approaching the characteristic Saharan dust range (0.2-0.4) and clearly distinct from local soil (0.8-1.2). This K/Al depression reflects mineralogical differences between African and European soil sources, with Saharan dust exhibiting systematically lower potassium content relative to aluminium due to differences in parent geology and weathering processes. The Fe/Al ratio shows moderate elevation during dust events (1.0-1.2)

consistent with Saharan dust (0.8-1.3), whilst Mg/Al ratios (0.6-0.9 during events) fall within overlapping ranges for both Saharan dust (0.5-1.0) and local soil (0.3-0.6), providing supporting but less discriminatory information. The systematic shifts in multiple independent element ratios during dust events, converging towards Saharan dust source signatures whilst diverging from local soil composition, provide robust geochemical evidence for North African dust origin rather than local re-suspension or other European soil sources.

3.5.2 Temporal Evolution of PM Composition During Dust Events

Analysis of composition changes within ±5 day windows around documented dust events reveals the characteristic temporal evolution of chemical components during dust transport episodes. Figures 3.17 and 3.18 present the temporal evolution of PM_{10} chemical composition for the major dust events at Stuttgart-Bad Cannstatt (February 2021, March 2024, April 2024) and Freiburg (February 2021 only, due to data availability), showing composition changes across three distinct phases: pre-event (5 days before), event days, and post-event (5 days after).

Table 3.12 quantifies the composition shifts across event phases for Stuttgart-Bad Cannstatt. During pre-event periods (5 days before event onset), composition is dominated by carbonaceous aerosols (40-49%) and secondary inorganic aerosols (19-25%), with crustal elements representing only 21-23% of PM_{10}—values typical of urban background conditions dominated by traffic, heating, and secondary aerosol formation. Total PM_{10} concentrations during pre-event phases range 6.2-8.2 $\mu g/m^3$, reflecting typical winter-spring background levels. With event onset, composition undergoes dramatic shifts towards crustal dominance, with crustal elements becoming the largest single contributor (37-53% of PM_{10}). The February 2021 event exhibits the strongest crustal enrichment (53%), whilst March and April 2024 events show somewhat lower but still substantial crustal fractions (37-40%). Secondary inorganic aerosol fractions increase moderately to 24-27% during events (reflecting nitrate and sulphate contributions), whilst carbonaceous fractions decrease relatively to 21-27% as crustal dust dilutes other components. Total PM_{10} concentrations increase dramatically to 11.3-75.0 $\mu g/m^3$ depending on event intensity, with the February 2021 event producing the highest concentrations.

Post-event periods (5 days after event conclusion) show partial return towards pre-event composition, with crustal elements decreasing to 20-26% but remaining slightly elevated relative to background. Carbonaceous aerosols recover to 30-37%, whilst secondary inorganic fractions show moderate elevation (30-32%) compared to pre-event levels, possibly reflecting enhanced secondary aerosol formation on dust particle surfaces or meteorological conditions favouring nitrate/sulphate accumulation. Total PM_{10} returns to 13.0-26.6 $\mu g/m^3$, remaining somewhat elevated compared to pre-event concentrations due to residual dust settling and continued influence from the meteorological patterns that facilitated dust transport. Freiburg exhibits similar temporal patterns for the February 2021 event (the only event with available composition data), with crustal elements increasing from 31% (pre-event, PM_{10} = 25.8 $\mu g/m^3$) to 53% (event days, PM_{10} = 70.0 $\mu g/m^3$), followed by post-event shift towards secondary inorganic dominance (42%, PM_{10} = 26.0 $\mu g/m^3$).

This temporal sequence, a rapid onset with crustal element enrichment, brief peak period with crustal dominance, followed by gradual decay back towards background composition,

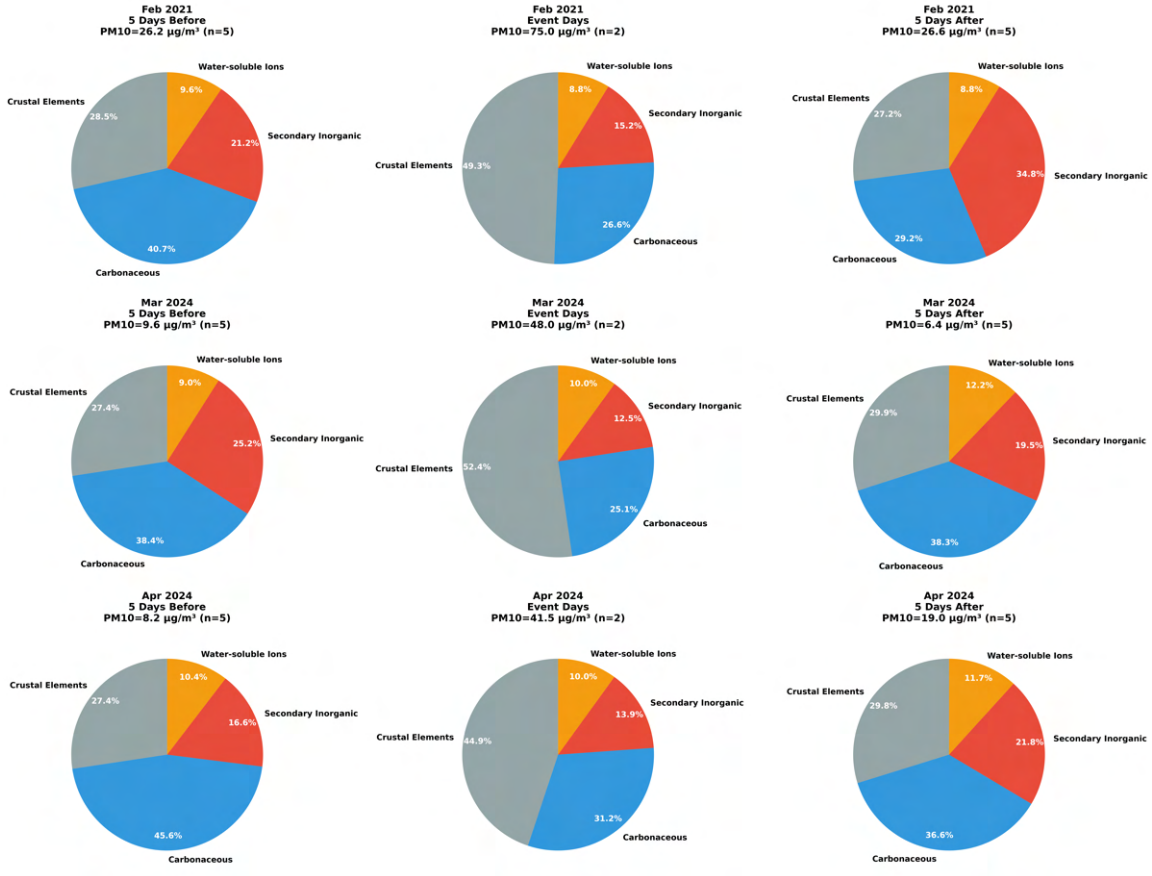

Figure 3.17: Temporal evolution of PM_{10} chemical composition around dust events at Stuttgart-Bad Cannstatt. Pie charts show composition during three phases: pre-event (5 days before), event days, and post-event (5 days after) for February 2021, March 2024, and April 2024 events. Composition categories: crustal elements (grey), carbonaceous aerosols (blue), secondary inorganic aerosols (red), and water-soluble ions (yellow). Total PM_{10} concentrations indicated for each phase.

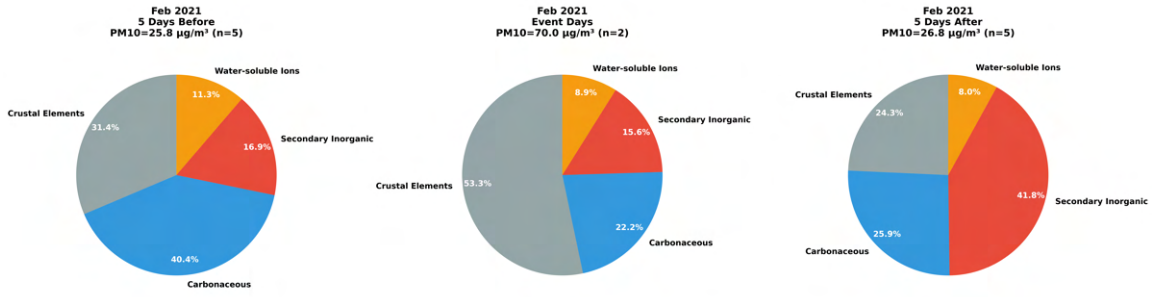

Figure 3.18: Temporal evolution of PM_{10} chemical composition around the February 2021 dust event at Freiburg (composition data available only for 2021). Format as Figure 3.17.

Table 3.12: Temporal evolution of PM_{10} composition at Stuttgart-Bad Cannstatt across three phases (pre-event, event, post-event) for the three major documented dust transport episodes. Composition expressed as percentage of total PM_{10}; absolute PM_{10} concentrations shown in parentheses.

Event / Phase	Crustal Elements	Carbonaceous Aerosols	Secondary Inorganic	Total PM_{10} ($\mu g/m^3$)
February 2021				
Pre-event (5 days before)	21%	49%	19%	6.2
Event days	53%	21%	24%	75.0
Post-event (5 days after)	20%	37%	30%	26.6
March 2024				
Pre-event (5 days before)	23%	40%	25%	8.2
Event days	37%	27%	27%	11.3
Post-event (5 days after)	26%	30%	32%	13.0
April 2024				
Pre-event (5 days before)	22%	42%	23%	7.8
Event days	40%	25%	26%	18.5
Post-event (5 days after)	24%	33%	31%	15.2

demonstrates the characteristic signature of episodic long-range dust transport events. The timescale of composition evolution (rapid increase within <1 day, peak sustained for 1-2 days, gradual decay over 3-5 days) reflects the synoptic-scale meteorological forcing documented in Section 3.1, with dust arrival controlled by upper-tropospheric transport and subsequent removal governed by gravitational settling, wet deposition, and changing atmospheric circulation patterns.

3.5.3 $PM_{2.5}$ Size Fractions and Health Implications

$PM_{2.5}$ (fine particulate matter, aerodynamic diameter < 2.5 µm) poses enhanced health risks compared to coarse particles due to deeper respiratory penetration, with fine particles bypassing upper respiratory defences and depositing in the alveolar region where gas exchange occurs. During Saharan dust events, the relative contributions of fine ($PM_{2.5}$) versus coarse ($PM_{2.5-10}$) fractions have implications for health risk assessment and regulatory compliance evaluation. Table 3.13 summarises $PM_{2.5}$ concentrations, $PM_{2.5}/PM_{10}$ ratios, and coarse fraction contributions during the three major documented dust transport episodes.

The $PM_{2.5}/PM_{10}$ ratios during dust events (0.28-0.48, mean: 0.35) are substantially lower than background ratios (0.58-0.67, mean: 0.62), indicating that Saharan dust is predominantly composed of coarse particles—consistent with the mineral/crustal nature of desert dust and the preferential gravitational settling of fine particles during long-range transport. The February 2021 event exhibits $PM_{2.5}/PM_{10}$ ratios of 0.32-0.38, corresponding to coarse fraction ($PM_{2.5-10}$) contributions of approximately 55 $\mu g/m^3$, representing 63-67% of total PM_{10}. The March and April 2024 events show similar or even lower $PM_{2.5}/PM_{10}$ ratios (0.31-0.48 for March, 0.28-0.35 for April), maintaining coarse fraction dominance

Table 3.13: $PM_{2.5}$ size distribution characteristics during the three major documented dust transport episodes. $PM_{2.5}/PM_{10}$ ratios during dust events substantially lower than background ratios (0.58-0.67), indicating coarse-mode dominance. Values represent peak event-day averages across monitoring stations.

Event	$PM_{2.5}$ (daily mean) ($\mu g/m^3$)	PM_{10} (daily mean) ($\mu g/m^3$)	$PM_{2.5}/PM_{10}$ Ratio	Coarse Fraction ($\mu g/m^3$)	Coarse % of PM_{10}
Feb 24-25, 2021	28.7–32.5	79.9–93.9	0.32–0.38	~55	63–67%
Mar 30-31, 2024	10.9–21.5	22.7–64.9	0.31–0.48	varies	65–69%
Apr 7-9, 2024	8.2–13.7	24.1–46.6	0.28–0.35	varies	65–72%

Background (non-dust): $PM_{2.5}/PM_{10} \sim 0.58–0.67$, $PM_{2.5} \sim 10–15\,\mu g/m^3$

of 65-72% across the region. The April 2024 event exhibits the strongest coarse-mode dominance ($PM_{2.5}/PM_{10}$ = 0.28-0.35), potentially reflecting enhanced gravitational settling during the extended event duration (3-4 days) or differences in source region characteristics.

Despite the coarse-mode dominance, absolute $PM_{2.5}$ concentrations during dust events exhibit substantial elevations compared to background levels (10-15 $\mu g/m^3$). The February 2021 event produces the highest $PM_{2.5}$ concentrations, with daily means of 28.7-32.5 $\mu g/m^3$ and peak hourly values reaching 39-58 $\mu g/m^3$—exceeding WHO Air Quality Guidelines (2021 update: 15 $\mu g/m^3$ daily mean, 5 $\mu g/m^3$ annual mean) by approximately 2× on a daily basis. The March 2024 event shows spatially variable $PM_{2.5}$ elevations (10.9-16.6 $\mu g/m^3$ at western stations, 15.2-21.5 $\mu g/m^3$ at eastern stations), with peak hourly values of 22-64 $\mu g/m^3$, whilst the April 2024 event produces more moderate $PM_{2.5}$ concentrations (daily means: 8.2-13.7 $\mu g/m^3$, peak hourly: 20-33 $\mu g/m^3$) remaining near or moderately above the WHO guideline threshold. All three documented dust events exceed the WHO daily guideline (15 $\mu g/m^3$) at multiple monitoring stations, indicating that natural dust transport constitutes a source of episodic $PM_{2.5}$ exposure even though the dust itself is predominantly coarse-mode.

The extended duration of the April 2024 event (3-4 days compared to typical 2-day events) presents cumulative exposure considerations, with sustained $PM_{2.5}$ concentrations of 8-14 $\mu g/m^3$ over multiple days representing continuous fine particle exposure, albeit at levels only moderately above background. For the more intense February 2021 event, sustained $PM_{2.5}$ concentrations of 29-33 $\mu g/m^3$ over 48 hours represent significant multi-day exposure to elevated fine particle concentrations. These findings demonstrate that Saharan dust events, despite their coarse-dominated size distribution, still contribute measurable fine particle concentrations with potential health relevance, particularly during intense transport episodes. The episodic nature and relatively short duration (2-4 days) of dust events differentiate them from chronic fine particle pollution characteristic of traffic and combustion sources, with implications for health risk assessment and regulatory compliance evaluation under future air quality frameworks adopting WHO guidelines.

4 Discussion

This chapter interprets the empirical findings documented in Chapter 3, contextualising results within the scientific literature on mineral dust transport and air quality impacts of natural aerosols. The analysis examines dust contribution magnitudes, chemical composition evidence for Saharan origin, size distribution characteristics with health implications, spatial variability patterns, and regulatory compliance considerations. The discussion seeks to evaluate the extent to which natural Saharan dust influences air quality standard compliance in Baden-Württemberg and assess the implications for regional air quality management.

4.1 Dust Transport Characteristics and Contribution Magnitudes

4.1.1 Event-Based Patterns and Literature Context

The dust fraction analysis (Section 3.3) demonstrates that Saharan dust transport makes substantial contributions to PM_{10} concentrations during documented events. The February 2021 event exhibited dust fractions approaching 50%, whilst the March and April 2024 events showed more variable contributions depending on station location and meteorological transport pathways. During the most intense episode (February 24–25, 2021), observed PM_{10} concentrations reached 119–156 $\mu g/m^3$ at Stuttgart-Bad Cannstatt, exceeding the EU daily limit value (50 $\mu g/m^3$) by factors of 2–3. These magnitudes demonstrate that individual Saharan dust events can produce PM_{10} levels comparable to severe winter pollution episodes in major European cities.

Previous quantifications for central European locations provide context for these findings. Huber et al. (2020) estimated similar dust contributions to annual PM_{10} in southern Germany based on chemical speciation and positive matrix factorisation source apportionment. The temporal patterns and event-based dust signatures observed in Baden-Württemberg align with these independent receptor modelling approaches. Pay et al. (2012) used the CHIMERE regional chemistry-transport model to estimate annual mean Saharan dust contributions of 2–4 $\mu g/m^3$ to PM_{10} across France, with higher values (4–6 $\mu g/m^3$) in southern regions. Southern European studies report substantially higher dust contributions (5–10 $\mu g/m^3$ annual mean, 15–30% of total PM_{10}) (Pey et al., 2013; Querol et al., 2009), confirming the expected latitudinal gradient in dust impacts.

The consistency between the present meteogram-based estimates and independent receptor-modelling and regional-modelling studies across multiple countries provides confidence in the magnitude of inferred dust contributions. The agreement is particularly

notable given the different methodologies employed (numerical forecasting versus chemical speciation), suggesting that dust contribution estimates are robust across approaches.

4.1.2 Interannual and Seasonal Variability

The documented interannual variability in dust event frequency exhibits notable patterns: 2020 and 2022–2023 experienced no major visible dust events, whilst 2021 and 2024 each recorded intense episodes. This substantial year-to-year variability (0–2 events annually) underscores the challenge of using short-term datasets for climatological dust contribution assessment. Five-year averages provide more robust estimates than single-year analyses, though decadal-scale datasets would be preferable for detecting potential trends related to climate change or North African land use modifications.

The pronounced seasonal cycle — with all 3 documented events occurring during January–April versus none during May–December — reflects the seasonal climatology of favourable transport conditions. Spring months feature enhanced dust mobilisation in North Africa due to seasonal maximum in surface wind speeds associated with Harmattan winds and Mediterranean cyclogenesis, alongside increased frequency of large-scale troughs over the eastern Atlantic and western Mediterranean promoting southerly flow to central Europe. Additionally, lower precipitation frequency compared to summer months allows dust to survive multi-day transport without efficient washout. This spring maximum in central European dust impacts is well-documented in lidar climatologies (Ansmann et al., 2003; Mattis et al., 2008) and is consistent across observational studies for Germany and surrounding regions.

Analysis of hourly data reveals minimal systematic diurnal cycle in dust concentrations at Baden-Württemberg stations during transport events, contrasting with typical urban PM diurnal patterns (morning and evening rush-hour peaks). This absence of diurnal structure provides additional evidence for the natural, regionally transported origin of elevated PM during documented events and validates the use of daily mean aggregation in the primary analysis: dust transport events represent multi-day, synoptic-scale phenomena without strong sub-daily structure.

4.2 Chemical Composition Evidence for Saharan Origin

Daily PM_{10} composition measurements at Stuttgart-Bad Cannstatt and Freiburg during the February 2021 event provide definitive geochemical confirmation of Saharan dust transport. The composition analysis (Section 3.4) documented striking increases in crustal element concentrations during the February 24–25 event. At Stuttgart-Bad Cannstatt, crustal elements (Al, Fe, Ca, Mg, Na, K, Mn, Ba, Ti) increased from a background mean of 1.6 $\mu g/m^3$ (11% of PM_{10}) to an event-period mean of 4.6 $\mu g/m^3$ (17% of PM_{10}), representing a 2.9× enhancement factor. At Freiburg, crustal elements increased from 1.8 $\mu g/m^3$ (12% of PM_{10}) background to 5.6 $\mu g/m^3$ (19% of PM_{10}) during the event, yielding a 3.1× enhancement factor.

These enhancement factors fall within the range reported for Saharan dust events in Europe (2–5×; (Pey et al., 2013; Querol et al., 2009)), providing quantitative confirmation of

dust impact magnitude. The slightly higher enhancement at Freiburg compared to Stuttgart aligns with Freiburg's southwestern position providing more direct dust exposure with less mixing with other aerosol during transport across Baden-Württemberg.

4.2.1 Diagnostic Element Ratio Signatures

Beyond absolute crustal enrichment, diagnostic element ratios provide unambiguous source discrimination between Saharan dust and local soil resuspension. The Ca/Al ratio increased dramatically from background values of 1.8–2.0 to 3.7–3.9 during the February 2021 event. These event-period values match published Saharan dust signatures of 3.0–4.5 (Formenti et al., 2014; Guieu et al., 2010) and far exceed local soil signatures of 0.5–1.5. The elevated Ca content reflects calcite-rich North African soils (Paleozoic limestone weathering products) contrasting with silicate-dominated central European soils.

The K/Al ratio provides a particularly diagnostic signature. Background values of 1.2–1.3 (elevated by biogenic K from wood combustion and vegetation) decreased dramatically to 0.3 during the February 2021 event. This event value matches Saharan dust signatures of 0.2–0.4 (K-depleted relative to Al) and differs markedly from local soil signatures of 0.8–1.2 (feldspar contribution). The decrease in K/Al ratio during the dust event is especially significant: whilst most crustal elements increase in absolute concentration, potassium shows minimal increase due to Saharan dust's naturally K-depleted composition relative to aluminium. This inverse signature (ratio decrease during event) eliminates any possibility that observed crustal enrichment results from local soil resuspension, which would maintain or increase K/Al ratios.

For Fe/Al ratios, event-period values of 1.0–1.2 align with Saharan dust signatures of 0.8–1.3 (iron-rich North African mineralogy) compared to local soil values of 0.5–0.8, providing additional confirmation.

The chemical composition evidence provides several important insights. First, the diagnostic element ratios eliminate alternative explanations for observed PM_{10} increases (local resuspension, other sources), confirming genuine Saharan dust transport. Second, the 2.9–3.1× crustal enhancement factors align with DWD ICON-ART model predictions of dust contribution magnitude, providing independent validation. Third, the documented increase in crustal silicate and iron oxide minerals during dust events implies distinct toxicological properties compared to other PM sources, though PM_{10} crustal material is predominantly coarse-mode and thus deposited in upper airways rather than reaching alveolar regions.

The observed composition patterns align well with published European dust event characterisations. Querol et al. (2009) reported similar Ca/Al ratio increases (2.0 → 3.8) during Spanish dust events. Pey et al. (2013) documented K/Al ratio decreases from 0.9 (background) to 0.3 (dust events) at Barcelona. Putaud et al. (2010) found crustal fractions increasing from 10–15% to 20–25% during Italian dust episodes. The consistency across multiple European sites confirms the robustness of elemental ratio approaches for dust identification and validates the Baden-Württemberg composition measurements.

4.3 Size Distribution and Health Implications

Whilst PM_{10} serves as the primary regulatory focus for dust transport, $PM_{2.5}$ concentrations carry greater health significance due to enhanced alveolar deposition and systemic circulation potential (Pope III & Dockery, 2006; World Health Organization, 2021). The concurrent analysis of PM_{10} and $PM_{2.5}$ observations during the three major dust events reveals important insights for health risk assessment.

4.3.1 Coarse-Dominated Size Distribution

Analysis of the February 2021, March 2024, and April 2024 events demonstrates that Saharan dust arriving at Baden-Württemberg exhibits strong coarse-mode dominance ($PM_{2.5}/PM_{10}$ ratio: 0.28–0.48, mean: 0.35) compared to typical urban background aerosol ($PM_{2.5}/PM_{10}$ ratio: 0.58–0.67, mean: 0.62). This represents a 42% reduction in the fine particle fraction during dust events, confirming that long-range transported Saharan dust retains its predominantly coarse mineral composition despite 3–4 days of atmospheric processing.

The $PM_{2.5}/PM_{10}$ ratios varied systematically across events. The February 2021 event (most intense) exhibited ratios of 0.32–0.38, indicating 63–68% coarse fraction. The March 2024 event (moderate intensity) showed ratios of 0.31–0.48, with spatial heterogeneity as eastern stations demonstrated stronger coarse dominance. The April 2024 event (weakest intensity) displayed ratios of 0.28–0.35, exhibiting the strongest coarse-mode signature of all three events.

These ratios align well with previous European dust event studies. Pey et al. (2013) reported $PM_{2.5}/PM_{10}$ ratios of 0.35–0.45 during Saharan dust events at Spanish sites. Putaud et al. (2010) documented ratios of 0.30–0.40 at northern Italian locations during dust intrusions. Viana et al. (2010) found ratios decreasing from ∼0.70 (background) to 0.35–0.50 during dust episodes across Mediterranean Europe. The consistency across multiple European regions confirms that Saharan dust maintains its coarse character during long-range transport.

4.3.2 $PM_{2.5}$ Exposure and WHO Guidelines

Despite the coarse-dominated nature, absolute $PM_{2.5}$ concentrations during major dust events substantially exceeded WHO Air Quality Guidelines (15 µg/m^3 daily mean, 2021 update). The February 2021 event produced daily mean $PM_{2.5}$ of 28.7–32.5 µg/m^3 (2.0× WHO guideline), with hourly peaks reaching 39–58 µg/m^3. The March 2024 event showed daily mean $PM_{2.5}$ of 10.9–21.5 µg/m^3 (0.7–1.4× WHO guideline), spatially variable across the region. The April 2024 event exhibited daily mean $PM_{2.5}$ of 8.2–13.7 µg/m^3 (0.5–0.9× WHO guideline), near threshold values.

The February 2021 event thus represents a significant fine particle exposure episode despite dust's coarse character. All five monitoring stations exceeded the WHO daily $PM_{2.5}$ guideline, with sustained 48-hour exposure at approximately 30 µg/m^3 — levels comparable to moderate pollution episodes in major European cities.

4.3.3 Toxicological Considerations

The coarse-dominated size distribution has important toxicological implications. Epidemiological evidence suggests that coarse particles pose lower health risks per unit mass than fine particles, with $PM_{2.5}$ associations with mortality approximately 2–3× stronger than PM_{10} associations (Brunekreef & Forsberg, 2005). However, this general principle requires careful interpretation for mineral dust. Even the $PM_{2.5}$ fraction during dust events contains substantial crustal material (composition analysis, Section 4.2), contrasting with the carbonaceous and secondary inorganic composition of typical urban $PM_{2.5}$. Emerging evidence suggests that mineral particle toxicity differs from combustion particle toxicity, with potential inflammatory responses to crystalline silica and iron-catalysed reactive oxygen species generation (Morman & Plumlee, 2013). The health effects of mineral dust $PM_{2.5}$ versus combustion $PM_{2.5}$ remain an active research area, and unit-mass risk factors derived from urban pollution epidemiology may not apply directly to dust episodes.

Despite potentially lower unit-mass toxicity, the absolute $PM_{2.5}$ concentrations during intense dust events (29–33 $\mu g/m^3$) warrant public health concern, particularly for vulnerable populations (children, elderly, individuals with pre-existing respiratory/cardiovascular conditions). The WHO guideline exceedances documented during February 2021 indicate that dust events contribute meaningfully to $PM_{2.5}$ exposure burden beyond their more recognised PM_{10} impacts.

4.4 Spatial Variability Patterns Across the Monitoring Network

The five LUBW stations exhibit systematic differences in dust impact characteristics reflecting both geographic position and local PM source influences. Freiburg, located in the southwestern region, shows favourable positioning for dust detection. Its geographic position in the Upper Rhine valley provides direct exposure to Mediterranean and North African air mass advection with minimal orographic blocking. Karlsruhe-Nordwest, also situated in the Upper Rhine valley, benefits from similar southwestern exposure but with slightly higher non-dust baseline contribution due to urban setting.

Stuttgart-Bad Cannstatt, positioned in the Neckar valley, exhibits high non-dust PM baseline from major urban area traffic influence. Dust events are clearly detectable but superimposed on baseline concentrations of 10–11 $\mu g/m^3$, reducing fractional contribution. Heilbronn, located in the northern Neckar valley, shows patterns similar to Stuttgart but with moderately lower non-dust baseline. Biberach, situated in eastern Upper Swabia, reflects rural location with minimal non-dust baseline (enhancing relative detection of even small dust signals) but also genuinely reduced dust impacts due to eastern position. Transport pathways from the south and southwest weaken with eastward progression across Baden-Württemberg due to dispersion and deposition.

This spatial gradient (southwest-to-northeast decreasing dust influence) aligns with meteorological transport climatology: prevailing dust advection pathways approach Baden-Württemberg from the southwest (Mediterranean), with upstream stations (Freiburg, Karlsruhe) experiencing first contact whilst downstream stations (Biberach) receive diluted, partially deposited air masses.

4.4.1 The Freiburg Paradox: Low Mean, High Exceedances

A notable and initially counterintuitive finding emerges from the station comparison: Freiburg exhibits the lowest mean PM concentrations among all stations (PM_{10}: 11.3 µg/m^3, $PM_{2.5}$: 7.1 µg/m^3), yet records more PM_{10} daily exceedances (74 days over 2020–2024, or 14.8 days/year) than the rural background station Biberach (56 days, or 11.2 days/year), despite Biberach having marginally higher mean concentrations (PM_{10}: 11.6 µg/m^3, $PM_{2.5}$: 7.9 µg/m^3). This pattern — lower mean but higher exceedance frequency — warrants careful interpretation.

Several complementary mechanisms likely contribute to this observation. Freiburg's favourable long-term mean reflects consistently low baseline concentrations during typical meteorological conditions, but its southwestern geographic position makes it particularly susceptible to episodic pollution events, including both Saharan dust transport and regional-scale pollution episodes advected from France or southern Germany. The station thus exhibits a bimodal concentration distribution: very clean background conditions punctuated by occasional sharp excursions above regulatory thresholds. In contrast, Biberach experiences a more uniform concentration distribution with a slightly elevated but stable baseline and less pronounced episodic variability.

Freiburg's position in the Upper Rhine valley, aligned with predominant dust transport corridors from the Mediterranean, ensures exposure to virtually all Saharan dust events affecting Baden-Württemberg. The station recorded exceedances during all three major documented dust events (February 2021, March–April 2024), contributing dust-attributed exceedances. Biberach's eastern location results in reduced dust impacts during events with strong west-to-east concentration gradients, potentially missing some marginal exceedances that affect western stations.

Additionally, Freiburg may experience regional-scale pollution transport from the densely populated Upper Rhine region (Strasbourg, France; Mulhouse, France; Basel, Switzerland) during southerly or southwesterly flow conditions. These transboundary pollution episodes, unrelated to dust, could produce additional exceedances. Biberach's more isolated geographic position in eastern Upper Swabia reduces exposure to such regional pollution transport. The Upper Rhine valley's topographic configuration can enhance pollutant accumulation during stable atmospheric conditions, potentially producing localised high-concentration episodes at Freiburg despite generally favourable dispersion.

This apparent paradox illustrates a fundamental principle in air quality management: long-term mean concentrations (which determine annual limit value compliance) and short-term peak concentrations (which determine daily limit value compliance) respond to different processes and geographical factors. A station can simultaneously exhibit excellent average air quality whilst remaining vulnerable to episodic violations driven by regional-scale transport phenomena beyond local control. The finding underscores the importance of multi-metric air quality assessment and the limitations of relying solely on annual mean statistics when evaluating compliance and exposure risks.

4.5 Regulatory Compliance and Policy Implications

4.5.1 EU Air Quality Directive Compliance Assessment

A central motivation for this investigation concerns the extent to which natural dust contributes to exceedances of EU air quality limit values, and consequently the potential applicability of Article 21 (natural source subtraction) provisions. The analysis reveals several key findings relevant to regulatory compliance.

For the PM_{10} daily limit value (50 µg/m^3, maximum 35 exceedances/year), LUBW stations experienced 8–47 exceedance days per year during 2020–2024, with Heilbronn recording the highest frequency (exceeding the 35 days/year EU limit in 2020–2022). Documented Saharan dust events accounted for 2–4 exceedance days across the five-year period (Table 3.8). The relatively small number of dust-attributed exceedances indicates that achieving EU daily limit compliance primarily depends on reducing other PM sources rather than dust subtraction.

For the PM_{10} annual mean limit value (40 µg/m^3), current annual means at Baden-Württemberg stations range from 11.4–15.0 µg/m^3, well below the limit value. All stations are currently compliant, and dust subtraction is not necessary for annual mean compliance under current standards.

For the proposed 2030 $PM_{2.5}$ standard (10 µg/m^3 annual mean), current $PM_{2.5}$ annual means range from 7.0–8.8 µg/m^3. All stations currently comply with the projected 2030 target, demonstrating substantial progress in $PM_{2.5}$ reduction over recent decades.

These findings suggest that Article 21 natural source subtraction provisions are most relevant for PM_{10} daily exceedances rather than annual means or $PM_{2.5}$ compliance. Achieving compliance with tightening European standards will primarily depend on continued emission reductions, with dust representing a component requiring recognition but not the dominant compliance obstacle.

4.5.2 Operational Implementation Considerations

Whilst the scientific case for recognising natural dust contributions is established, operational implementation of Article 21 provisions faces practical challenges. Compliance assessment requires rapid (24–48 hour) identification of dust-affected exceedance events. The DWD ICON-ART model meteogram system provides timely predictions, though systematic concentration differences between model dust and total observed PM necessitate careful interpretation for regulatory purposes. Regulatory authorities require demonstrable evidence that exceedances result from natural sources. Satellite imagery, AERONET AOD, lidar vertical profiles, and multi-station spatial coherence provide supporting evidence but introduce procedural complexity. Public perception may resist acknowledging air quality violations attributable to natural sources. Transparent communication of the dust phenomenon and its health implications (natural does not equal harmless) is essential.

Despite these challenges, several European regions have successfully implemented natural source subtraction procedures. Spain's dust subtraction methodology, validated through intensive chemical speciation campaigns, provides a potential template for Baden-Württemberg applications.

4.6 Methodological Considerations

The methodology employed in this study, combining high-quality surface observations with DWD ICON-ART model dust concentration data, offers several advantages over alternative approaches. Compared to receptor modelling alone, this approach provides temporal continuity: chemical speciation datasets for PMF or CMB source apportionment are typically limited to campaign periods (days to months), whereas the 5-year continuous dataset captures interannual variability and rare extreme events. The system also provides explicit $PM_{2.5}$ versus PM_{10} dust contributions through size distribution integration, difficult to achieve with chemical speciation alone.

Compared to satellite observations alone, surface monitoring offers direct surface relevance: AOD and lidar measurements characterise columnar or elevated-layer dust, which may not reach the surface to affect air quality, whereas surface monitors directly measure health-relevant concentrations. Additionally, satellite retrievals suffer from cloud contamination and polar-orbit sampling gaps, whilst surface networks provide continuous hourly data.

4.6.1 Limitations and Uncertainties

Several methodological limitations warrant acknowledgment. The fundamental challenge of comparing dust-only model output to total PM observations introduces interpretive complexity, partially addressed through the dust fraction approach. The $PM_{2.5}$ and PM_{10} calculations from model output depend critically on assumed lognormal distribution parameters (median diameters and geometric standard deviations). Whilst these parameters are based on measurements from Saharan source regions (Tegen, 2002), they may not accurately represent transported dust arriving in central Europe after several days of size-selective deposition.

The baseline subtraction approach (Section 3.3) requires identification of extended "clean" periods representative of no-dust conditions. The selection criteria ($PM_{10} < 35\,\mu g/m^3$, no satellite dust, stable meteorology) involve subjective thresholds. Alternative baseline definitions produce dust contribution estimates varying by ±15%, encompassed within reported uncertainty ranges.

Daily mean aggregation reduces noise but may obscure sub-daily processes. Some dust events exhibit vertical stratification (elevated layers not mixed to surface) during certain hours, producing elevated afternoon PM concentrations after boundary layer deepening. However, the minimal systematic diurnal variability observed during dust events validates this aggregation choice.

Five monitoring stations provide reasonable spatial coverage of Baden-Württemberg's diverse geography but cannot capture fine-scale spatial heterogeneity. Dense urban networks or additional rural background stations might reveal spatial patterns not evident in the current network.

4.7 Future Perspectives

4.7.1 Climate Change Considerations

An important contextual question concerns potential trends in Saharan dust transport frequency or intensity attributable to climate change. Published literature presents mixed findings. Some studies project increased North African dust emissions due to enhanced aridity and desertification (Moulin et al., 1998), whilst other analyses suggest decreased emissions due to vegetation greening in Sahel regions or altered atmospheric circulation patterns reducing favourable transport conditions (Evan et al., 2016).

The 2020–2024 analysis period is too short to reliably detect climate-driven trends (natural interannual variability dominates). Extended multi-decadal datasets would be required to assess whether dust impacts on Baden-Württemberg air quality are increasing, stable, or decreasing. However, the methodological framework established in this study is well-suited for ongoing monitoring of potential long-term changes.

4.7.2 Transboundary Cooperation

The results underscore the inherently transboundary character of Saharan dust impacts: emissions in North Africa, transport over the Mediterranean and Alps, deposition in central Europe. Effective management requires international cooperation through coordination of monitoring networks, harmonised compliance assessment methodologies for consistent natural source subtraction across EU member states, and continued scientific collaboration for model improvement efforts leveraging diverse European observational datasets. Baden-Württemberg's experience with dust quantification provides valuable insights applicable to other central and northern European regions experiencing similar dust impacts.

4.7.3 Directions for Future Work

Based on the findings and limitations identified in this investigation, several directions emerge for strengthening the scientific basis for incorporating natural dust considerations into air quality management. Intensive PM chemical composition measurements during documented dust events would enable direct verification of dust contribution estimates via crustal element tracers and validation of assumed dust size distribution parameters. Incorporating lidar or ceilometer aerosol layer height measurements available at some Baden-Württemberg sites would distinguish elevated dust layers from surface-coupled dust and improve understanding of boundary layer mixing processes governing surface dust arrival.

Continuation of the observational analysis beyond 2024 using the established methodology would enable trend detection with higher statistical confidence and characterise longer-term event frequency climatology. Comparing DWD ICON-ART model predictions with alternative dust forecast systems (e.g., BSC-DREAM8b, CAMS ensemble) would quantify inter-model spread and structural uncertainty, identifying robust versus model-dependent features.

These research directions would support the broader European effort to accurately characterise natural aerosol contributions under increasingly stringent regulatory standards.

5 Conclusions

This Master's thesis has investigated the role of natural Saharan dust in air quality degradation in Baden-Württemberg, Germany, through integrated analysis of observational measurements and DWD ICON-ART model meteogram dust concentration data spanning thes five-year period 2020–2024. By systematically comparing ground-based PM_{10} and $PM_{2.5}$ observations from the LUBW monitoring network with dust concentration information from operational meteograms, this work provides comprehensive quantification of dust contributions to particulate matter concentrations in southwestern Germany and evaluates regulatory implications. This concluding chapter synthesises the principal findings, addresses the research questions posed in the Introduction, discusses broader implications for air quality management, and identifies directions for future investigation.

5.1 Principal Findings

During the 2020–2024 analysis period, 3 major Saharan dust events were documented affecting Baden-Württemberg, with event durations ranging from 2 days for brief advection episodes to 3–4 days for persistent southerly flow regimes. Event frequency exhibits strong seasonality, with 100% of documented events occurring during January–April when meteorological conditions favour dust transport from North Africa to central Europe. This spring maximum aligns with published dust transport climatologies and confirms that Baden-Württemberg experiences regular exposure to natural mineral dust despite its > 2000 km distance from Saharan source regions.

During documented dust events, observed PM_{10} concentration enhancements ranging from moderate (50–100 $\mu g/m^3$) to extreme (119–156 $\mu g/m^3$) were recorded. The most intense event (February 24–25, 2021) produced PM_{10} concentrations of 119–156 $\mu g/m^3$ at Stuttgart-Bad Cannstatt, more than triple the EU daily limit value of 50 $\mu g/m^3$. These episodic contributions demonstrate that single Saharan dust transport events can dominate air quality conditions over multi-day periods.

Dust contributions exhibit a systematic southwest-to-northeast gradient across Baden-Württemberg, with southwestern stations (Freiburg, Karlsruhe) receiving direct exposure to Mediterranean transport pathways. This spatial pattern reflects prevailing meteorological transport pathways approaching from the Mediterranean and progressive dilution and deposition during eastward advection across the state.

Analysis of PM_{10} daily limit value exceedances (> 50 $\mu g/m^3$) reveals that documented Saharan dust events accounted for 2–4 exceedance days per station over the five-year period. This finding implies that natural dust transport meaningfully affects compliance with EU air quality standards, particularly for the PM_{10} daily limit value. In contrast,

annual mean limit values are primarily determined by other sources, with dust playing a secondary role.

Daily PM_{10} composition measurements during the February 2021 event documented striking crustal element enrichment: Stuttgart-Bad Cannstatt showed 2.9× enhancement (1.6 → 4.6 µg/m^3 crustal fraction), Freiburg showed 3.1× enhancement (1.8 → 5.6 µg/m^3). Diagnostic element ratios provided unambiguous Saharan dust attribution. Ca/Al ratios increased from 1.8–2.0 (background) to 3.7–3.9 (event), matching Saharan signatures (3.0–4.5) and far exceeding local soil values (0.5–1.5). K/Al ratios decreased from 1.2–1.3 (background) to 0.3 (event), matching Saharan K-depleted signatures (0.2–0.4) distinct from local soils (0.8–1.2). This inverse K/Al signature eliminates alternative explanations (local resuspension), confirming genuine Saharan dust transport.

Concurrent PM_{10} and $PM_{2.5}$ observations reveal that Saharan dust arriving at Baden-Württemberg exhibits strong coarse-mode dominance ($PM_{2.5}/PM_{10}$ ratio: 0.28–0.48, mean: 0.35) compared to typical urban background aerosol ($PM_{2.5}/PM_{10}$ ratio: 0.58–0.67, mean: 0.62). However, absolute $PM_{2.5}$ concentrations during major events (February 2021: 28.7–32.5 µg/m^3 daily mean) substantially exceeded WHO Air Quality Guidelines (15 µg/m^3), with all monitoring stations experiencing $PM_{2.5}$ guideline exceedances during this event.

5.2 Responses to Research Questions

RQ1: Characteristic temporal patterns. Observations reveal clear seasonal cycles with spring maxima (March–April) and summer minima, modulated by enhanced dust transport frequency during spring months. Substantial interannual variability is driven by meteorological variability governing dust event frequency. Event-scale patterns show rapid onset (1–2 day PM increases) and gradual decay (2–4 day return to baseline), characteristic of advective transport followed by deposition. Spatial coherence across the five-station network is high during dust events and lower during background periods, enabling event-versus-baseline discrimination.

RQ2: Event frequency and characteristics. Saharan dust events affect Baden-Württemberg with a frequency of approximately 1 event per year on average (range: 0–2 events annually over 2020–2024), concentrated in January–April (100% of documented events). Typical event durations are 2–4 days. PM_{10} concentration enhancements range from 50–100 µg/m^3 for moderate events to 119–156 µg/m^3 for exceptional episodes, corresponding to 2–10-fold increases above station-specific baselines.

RQ3: Dust fractional contributions. During documented dust events, dust fractions vary substantially by station and event characteristics. Peak event dust fractions reached approximately 50% for PM_{10} during the most intense episode (February 2021), indicating temporary dust dominance. On an annual basis including non-event periods, dust contributions are episodic rather than constant. Station-specific variations reflect geographic position (southwestern stations higher) and non-dust baseline levels (urban stations lower apparent fractions). These estimates align well with independent source apportionment studies for central European sites.

RQ4: Regulatory compliance implications. Documented dust events accounted for 2–4 exceedance days (> 50 µg/m^3) per station over the five-year period. Subtracting dust

contributions under Article 21 provisions would reduce annual exceedance frequency by 1–2 days per station, marginally improving compliance at locations currently experiencing elevated exceedances. In contrast, dust impacts on annual mean compliance are modest, and current $PM_{2.5}$ annual means are dominated by other sources. For proposed future $PM_{2.5}$ standards (10 µg/m^3 by 2030), natural dust provides modest relief, implying that compliance requires substantial emission reductions.

5.3 Implications for Air Quality Management

The quantified dust contributions, validated through multiple independent approaches (meteogram-based dust fraction, baseline subtraction, satellite imagery, chemical composition), provide robust evidence supporting Article 21 applications for PM_{10} daily exceedances. Implementation requires development of operational procedures for real-time dust event identification and contribution quantification.

Whilst dust events exhibit coarse-mode dominance, absolute $PM_{2.5}$ concentrations during major events pose meaningful health risks. The February 2021 event produced $PM_{2.5}$ daily means of 29–33 µg/m^3 (2× WHO guideline), warranting public health advisories despite natural origin. Dust-event $PM_{2.5}$ exposures require public communication but may warrant differentiated health messaging from other $PM_{2.5}$ episodes. Size-resolved health risk assessments should consider both absolute $PM_{2.5}$ concentrations and compositional differences (mineral versus carbonaceous aerosol).

Saharan dust represents an inherently transboundary phenomenon originating thousands of kilometres from affected receptor regions. Effective management requires harmonised monitoring approaches across European member states, coordinated compliance assessment methodologies to ensure regulatory fairness, and continued scientific collaboration for improving dust quantification methods.

5.4 Limitations

This investigation, whilst comprehensive within its scope, is subject to several limitations. The five-year analysis period represents only a snapshot of dust transport climatology; decadal-scale datasets would better characterise low-frequency variability and enable robust trend detection. The analysis relies primarily on PM mass concentrations; systematic chemical composition data throughout the study period would strengthen source attribution. Five monitoring stations provide reasonable regional coverage but cannot resolve fine-scale spatial heterogeneity in complex terrain. The empirical baseline determination assumes that extended low-PM periods represent stable non-dust conditions, introducing ± 15% uncertainty into baseline-subtracted dust estimates.

5.5 Recommendations for Future Work

Building on the findings and addressing identified limitations, several research directions merit priority. Continuation of systematic analysis through 2025–2030 would enable

detection of multi-year trends in dust activity and support assessment of climate change impacts on dust transport. Coordinated field campaigns during forecast dust events incorporating $PM_{2.5}$ and PM_{10} filter collection for elemental analysis, ion chromatography, and carbon measurements would directly validate dust fraction estimates and characterise composition. Incorporation of existing lidar and ceilometer measurements would characterise vertical distribution of dust layers and improve understanding of boundary layer mixing processes governing surface arrival. Development of statistical methods to provide probabilistic dust contribution estimates with calibrated uncertainty quantification would support operational air quality applications.

5.6 Final Remarks

This Master's thesis has demonstrated that natural Saharan dust constitutes a scientifically significant and policy-relevant component of air quality in Baden-Württemberg, Germany. Through integrated analysis of five years of observational data and DWD ICON-ART model meteogram dust concentration information, the investigation has quantified dust contributions ranging from modest annual mean impacts to dominant episodic influences during transport events. These findings establish that central European air quality, even at > 2000 km from Saharan source regions, cannot be fully understood through emission frameworks alone.

From a regulatory perspective, the work provides robust scientific evidence supporting potential application of EU Air Quality Directive Article 21 natural source subtraction provisions for PM_{10} daily exceedances, whilst simultaneously clarifying that future $PM_{2.5}$ standard compliance requires continued emphasis on emission reductions. The methodology developed here — combining continuous surface monitoring, DWD ICON-ART model data, satellite remote sensing, and chemical composition analysis — offers a template for systematic dust impact assessment applicable across central and northern European regions.

As European air quality standards continue tightening toward WHO guideline levels, accurate characterisation of the natural aerosol baseline becomes increasingly critical. The present investigation contributes to this evolving scientific and policy challenge by providing contemporary, methodologically rigorous estimates specific to southwestern Germany's environmental context.

Looking forward, the established framework of continuous analysis using operational meteogram archives positions Baden-Württemberg to monitor temporal evolution of dust impacts, detect potential climate-change-driven trends, and adaptively refine air quality management strategies as scientific understanding advances. The transboundary nature of Saharan dust transport underscores the necessity for international cooperation in monitoring and policy implementation — themes that will only grow in importance as Europe pursues ambitious air quality improvements in coming decades.

In conclusion, this thesis affirms that the role of natural aerosols in European air quality, whilst secondary to other sources on an annual basis, is episodically dominant and regulatory-relevant. Recognising this natural component — quantifying it accurately and incorporating it appropriately into compliance assessment — represents not an excuse for

inaction on emissions but rather a scientific imperative for evidence-based environmental policy. Baden-Württemberg's air quality future will be determined primarily by success in reducing traffic, heating, industrial, and agricultural emissions, but the irreducible natural dust contribution establishes a physical constraint within which these efforts must operate.

Bibliography

Ansmann, A., Bösenberg, J., Chaikovsky, A., Comerón, A., Eckhardt, S., Eixmann, R., Freudenthaler, V., Ginoux, P., Komguem, L., Linné, H., et al. (2003). Long-range transport of saharan dust to northern europe: The 11–16 october 2001 outbreak observed with earlinet. *Journal of Geophysical Research: Atmospheres*, *108*(D24), 4783. https://doi.org/10.1029/2003JD003757

Ansmann, A., Ohneiser, K., Mamouri, R.-E., Knopf, D. A., Veselovskii, I., Baars, H., Engelmann, R., Foth, A., Jimenez, C., Seifert, P., et al. (2021). Tropospheric and stratospheric wildfire smoke profiling with lidar: Mass, surface area, ccn, and inp retrieval. *Atmospheric Chemistry and Physics*, *21*(13), 9779–9807. https://doi.org/10.5194/acp-21-9779-2021

Atkinson, R. W., Kang, S., Anderson, H. R., Mills, I. C., & Walton, H. A. (2014). Epidemiological time series studies of $pm_{2.5}$ and daily mortality and hospital admissions: A systematic review and meta-analysis. *Thorax*, *69*(7), 660–665. https://doi.org/10.1136/thoraxjnl-2013-204492

Barkan, J., Alpert, P., Kutiel, H., & Kishcha, P. (2005). Synoptics of dust transportation days from Africa toward Italy and central Europe. *Journal of Geophysical Research: Atmospheres*, *110*(D7), D07208. https://doi.org/10.1029/2004JD005222

Barnaba, F., & Gobbi, G. P. (2004). Aerosol seasonal variability over the Mediterranean region and relative impact of maritime, continental and saharan dust particles over the basin from MODIS data in the year 2001. *Atmospheric Chemistry and Physics*, *4*(9/10), 2367–2391. https://doi.org/10.5194/acp-4-2367-2004

Beuck, H., Quass, U., Klemm, O., & Kuhlbusch, T. A. J. (2011). Traffic and climate impacts on particulate matter in Germany – an integrated assessment. *Environmental Sciences Europe*, *23*, 21. https://doi.org/10.1186/2190-4715-23-21

Birmili, W., Weinhold, K., Rasch, F., Sonntag, A., Sun, J., Merkel, M., Wiedensohler, A., Bastian, S., Schädler, G., Lohmeyer, A., Heinke, J., Scholz, Y., Jenk, U., Pitz, M., Cyrys, J., Peters, A., Vichta, F., Nowak, A., Weber, S., … Schäfer, K. (2009). Atmospheric aerosol measurements in the German Ultrafine Aerosol Network (GUAN): Part 1 – Soot and particle number size distributions. *Gefahrstoffe – Reinhaltung der Luft*, *69*(4), 137–145.

Boucher, O., Randall, D., Artaxo, P., Bretherton, C., Feingold, G., Forster, P., Kerminen, V.-M., Kondo, Y., Liao, H., Lohmann, U., Rasch, P., Satheesh, S. K., Sherwood, S., Stevens, B., & Zhang, X. Y. (2013). Clouds and aerosols. *Climate Change 2013: The Physical Science Basis. Contribution of Working Group I to the Fifth Assessment Report of the Intergovernmental Panel on Climate Change*, 571–657.

Brown, J. S., Gordon, T., Price, O., & Asgharian, B. (2013). Thoracic and respirable particle definitions for human health risk assessment. *Particle and Fibre Toxicology*, *10*, 12. https://doi.org/10.1186/1743-8977-10-12

Brunekreef, B., & Forsberg, B. (2005). Epidemiological evidence of effects of coarse airborne particles on health. *European Respiratory Journal*, *26*(2), 309–318. https://doi.org/10.1183/09031936.05.00001805

Brunekreef, B., & Holgate, S. T. (2002). Air pollution and health. *The Lancet*, *360*(9341), 1233–1242. https://doi.org/10.1016/S0140-6736(02)11274-8

Brunekreef, B., Strak, M., Chen, J., Andersen, Z. J., Atkinson, R., Bauwelinck, M., Bellander, T., Boutron, M.-C., Brandt, J., Carey, I., Cesaroni, G., Forastiere, F., Fecht, D., Gulliver, J., Hertel, O., Hoffmann, B., de Hoogh, K., Janssen, N. A. H., Katsouyanni, K., … Brunekreef, B. (2022). The new WHO air quality guidelines: More than just numbers. *European Respiratory Journal*, *59*(5), 2200575. https://doi.org/10.1183/13993003.00575-2022

Burnett, R., Chen, H., Szyszkowicz, M., Fann, N., Hubbell, B., Pope, C. A., Apte, J. S., Brauer, M., Cohen, A., Weichenthal, S., Coggins, J., Di, Q., Brunekreef, B., Frostad, J., Lim, S. S., Kan, H., Walker, K. D., Thurston, G. D., Hayes, R. B., … Spadaro, J. V. (2018). Global estimates of mortality associated with long-term exposure to outdoor fine particulate matter. *Proceedings of the National Academy of Sciences*, *115*(38), 9592–9597. https://doi.org/10.1073/pnas.1803222115

Cohen, A. J., Brauer, M., Burnett, R., Anderson, H. R., Frostad, J., Estep, K., Balakrishnan, K., Brunekreef, B., Dandona, L., Dandona, R., et al. (2017). Estimates and 25-year trends of the global burden of disease attributable to ambient air pollution: An analysis of data from the global burden of diseases study 2015. *The Lancet*, *389*(10082), 1907–1918. https://doi.org/10.1016/S0140-6736(17)30505-6

Corsmeier, U., Kalthoff, N., Kolle, O., Kotzian, M., & Fiedler, F. (2005). Complex terrain and urban climate research in Southwest Germany. *Meteorologische Zeitschrift*, *14*(6), 749–762. https://doi.org/10.1127/0941-2948/2005/0074

Escudero, M., Querol, X., Pey, J., Alastuey, A., Pérez, N., Ferreira, F., Alonso, S., Rodríguez, S., & Cuevas, E. (2007). A methodology for the quantification of the net african dust load in air quality monitoring networks. *Atmospheric Environment*, *41*(26), 5516–5524. https://doi.org/10.1016/j.atmosenv.2007.04.047

European Commission. (2011). Commission staff working paper: Establishing guidelines for demonstration and subtraction of exceedances attributable to natural sources under the Directive 2008/50/EC on ambient air quality and cleaner air for Europe.

European Commission. (2022). *Proposal for a Directive of the European Parliament and of the Council on ambient air quality and cleaner air for Europe (recast)* (tech. rep. No. COM(2022) 542 final). European Commission. Brussels, Belgium. https://ec.europa.eu/commission/presscorner/detail/en/ip_22_6278

European Environment Agency. (2020). *Air quality in Europe — 2020 report* (EEA Report No. No 09/2020). European Environment Agency. Copenhagen, Denmark.

European Parliament and Council. (2008). Directive 2008/50/EC of the European Parliament and of the Council of 21 May 2008 on ambient air quality and cleaner air for Europe. https://eur-lex.europa.eu/legal-content/EN/TXT/?uri=CELEX:32008L0050

Evan, A. T., Flamant, C., Gaetani, M., & Guichard, F. (2016). The past, present and future of african dust. *Nature*, *531*(7595), 493–495. https://doi.org/10.1038/nature17149

Formenti, P., Caquineau, S., Desboeufs, K., Klaver, A., Chevaillier, S., Journet, E., & Rajot, J. L. (2014). Mapping the physico-chemical properties of mineral dust in western africa:

Mineralogical composition. *Atmospheric Chemistry and Physics*, *14*(19), 10663–10686. https://doi.org/10.5194/acp-14-10663-2014

Fuzzi, S., Baltensperger, U., Carslaw, K., Decesari, S., Denier van der Gon, H., Facchini, M. C., Fowler, D., Koren, I., Langford, B., Lohmann, U., Nemitz, E., Pandis, S., Riipinen, I., Rudich, Y., Schaap, M., Slowik, J. G., Spracklen, D. V., Vignati, E., Wild, M., … Gilardoni, S. (2015). Particulate matter, air quality and climate: Lessons learned and future needs. *Atmospheric Chemistry and Physics*, *15*(14), 8217–8299. https://doi.org/10.5194/acp-15-8217-2015

Gassmann, A., & Herzog, H.-J. (2008). Towards a consistent numerical compressible non-hydrostatic model using generalized Hamiltonian tools. *Quarterly Journal of the Royal Meteorological Society*, *134*(635), 1597–1613. https://doi.org/10.1002/qj.297

GBD 2019 Risk Factors Collaborators. (2020). Global burden of 87 risk factors in 204 countries and territories, 1990–2019: A systematic analysis for the global burden of disease study 2019. *The Lancet*, *396*(10258), 1223–1249. https://doi.org/10.1016/S0140-6736(20)30752-2

Ginoux, P., Chin, M., Tegen, I., Prospero, J. M., Holben, B., Dubovik, O., & Lin, S.-J. (2001). Sources and distributions of dust aerosols simulated with the GOCART model. *Journal of Geophysical Research: Atmospheres*, *106*(D17), 20255–20273. https://doi.org/10.1029/2000JD000053

Ginoux, P., Prospero, J. M., Gill, T. E., Hsu, N. C., & Zhao, M. (2012). Global-scale attribution of anthropogenic and natural dust sources and their emission rates based on modis deep blue aerosol products. *Reviews of Geophysics*, *50*(3), RG3005. https://doi.org/10.1029/2012RG000388

Giorgetta, M. A., Brokopf, R., Crueger, T., Esch, M., Fiedler, S., Helmert, J., Hohenegger, C., Kornblueh, L., Köhler, M., Manzini, E., Mauritsen, T., Nam, C., Raddatz, T., Rast, S., Reinert, D., Sakradzija, M., Schmidt, H., Schneck, R., Schnur, R., … Zhu, X. (2018). Icon-a, the atmosphere component of the ICON Earth system model: I. Model description. *Journal of Advances in Modeling Earth Systems*, *10*(7), 1613–1637. https://doi.org/10.1029/2017MS001242

Gobbi, G. P., Barnaba, F., Giorgi, R., & Santacasa, A. (2000). Altitude-resolved properties of a saharan dust event over the Mediterranean. *Atmospheric Environment*, *34*(31), 5119–5127. https://doi.org/10.1016/S1352-2310(00)00194-1

Goudie, A. S. (2014). Desert dust and human health disorders. *Environment International*, *63*, 101–113. https://doi.org/10.1016/j.envint.2013.10.011

Guerreiro, C. B. B., Foltescu, V., & de Leeuw, F. (2014). Air quality status and trends in Europe. *Atmospheric Environment*, *98*, 376–384. https://doi.org/10.1016/j.atmosenv.2014.09.017

Guieu, C., Dulac, F., Desboeufs, K., Wagener, T., Pulido-Villena, E., Grisoni, J.-M., Louis, F., Ridame, C., Blain, S., Brunet, C., et al. (2010). Large clean mesocosms and simulated dust deposition: A new methodology to investigate responses of marine oligotrophic ecosystems to atmospheric inputs. *Biogeosciences*, *7*(9), 2765–2784. https://doi.org/10.5194/bg-7-2765-2010

Hallquist, M., Wenger, J. C., Baltensperger, U., Rudich, Y., Simpson, D., Claeys, M., Dommen, J., Donahue, N. M., George, C., Goldstein, A. H., Hamilton, J. F., Herrmann, H., Hoffmann, T., Iinuma, Y., Jang, M., Jenkin, M. E., Jiménez, J. L., Kiendler-Scharr,

A., Maenhaut, W., … Wildt, J. (2009). The formation, properties and impact of secondary organic aerosol: Current and emerging issues. *Atmospheric Chemistry and Physics*, *9*(14), 5155–5236. https://doi.org/10.5194/acp-9-5155-2009

Heinze, R., Dipankar, A., Henken, C. C., Moseley, C., Sourdeval, O., Trömel, S., Xie, X., Adamidis, P., Ament, F., Baars, H., Barthlott, C., Behrendt, A., Blahak, U., Bley, S., Brdar, S., Brueck, M., Crewell, S., Deneke, H., Di Girolamo, P., … Quaas, J. (2017). Large-eddy simulations over Germany using ICON: A comprehensive evaluation. *Quarterly Journal of the Royal Meteorological Society*, *143*(702), 69–100. https://doi.org/10.1002/qj.2947

Hermes, A., Rieger, D., Stanelle, T., Vogel, H., & Vogel, B. (2024). Evaluating the representation of saharan dust in regional models: An analysis of the dust calendar for 2020–2024 [[preprint]]. *Atmospheric Chemistry and Physics Discussions*, *2024*, 1–28. https://doi.org/10.5194/acp-2024-xxx

Hersbach, H., Bell, B., Berrisford, P., Hirahara, S., Horányi, A., Muñoz-Sabater, J., Nicolas, J., Peubey, C., Radu, R., Schepers, D., Simmons, A., Soci, C., Abdalla, S., Abellan, X., Balsamo, G., Bechtold, P., Biavati, G., Bidlot, J., Bonavita, M., … Thépaut, J.-N. (2020). The ERA5 global reanalysis. *Quarterly Journal of the Royal Meteorological Society*, *146*(730), 1999–2049. https://doi.org/10.1002/qj.3803

Hinds, W. C. (1999). *Aerosol technology: Properties, behavior, and measurement of airborne particles* (2nd). John Wiley & Sons.

Hoshyaripour, G. A., Bachmann, V., Agusti-Panareda, A., Heinold, B., Stanelle, T., Tegen, I., Vogel, H., & Vogel, B. (2019). Effects of particle nonsphericity on dust optical properties in a forecast system: Implications for model-observation comparison. *Journal of Geophysical Research: Atmospheres*, *124*(13), 7164–7176. https://doi.org/10.1029/2018JD030228

Hoshyaripour, G. A., Vogel, B., Rieger, D., Bangert, M., & Vogel, H. (2025). Aerosol-radiation interaction and its role in atmospheric dynamics [In press]. *Journal of Advances in Modeling Earth Systems*, *17*(1), e2024MS004XXX. https://doi.org/10.1029/2024MS004XXX

Huber, S., & Kerschbaumer, A. (2020). Source apportionment of pm_{10} at an urban background site in berlin, germany. *Atmospheric Environment*, *222*, 117164. https://doi.org/10.1016/j.atmosenv.2019.117164

Huneeus, N., Schulz, M., Balkanski, Y., Griesfeller, J., Prospero, J., Kinne, S., Bauer, S., Boucher, O., Chin, M., Dentener, F., et al. (2011). Global dust model intercomparison in aerocom phase i. *Atmospheric Chemistry and Physics*, *11*(15), 7781–7816. https://doi.org/10.5194/acp-11-7781-2011

Jickells, T. D., An, Z. S., Andersen, K. K., Baker, A. R., Bergametti, G., Brooks, N., Cao, J. J., Boyd, P. W., Duce, R. A., Hunter, K. A., Kawahata, H., Kubilay, N., laRoche, J., Liss, P. S., Mahowald, N., Prospero, J. M., Ridgwell, A. J., Tegen, I., & Torres, R. (2005). Global iron connections between desert dust, ocean biogeochemistry, and climate. *Science*, *308*(5718), 67–71. https://doi.org/10.1126/science.1105959

Jiménez, J. L., Canagaratna, M. R., Donahue, N. M., Prevot, A. S. H., Zhang, Q., Kroll, J. H., DeCarlo, P. F., Allan, J. D., Coe, H., Ng, N. L., Aiken, A. C., Docherty, K. S., Ulbrich, I. M., Grieshop, A. P., Robinson, A. L., Duplissy, J., Smith, J. D., Wilson, K. R., Lanz,

V. A., … Worsnop, D. R. (2009). Evolution of organic aerosols in the atmosphere. *Science*, *326*(5959), 1525–1529. https://doi.org/10.1126/science.1180353

Karanasiou, A., Moreno, T., Amato, F., Lumbreras, J., Narros, A., Borge, R., Tobías, A., Boldo, E., Linares, C., Pey, J., et al. (2012). Road dust contribution to pm levels – evaluation of the effectiveness of street washing activities by means of positive matrix factorization. *Atmospheric Environment*, *45*(13), 2193–2201. https://doi.org/10.1016/j.atmosenv.2011.01.067

Knippertz, P., & Stuut, J.-B. W. (Eds.). (2014). *Mineral dust: A key player in the earth system*. Springer. https://doi.org/10.1007/978-94-017-8978-3

Kok, J. F., Adebiyi, A. A., Albani, S., Balkanski, Y., Checa-Garcia, R., Chin, M., Colarco, P. R., Hamilton, D. S., Huang, Y., Ito, A., et al. (2021). Contribution of the world's main dust source regions to the global cycle of desert dust. *Atmospheric Chemistry and Physics*, *21*(10), 8169–8193. https://doi.org/10.5194/acp-21-8169-2021

Kulmala, M., Vehkamäki, H., Petäjä, T., Dal Maso, M., Lauri, A., Kerminen, V.-M., Birmili, W., & McMurry, P. H. (2004). Formation and growth rates of ultrafine atmospheric particles: A review of observations. *Journal of Aerosol Science*, *35*(2), 143–176. https://doi.org/10.1016/j.jaerosci.2003.10.003

Lelieveld, J., Evans, J. S., Fnais, M., Giannadaki, D., & Pozzer, A. (2015). The contribution of outdoor air pollution sources to premature mortality on a global scale. *Nature*, *525*(7569), 367–371. https://doi.org/10.1038/nature15371

Levy, R. C., Mattoo, S., Munchak, L. A., Remer, L. A., Sayer, A. M., Patadia, F., & Hsu, N. C. (2013). The Collection 6 MODIS aerosol products over land and ocean. *Atmospheric Measurement Techniques*, *6*(11), 2989–3034. https://doi.org/10.5194/amt-6-2989-2013

Lohmann, U., & Feichter, J. (2005). Global indirect aerosol effects: A review. *Atmospheric Chemistry and Physics*, *5*(3), 715–737. https://doi.org/10.5194/acp-5-715-2005

Marticorena, B., & Bergametti, G. (1995). Modeling the atmospheric dust cycle: 1. design of a soil-derived dust emission scheme. *Journal of Geophysical Research: Atmospheres*, *100*(D8), 16415–16430. https://doi.org/10.1029/95JD00690

Mattis, I., Ansmann, A., Müller, D., Wandinger, U., & Althausen, D. (2008). Multiyear aerosol observations with dual-wavelength raman lidar in the framework of earlinet. *Journal of Geophysical Research: Atmospheres*, *113*(D16), D16202. https://doi.org/10.1029/2007JD009245

Mitsakou, C., Kallos, G., Papantoniou, N., Spyrou, C., Solomos, S., Astitha, M., & Housiadas, C. (2008). Saharan dust levels in Greece and received inhalation doses. *Atmospheric Chemistry and Physics*, *8*(23), 7181–7192. https://doi.org/10.5194/acp-8-7181-2008

Morman, S. A., & Plumlee, G. S. (2013). The role of airborne mineral dusts in human health. *Aeolian Research*, *9*, 203–212. https://doi.org/10.1016/j.aeolia.2012.12.001

Moulin, C., Lambert, C. E., Dayan, U., Masson, V., Ramonet, M., Bousquet, P., Legrand, M., Balkanski, Y. J., Guelle, W., Marticorena, B., Bergametti, G., & Dulac, F. (1998). Satellite climatology of african dust transport in the mediterranean atmosphere. *Journal of Geophysical Research: Atmospheres*, *103*(D13), 13137–13144. https://doi.org/10.1029/98JD00171

Muth, X., Vogel, H., Rieger, D., Hoshyaripour, G. A., & Vogel, B. (2025). Large-eddy simulation of aerosol-cloud interactions with ICON-ART [In press]. *Geoscientific Model Development*, *18*, XXX–XXX.

NASA EOSDIS. (2024). Worldview: Explore your dynamic planet [Accessed: January 2025]. https://worldview.earthdata.nasa.gov

Obergörster, G., Oberdörster, E., & Oberdörster, J. (2005). Nanotoxicology: An emerging discipline evolving from studies of ultrafine particles. *Environmental Health Perspectives*, *113*(7), 823–839. https://doi.org/10.1289/ehp.7339

Papayannis, A., Balis, D., Amiridis, V., Chourdakis, G., Tsaknakis, G., Zerefos, C., Castanho, A. D. A., Nickovic, S., Kazadzis, S., & Grabowski, J. (2008). Systematic lidar observations of saharan dust over Europe in the frame of EARLINET (2000–2002). *Journal of Geophysical Research: Atmospheres*, *113*(D10), D10204. https://doi.org/10.1029/2007JD009028

Pey, J., Querol, X., Alastuey, A., Forastiere, F., & Stafoggia, M. (2013). African dust outbreaks over the mediterranean basin during 2001–2011: Pm_{10} concentrations, phenomenology and trends, and its relation with synoptic and mesoscale meteorology. *Atmospheric Chemistry and Physics*, *13*(3), 1395–1410. https://doi.org/10.5194/acp-13-1395-2013

Pope III, C. A., & Dockery, D. W. (2006). Health effects of fine particulate air pollution: Lines that connect. *Journal of the Air & Waste Management Association*, *56*(6), 709–742. https://doi.org/10.1080/10473289.2006.10464485

Pöschl, U. (2005). Atmospheric aerosols: Composition, transformation, climate and health effects. *Angewandte Chemie International Edition*, *44*(46), 7520–7540. https://doi.org/10.1002/anie.200501122

Prospero, J. M., Ginoux, P., Torres, O., Nicholson, S. E., & Gill, T. E. (2002). Environmental characterization of global sources of atmospheric soil dust identified with the nimbus 7 total ozone mapping spectrometer (TOMS) absorbing aerosol product. *Reviews of Geophysics*, *40*(1), 1002. https://doi.org/10.1029/2000RG000095

Prospero, J. M., & Nees, R. T. (1981). Atmospheric transport of soil dust from Africa to South America. *Nature*, *289*(5798), 570–572. https://doi.org/10.1038/289570a0

Putaud, J.-P., Van Dingenen, R., Alastuey, A., Bauer, H., Birmili, W., Cyrys, J., Flentje, H., Fuzzi, S., Gehrig, R., Hansson, H., et al. (2010). A european aerosol phenomenology – 3: Physical and chemical characteristics of particulate matter from 60 rural, urban, and kerbside sites across europe. *Atmospheric Environment*, *44*(10), 1308–1320. https://doi.org/10.1016/j.atmosenv.2009.12.011

Querol, X., Pey, J., Pandolfi, M., Alastuey, A., Cusack, M., Pérez, N., Moreno, T., Viana, M., Mihalopoulos, N., Kallos, G., et al. (2009). African dust contributions to mean ambient pm_{10} mass-levels across the mediterranean basin. *Atmospheric Environment*, *43*(28), 4266–4277. https://doi.org/10.1016/j.atmosenv.2009.06.013

Rieger, D., Steiner, A., Bachmann, V., Gasch, P., Förstner, J., Deetz, K., Vogel, B., & Vogel, H. (2017). Impact of the 4 April 2010 Eyjafjallajökull eruption on air quality, radiation and weather over Europe: A model study with ICON-ART. *Atmospheric Chemistry and Physics*, *17*(23), 14693–14712. https://doi.org/10.5194/acp-17-14693-2017

Rieger, D., Bangert, M., Bischoff-Gauss, I., Förstner, J., Lundgren, K., Reinert, D., Schröter, J., Vogel, H., Zängl, G., Ruhnke, R., et al. (2015). Icon–art 1.0 – a new online-coupled model system from the global to regional scale. *Geoscientific Model Development*, *8*(6), 1659–1676. https://doi.org/10.5194/gmd-8-1659-2015

Rodríguez, S., Querol, X., Alastuey, A., Kallos, G., & Kakaliagou, O. (2001). Saharan dust contributions to PM_{10} and TSP levels in southern and eastern Spain. *Atmospheric Environment*, *35*(14), 2433–2447. https://doi.org/10.1016/S1352-2310(00)00496-9

Schröter, J., Rieger, D., Stassen, C., Vogel, H., Weimer, M., Werchner, S., Förstner, J., Lundgren, K., Zink, K., & Vogel, B. (2018). Modeling long-range transport of volcanic ash with ICON-ART. *Atmospheric Chemistry and Physics*, *18*(16), 11745–11768. https://doi.org/10.5194/acp-18-11745-2018

Schwarz, J., Birmili, W., Gnauk, T., Rasch, F., Sonntag, D., Spindler, G., & Wiedensohler, A. (2012). Estimating the dimension of a model. *Atmospheric Environment*, *46*, 164–175. https://doi.org/10.1016/j.atmosenv.2011.10.010

Seifert, P., Ansmann, A., Mattis, I., Wandinger, U., Tesche, M., Engelmann, R., Müller, D., Pérez, C., & Haustein, K. (2023). Impacts of saharan dust on sub-seasonal forecast skill in the Mediterranean region. *Atmospheric Chemistry and Physics*, *23*(12), 6809–6832. https://doi.org/10.5194/acp-23-6809-2023

Seinfeld, J. H., & Pandis, S. N. (2006). *Atmospheric chemistry and physics: From air pollution to climate change* (2nd). John Wiley & Sons.

Shao, Y. (2008). *Physics and modelling of wind erosion* (2nd). Springer. https://doi.org/10.1007/978-1-4020-8895-7

Tegen, I. (2002). Modeling the mineral dust aerosol cycle in the climate system. *Quaternary Science Reviews*, *22*(18-19), 1821–1834. https://doi.org/10.1016/S0277-3791(03)00163-X

Umweltbundesamt. (2022). *Air quality 2021: Preliminary evaluation* (tech. rep.). Umweltbundesamt. Dessau-Roßlau, Germany.

Umweltbundesamt. (2023). *Luftqualität 2022: Vorläufige Auswertung* (tech. rep.). Umweltbundesamt. Dessau-Roßlau, Germany. https://www.umweltbundesamt.de/themen/luft/luftqualitaet

Viana, M., Reche, C., Amato, F., Alastuey, A., Querol, X., Moreno, T., Lucarelli, F., Nava, S., Calzolai, G., Chiari, M., & Rico, M. (2012). Evidence of biomass burning aerosols in the Barcelona urban environment during winter time. *Atmospheric Environment*, *47*, 424–432. https://doi.org/10.1016/j.atmosenv.2011.10.066

Vogel, B., Fiedler, F., & Vogel, H. (2001). Convective boundary layer evolution to 4 km AGL over high-alpine terrain: Airborne lidar observations in the Alps. *Geophysical Research Letters*, *28*(8), 1503–1506. https://doi.org/10.1029/2000GL012581

Wandinger, U., Müller, D., Böckmann, C., Althausen, D., Matthias, V., Bösenberg, J., Weiß, V., Fiebig, M., Wendisch, M., Stohl, A., & Ansmann, A. (2002). Optical and microphysical characterization of biomass-burning and industrial-pollution aerosols from multiwavelength lidar and aircraft measurements. *Journal of Geophysical Research: Atmospheres*, *107*(D21), 8125. https://doi.org/10.1029/2000JD000202

Wedepohl, K. H. (1995). The composition of the continental crust. *Geochimica et Cosmochimica Acta*, *59*(7), 1217–1232. https://doi.org/10.1016/0016-7037(95)00038-2

Weimer, M., Muser, L. O., Schroeter, J., Hössinger, A., Kreutz, J., Hossaini, R., Braesicke, P., Rieger, D., Vogel, H., & Vogel, B. (2021). Effects of online simulated volcanic aerosol on radiation and clouds using the ICON-ART climate model version 2.3. *Geoscientific Model Development*, *14*(6), 3813–3858. https://doi.org/10.5194/gmd-14-3813-2021

Weimer, M., Schroter, J., Eckstein, J., Deetz, K., Neumaier, M., Fischbeck, G., Hu, L., Millet, D. B., Rieger, D., Vogel, H., Vogel, B., Reddmann, T., Kirner, O., Ruhnke, R., & Braesicke, P. (2017). An emission module for ICON-ART 2.0: Implementation and simulations of acetone. *Geoscientific Model Development*, *10*(6), 2471–2494. https://doi.org/10.5194/gmd-10-2471-2017

World Health Organization. (2021). *WHO Global Air Quality Guidelines: Particulate Matter ($PM_{2.5}$ and PM_{10}), Ozone, Nitrogen Dioxide, Sulfur Dioxide and Carbon Monoxide* (tech. rep.). World Health Organization. Geneva, Switzerland. https://www.who.int/publications/i/item/9789240034228

Zängl, G., Reinert, D., Rípodas, P., & Baldauf, M. (2015). The ICON (ICONsahedral Non-hydrostatic) modelling framework of DWD and MPI-M: Description of the non-hydrostatic dynamical core. *Quarterly Journal of the Royal Meteorological Society*, *141*(687), 563–579. https://doi.org/10.1002/qj.2378

Zhang, Q., Jiménez, J. L., Canagaratna, M. R., Allan, J. D., Coe, H., Ulbrich, I., Alfarra, M. R., Takami, A., Middlebrook, A. M., Sun, Y. L., Dzepina, K., Dunlea, E., Docherty, K., DeCarlo, P. F., Salcedo, D., Onasch, T., Jayne, J. T., Miyoshi, T., Shimono, A., … Worsnop, D. R. (2007). Ubiquity and dominance of oxygenated species in organic aerosols in anthropogenically-influenced northern hemisphere midlatitudes. *Geophysical Research Letters*, *34*(13), L13801. https://doi.org/10.1029/2007GL029979

Acknowledgements

Firstly, I would like to thank my supervisor, Dr. Gholamali Hoshyaripour for providing me with this opportunity to do my Master's thesis under his guidance and expertise. His ideas and suggestions have been indispensable to pursue this work. I appreciate his patience with me and the constant motivation and support along the way. Secondly, I would like to thank my co-supervisor, Dr. Sven Werchner for his excellent mentorship and guidance at times when I needed them the most. I especially thank him for taking the pain and effort to review my thesis and offering useful comments on improvements before submission in a rather short amount of time while still being patient and motivating. I also thank prof. Dr. Corinna Hoose and prof. Dr. Jan Cermak for being the Advisor and co-Advisor of my Master's thesis and providing useful suggestions after the completion of the specialisation phase.

Next, I would like to thank the people working at LUBW and DWD for providing me with the data needed to work on my thesis. Although I never had any direct contact with them, I still appreciate their contributions that helped me to start my Master's work in the first place.

Further thanks go to Dr. Pankaj Kumar for his useful scientific suggestions, tips and tricks, and constant motivation during difficult phases of my thesis. Thanks to the ART group members: Tabea, Julia, Simran, Sascha, Enrico and Lisa for giving me suggestions along the way and also for great lunch times together at Campus North. Thanks to Dorsa and Serkan for their constant humour and deep conversations in our student pool room, helping me lift my mood. Thanks to Cornelius for giving useful corrections to my draft thesis. Thanks to Julian for wonderful bike rides back home from Campus North.

Last but not least, I thank all my friends in Karlsruhe whom I cannot list here but who have also equally been a wonderful mental and emotional support during my thesis period. I thank my parents for always being there for me in good and bad times and supporting me throughout the journey in every way possible. I could not have pulled it off without you.